ELECTROCHEMICAL BEHAVIOR OF Fe_3Al-5M (M=Ti, Zr, V, Nb, Ta, Cr, Mo AND W) INTERMETALLICS

by

Shalin Astha

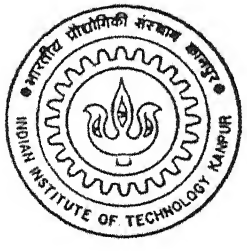

Department of Materials and Metallurgical Engineering

INDIAN INSTITUTE OF TECHNOLOGY KANPUR

March, 1996

ELECTROCHEMICAL BEHAVIOR OF Fe_3Al-5M (M = Ti, Zr, V, Nb, Ta, Cr, Mo AND W) INTERMETALLICS

A Thesis Submitted

in Partial Fulfillment of the Requirements

for the Degree of

MASTER OF TECHNOLOGY

by

SHALIN ASTHA

to the

DEPARTMENT OF MATERIALS AND METALLURGICAL ENGINEERING

INDIAN INSTITUTE OF TECHNOLOGY KANPUR

MARCH, 1996

MME-1996-M-AST-ELE

aluminide showed active-passive behavior but corrodes in a localized manner (pitting) [39].

As discussed earlier, the room temperature ductility of Fe_3Al is very low (3-5%), a characteristic which has restricted the ease of fabrication and engineering utility of the intermetallic. For improving the room temperature ductility and high temperature strength, alloying additions of Cr and Mo have been done [1,11]. In this context, Buchanan and Kim [36] have studied the effect of Cr and Mo additions on the corrosion characteristics of the alloyed Fe_3Al-based iron aluminides. They employed both electrochemical and immersion techniques for this purpose. They used Fe-28Al alloy containing different amount of (0-6 at %) Cr and (0-2 at %) Mo. The medium employed was H_2SO_4 (pH=4) containing 200 ppm chloride ions. They report that in cyclic anodic polarization of these alloys, passivity is exhibited but with a relatively low breakdown potential for pitting corrosion and a protection potential lower than the open free corrosion circuit potential thereby implying the poor re-passivation characteristics of the base Fe_3Al intermetallic. Although Cr addition increased the pitting potential, even with the addition of 6 at % of the same, the protection potential of the alloyed intermetallic was lower than the corrosion potential (Figure 2.5). This indicates that even upto 6 at% Cr addition is not sufficient for good corrosion resistance since pitting can initiate after an incubation period. It was found by them that Mo addition raises the protection potential (Figure 2.6). The combined addition of 1 to 2 at % Mo to 4 at% Cr alloy raises the protection potential above the corrosion potential thereby imparting significant improvement in resistance to initiation of localized corrosion [36]. This same alloy (1-2 at% Mo with 4 at% Cr) on immersion testing remained passivated with no localized corrosion for a period of four months (at which point the tests were terminated).

Buchanan *et al.* [40] have recently reviewed the corrosion behavior of iron aluminides. They have studied iron aluminides having compositions listed in Table 2.5. They report that the

DEDICATED TO MY MOTHER

Sample	Free corrosion potential (mV vs SCE)	Complete passivation potential (mV vs SCE)	Pitting potential (mV vs SCE)	Passivity range (mV)
Fe_3Al	-363	-950	100	1050
Fe_3Al-Cr	-330	-1333	400	1733
Fe_3Al-Ti	-350	-1196	444	1640
Fe_3Al-Mo	-334	-1360	585	1945
Fe_3Al-Ta	-293	-1264	454	1718

Table 2.7 Corrosion characteristics of Fe_3Al-5M and Fe_3Al in H_2SO_4 electrolyte of pH 4 [10].

corrosion rates 2C and 3D in the passive state are both very low.

It can therefore be predicted about the choice of the alloy according to the parameters derived from potentiostatic anodic polarization :

1. i_{corr} should be as low as possible.
2. i_{crit} should be as low as possible.
3. E_{cp} should be as low as possible.
4. E_{pp} should be as low as possible.
5. E_{pit} should be as high as possible.
6. Range of passivity should be as high as possible.

CERTIFICATE

This is to certify that the work contained in the thes
entitled "ELECTROCHEMICAL BEHAVIOR OF Fe_3Al-5M (M = Ti, Zr, V, N
Ta, Cr, Mo ANd W) INTERMETALLICS" has been carried out by
Shalin Astha under my supervision and that it has not be
submitted elsewhere for a degree.

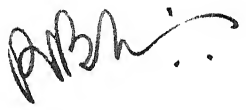

(R.BALASUBRAMANIAM)
Assistant Professor
Department of Materials and Metallurgical Engineering
Indian Institute of Technology
Kanpur 208016

March, 1996

ACKNOWLEDGEMENT

I wish to express my sincere gratitude to Dr R. Balasubramaniam for his continuous guidance and encouragement. I am extremely thankful to him for helping me gain confidence in all my endeavors.

I also express my sincere thanks to Mr Sanjeev Kumar Shukla for making things work for me whenever they got held up.

I am also thankful to Dr M.N.Mangole and all my labmates (Arvind Agarwal, C. Thakur, K.S. Rao and P. Banerjee) for their timely help with many aspects of the experimental program.

My special thanks to my friends Neera, Dheeraj, Moushmi, Piyush, and all the others whose names I missed out for the lack of adequate space.

Last but not the least I want to express my love to my dear brother ABHOY BHAKTWATSALAM who made me feel so much at home during my stay here at I.I.T. Kanpur.

March, 1996 SHALIN ASTHA

3.6.2 X-RAY DIFFRACTION (XRD)

XRD patterns of Fe_3Al and Fe_3Al-M intermetallics were recorded with a Rich-Siefert 2002 X-ray diffractometer using CuK_α radiation. The specimens were in the form of strips in the case of thermomechanically treated intermetallics and as buttons for the un-processed alloyed intermetallics. All the conditions (scanning rate, multiplication factor and voltage) were maintained constant in the XRD experiments. It was found that when the amplification of the diffracted signal was low and when the scan speed was relatively high (3 degree per minute), the small intensity peaks were not resolved. Therefore, the patterns were also obtained keeping the amplification of the pattern high and the scan speed low (1.2 degree per minute) so that the small intensity peaks could be identified.

TABLE OF CONTENTS

Table 4.2

Free Corrosion Potential (E_{corr}) of the Intermetallics in 0.05 mol/l NaOH, without and with 200 ppm chloride ions. All the potentials are in Volt versus SCE.

INTERMETALLIC	Alkaline	Alkaline + Cl^-
Fe_3Al	-0.32	-0.38
Fe_3Al-5Ti	-0.21	-0.28
Fe_3Al-5Zr	-0.45	-0.44
Fe_3Al-5V	-0.44	-0.25
Fe_3Al-5Nb	-0.26	-0.46
Fe_3Al-5Ta	-0.52	-0.48
Fe_3Al-5Cr	-0.46	-0.21
Fe_3Al-5Mo	-0.49	-0.25
Fe_3Al-5W	-0.16	-0.13

from the forward polarization curve (namely at 0.2 V and 0.5 V). Similar to the case of the Fe_3Al-5Ti intermetallic discussed earlier, this intermetallic also pits heavily once the second breakdown potential is attained and a large current density is drawn because of this reason. The passive range is lower on reverse scanning from the noble to active potential. The nature of the curve on reverse scanning indicates the moderate re-passivation characteristics of the Zr-alloyed intermetallic as the reverse scan does not trace the original forward scan in the initial period of the scan and intersects the forward scan only after the ZCP of the forward scan, thereby indicating the poor pitting resistance of the Zr-alloyed intermetallic. Higher currents are drawn during the reversal of scan further indicating the poor pitting resistance of this intermetallic. As noted earlier, the ZCP on reverse scanning occurs at a lower potential than the ZCP on forward scanning.

The potentiodynamic polarization curves (forward and reverse scans) for Fe_3Al-5Zr in the acidic H_2SO_4 solution with 200 ppm chloride ions are presented in Figure 4.10. The polarization curve exhibits active-passive behavior in the forward scan. Similar to the behavior in the solution without chloride ions, the zero current potential (-0.45 V vs SCE) on forward scanning is nearly the same as the stabilized free corrosion potential (-0.46 V vs SCE). Note that the i_{crit} in the chloride containing solution (11.0 mA/cm^2) is lower than that obtained in the earlier case without chloride ions and this is similar to the behavior observed above for the Fe_3Al-5Ti intermetallic. The i_{pass} is slightly lower in the presence of chloride ions (0.03 mA/cm^2) compared to the earlier case without chloride ions (0.4 mA/cm^2). Interestingly, the most striking feature about the passive behavior in the chloride containing solution is that the passive range (0.15 V) in this case is drastically lower than in the earlier case without chlorides (0.7 V). This indicates that the chloride ions destabilize the passive layer on the surface of Fe_3Al-5Ti in acidic solutions and this is supported by the fact that the

ABSTRACT

The polarization behavior of Fe_3Al and Fe_3Al-5M (M=Ti, Zr, V, Nb, Ta, Cr, Mo and W) alloyed iron aluminide intermetallics has been studied by the cyclic potentiodynamic method in 0.05 mol/l H_2SO_4 and 0.1 mol/l NaOH solutions, with and without 200 ppm of chloride ions. The addition of these elements, except V, induced passivity to the base iron aluminide in the acidic medium whereas the base intermetallic exhibited active behavior in the forward scan and passive behavior in the reverse polarization scan. The critical current density for passivation, the passive current density the primary passivation potential and the complete passivation potential for the alloyed intermetallics are lower than the base intermetallic. The breakdown potential and the passive range is higher for the alloyed intermetallics. The variation of these parameters with alloying strongly suggest that passivity is enhanced on alloying. The presence of chloride ions in the acidic solution leads to lowering of the breakdown potential and the passive region.The presence of chloride ions generally results in poorer repassivation behavior and this is due to the destabilizing effect of chloride ions on the passive layer. In the alkaline solution, the polarization behavior of Fe_3Al and Fe_3Al-5M (M=Ti,Ta, Cr and Mo) were similar and they exhibited stable passive behavior in the absence of chloride ions. The polarization behavior of the other intermetallics Fe_3Al-5M (M=Zr, V, Nb, and W) in the alkaline solution are poorly understood. The characterization of the phases that form on alloying the base intermetallic with passivity-inducing elements was performed by x-ray diffraction. The study indicated that Cr and Ti additions dissolve as solid solutions in the base intermetallic whereas additional phases form in the other alloyed intermetallics.

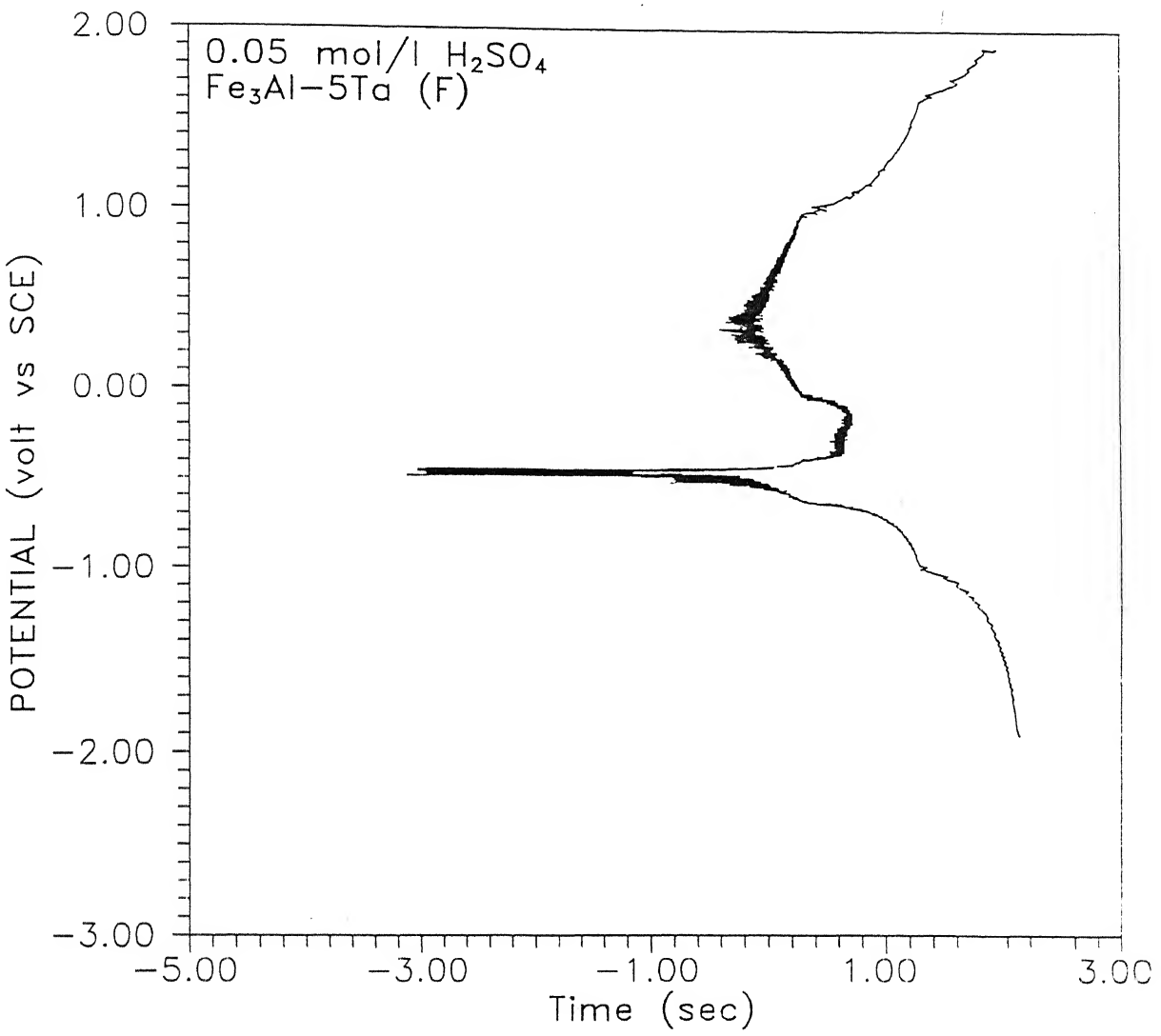

Figure 4.16 **Forward** polarization curve of Fe_3Al-5Ta intermetallic in 0.05 mol/l H_2SO_4.

enhances the passive behavior of the base intermetallic. In an earlier study, the enhanced passivity due to chromium addition was also observed in H_2SO_4 solution of pH 4 [10] and the probable reasons for this behavior has also been elucidated. It is interesting to note that addition of Cr to the base intermetallic also provides sufficient ductilities to the intermetallic [7,10] and the effect of passivity in affecting ductilities has been explained by electrochemical mixed potential theory [8]. Therefore the present study further validates the enhancement in passivity in acidic solutions due to Cr addition.

4.3.8 Fe_3Al-5Mo

The potentiodynamic polarization curve (both forward and reverse scans) for Fe_3Al-5Mo in the acidic H_2SO_4 solution without chloride ions are presented in Figure 4.21. The intermetallic exhibited active-passive behavior in this electrolyte as can be seen from the forward scan and this is in contrast to the active behavior observed earlier for the base Fe_3Al intermetallic. The stabilized FCP for this intermetallic was -0.40 V vs SCE and the ZCP on scanning from the cathodic to the anodic (active to noble) direction is -0.48 V vs SCE. The value of the critical current density for passivation (i_{crit}) is 1.99 mA/cm^2 and this is lower than the i_{crit} of unalloyed Fe_3Al during the reverse scan in the same electrolyte. The passive range extends to about 0.5 V and this is higher than the passive range obtained in unalloyed Fe_3Al in the reverse scan. Two breakdown potentials can be identified from the forward polarization curve (namely at 0.8 V and 1.5 V). Similar to the case of the Fe_3Al-5Cr intermetallic, this intermetallic also pits heavily once the second breakdown potential is attained and a large current density is drawn because of this reason. The passive range is lower on reverse scanning from the noble to active potential. The nature of the curve on reverse scanning indicates the moderate re-passivation characteristics of the Cr-alloyed intermetallic as the reverse scan does not trace the original forward scan in the initial period of the scan and the forward scan is intersected at a much

LIST OF FIGURES

with and without chlorides) for all the intermetallics (Table 4.1). The FCP is also similar in both the electrolytes. Moreover, the ZCP in both the electrolytes is similar for all the intermetallics. The primary passivation and complete passivation potentials for the intermetallics in both the electrolytes have been compiled in Table 4.3. It can be observed that both these potentials decrease with the addition of the passivity inducing element when compared with the same potentials for the base Fe_3Al obtained on the reverse scan. This implies that the addition of these elements would enhance passivity and therefore the additions are beneficial from this point of view. The maximum shift in E_{pp} and E_{cp} is observed for Zr addition with that for Cr addition close behind. Moreover, it can be noted that the effect of chloride ions on these potentials is insignificant for all the intermetallics implying that the presence of chloride ions do not drastically change these parameters.

The passive region breaks down after the first breakdown potential and a large current density is drawn after this process. This break down of passivity was observed in all the cases when active-passive behavior was exhibited and these potentials have been tabulated in Table 4.4 for the intermetallics under study. It can be observed from this table that the breakdown potential of Fe_3Al (obtained on the reverse scan) is increased with the addition of the passivity-inducing elements. The maximum shift in E_{bI} is observed for the Ta-containing intermetallic in the solution without chloride and for the Mo-containing intermetallic in the solution containing chloride. The general behavior again implies that the addition of the passivity-inducing elements are beneficial in enhancing the passivity of the base intermetallic. The second observation that can be made from the table is that the breakdown potential decreases in the presence of chloride ions thereby indicating that chloride ions destabilize the passive layer at a lower value of potential compared to the case without chloride ion presence. This behavior is expected as chloride ions are known to destabilize passive layers on the surfaces of

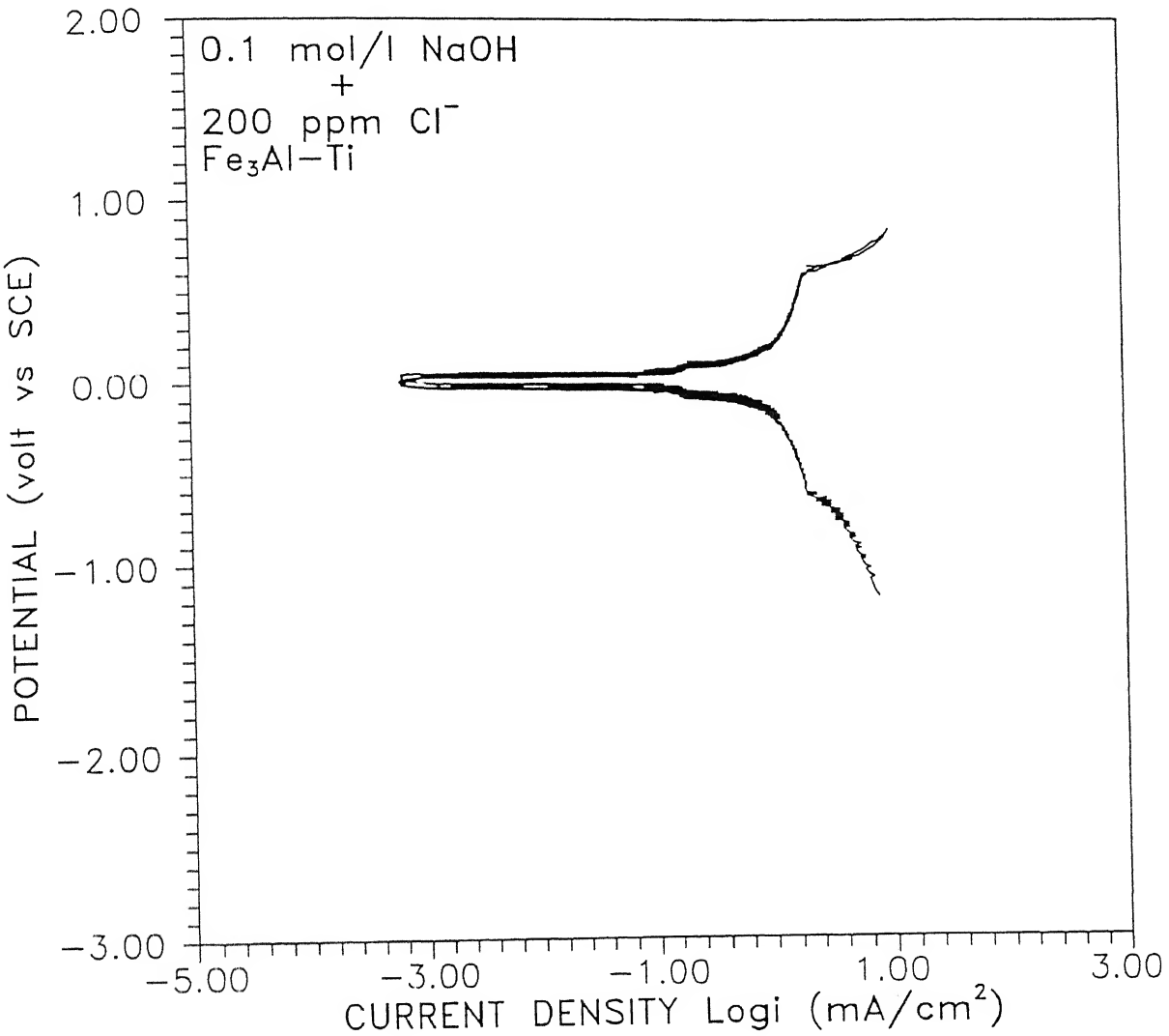

Figure 4.28 Forward polarization curve of Fe_3Al-5Ti intermetallic in 0.1 mol/l NaOH with 200 ppm Cl^-.

Table 4.7

Passive Range of the Intermetallics in 0.1 mol/l NaOH, without and with 200 ppm chloride ions.

INTERMETALLIC	RANGE (V)
Fe_3Al	0.3
Fe_3Al-5Ti	0.3
Fe_3Al-5Ta	0.8
Fe_3Al-5Cr	0.3
Fe_3Al-5Mo	0.5

LIST OF TABLES

APPENDICES

Appendix A X-RAY DIFFRACTION PATTERNS OF THE BASE AND ALLOYED INTERMETALLICS

Appendix B ANALYSIS OF X-RAY DIFFRACTION PATTERNS OF THE BASE AND ALLOYED INTERMETALLICS.

TABLE B8

Analysis of XRD pattern of intermetallic Fe_3Al-5Cr thermomechanically processed at 1000°C.

2θ ($Cr_{k\alpha}$) (deg)	d Obs (Å)	d Theor (Å)	Int Obs (%)	Int Theor (%)	plane (hkl)	phase
32.4	4.10					
34.3	3.88					
35.0	3.81					
36.4	3.68					
46.6	2.90	2.89	20	50	(200)	Fe_3Al
54.1	2.52					
58.2	2.36					
68.0	2.05	2.04	100	100	(220)	Fe_3Al
78.3	1.81					
85.3	1.69	1.67	8	10	(222)	Fe_3Al
104.0	1.45	1.45	76	80	(400)	Fe_3Al

CHAPTER 1

INTRODUCTION

1.1 ALLOY DEVELOPMENT OF IRON ALUMINIDES

The iron rich Fe_3Al-based intermetallics are highly oxidation resistant (due to the formation of protective alumina scale) and have excellent sulphidation and carburization resistance. They are therefore considered as candidate materials for elevated temperature applications especially in sulphur containing energy conversion systems. Compared to stainless steels, the principal advantages of Fe_3Al-based intermetallics are : the low cost of iron and aluminum, lower density, adequate strength at low temperatures, and reduced consumption of strategic elements such as chromium. Iron aluminides are therefore candidate materials to replace stainless steels in structural parts for many industrial applications.

The major obstacle to their widespread use is their lack of ductility and brittle fracture at ambient temperatures and a rapid drop of strength and poor creep resistance at high temperatures.

The major cause for their poor ambient temperature ductility is moisture-induced hydrogen embrittlement (HE) [1-6]. Iron aluminides exhibit low ductilities in environments containing hydrogen. It is interesting to note that higher ductilities are observed in a dry oxygen environment rather than in vacuum because oxygen reacts with aluminum to form Al_2O_3 directly [7] as given by

$$2Al + 3/2\ O_2 = Al_2O_3 \qquad (1.1)$$

and thereby suppressing the aluminum-moisture reaction which provides nascent hydrogen as per the reaction

$$2Al + 3H_2O = Al_2O_3 + 6H \qquad (1.2)$$

Generation of atomic hydrogen is suppressed and thus higher ductility is observed in dry oxygen environment. The nascent hydrogen of reaction (1.2) embrittles iron aluminides. The propensity of the above reaction increases with increasing

aluminum concentration in iron aluminides [1]. The reaction of condensed moisture from ambient environments with aluminum at crack tips and freshly created metal surfaces (due to oxide spallation) results in the generation of high fugacity atomic hydrogen that causes severe embrittlement.

The hydrogen embrittlement can be minimized by several approaches. Most important among them is chromium additions to the base Fe_3Al intermetallic [7]. The role of chromium in enhancing room temperature ductilities has been elucidated recently from an electrochemical viewpoint [8]. According to this theory, Cr induces passivity in iron aluminides and hydrogen liberation rates are lowered on freshly created surfaces of Cr-alloyed iron aluminides [8]. It has also been proposed that Cr provides a surface layer that decreases hydrogen diffusion into the material [1].

Based on the effect of chromium in minimizing HE in iron aluminides, an alloy development philosophy has been proposed [8] according to which optimum additions of passivity-inducing elements like Ni, Mo, W, V, Nb, Ta, Si, Ti and Zr, apart from Cr, would increase ductility of iron aluminides by inducing passivity. Some of the recently developed iron aluminides that show enhanced ductilities contain some of these elements [1-3] and passivity may be indirectly responsible for this. It has also been recently shown that addition of small amount of cerium enhances the ductile of Cr-alloyed Fe_3Al [9], reasons for which are not clearly known at present. Therefore, the development of ductile iron aluminides is still in its infancy and active research is conducted by several groups in order to ductilize iron aluminides.

1.2 OBJECTIVE OF STUDY

Addition of passivity-inducing elements should ideally result in enhanced ductilities, assuming that there is no additional ternary brittle intermetallic formation which would result in low ductilities. Ternary additions of passivity-inducing elements (Ni, Cr, Mo, Ta, Ti, Nb, Zr, W, V and Si) have been alloyed to iron

aluminides of composition Fe_3Al, so as to produce alloyed intermetallics of type Fe_3Al-5M. The addition were made for modifying mechanical properties, mainly ductility at ambient temperatures. The thermomechanical and mechanical behaviors of these alloyed intermetallics has been previously studied [10]. The electrochemical behavior of these intermetallics has also been studied in H_2SO_4 solution of pH 4 and NaOH solution of pH 9 and the effect of chloride ions on the behavior has also been addressed [10]. It was seen that all the intermetallics exhibited stable passivity in both the solutions and therefore the passivation behavior of the intermetallics needed to be studied in more concentrated acidic and alkaline media. The present investigation aims at the study of the electrochemical behavior of Fe_3Al intermetallics in alkaline and acidic media with the use of cyclic potentiodynamic polarization technique. The effect of chloride ions on the electrochemical behavior is also to be studied. The secondary aim of the present work is to structurally characterize the alloyed intermetallics by x-ray diffraction and scanning electron microscopy.

1.3 PLAN OF WORK

The following plan of work was adopted for the thesis:

(a) Preparation of iron aluminides alloyed with Cr, Mo, Ti, Ta, Nb, Zr, V, W and Si.

(b) Characterization of alloyed intermetallics using characterization techniques like electron probe micro analysis, scanning electron microscopy and x-ray diffraction analysis.

(c) Cyclic potentiodynamic polarization studies of these alloys in acid (0.05 mol/l H_2SO_4) and alkaline (0.1 mol/l NaOH) media, with and without chloride ions.

CHAPTER 2

LITERATURE REVIEW

2.1 IRON ALUMINIDES

Iron aluminides have very low density, of the order of 5.4-6.7 gcm^{-3} which is about 30% lower than that of commercial high temperature structural materials such as stainless steels and superalloys. They, therefore, offer better strength to weight ratios compared to most of the high temperature materials. The following sections would provide a brief review of the literature of various characteristics of iron aluminides.

2.1.1. Fe-Al Phase Diagram

In order to obtain a better understanding of the mechanical behavior and properties of iron aluminides, it is imperative to discuss the Fe-Al phase diagram that which is presented in Figure 2.1 [11]. It can be seen from the phase diagram at very low Al contents, the α-Fe is stable which is a disordered phase. With increasing Al contents, ordering of Al atoms around Fe atoms leads to the formation of the imperfectly ordered B2 structure (which is the structure of α2 phase shown in the phase diagram). The B2 structure can also be visualized as a BCC structure with Fe at its centre and Al at corners and vice versa (Figure 2.2). The stoichiometric intermetallic FeAl possesses the ordered cubic B2 structure in the range 30-50 at% Al. The stoichiometric Fe_3Al can exist in different forms depending upon the temperature. It exists as an ordered phase at low temperature and as disordered/partially disordered phases at high temperature. Fe_3Al transforms from the DO_3 crystal structure (Figure 2.3) to a defective ordered cubic B2 crystal structure at temperatures above the critical ordering temperature T_c of ~ 814 K. Notice that as the amount of Al in Fe-Al alloys increases, its melting temperature decreases. Therefore, Fe_3Al has a reasonably high melting temperature.

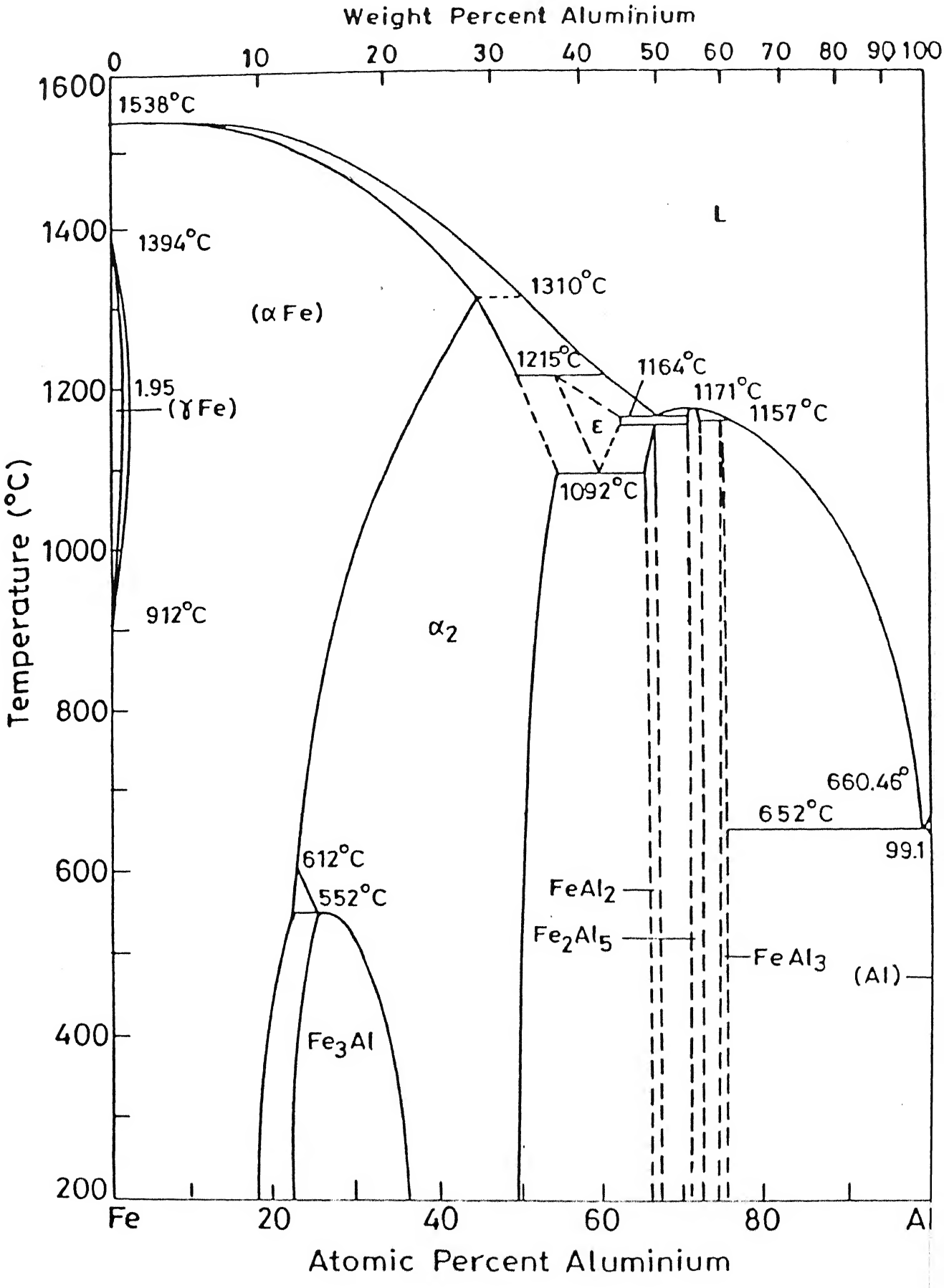
Weight Percent Aluminium
0
10
20
30
40
50
60
70
80
90
100
1600
1400
1200
1000
800
600
400
200
Temperature (°C)
1538°C
1394°C
1.95
(γ Fe)
912°C
(α Fe)
1310°C
1215°C
1164°C
1171°C
1157°C
ε
1092°C
L
α2
660.46°
652°C
99.1
612°C
552°C
FeAl2
Fe2Al5
FeAl3
(Al)
Fe3Al
Fe
20
40
60
80
Al
Atomic Percent Aluminium

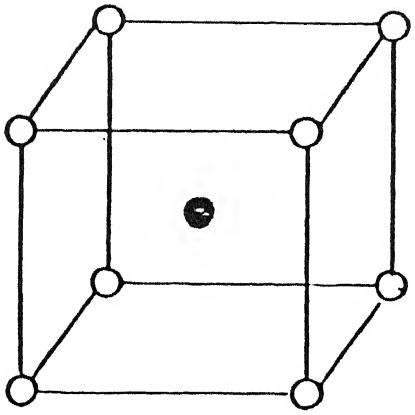

Figure 2.2 The B2 ordered crystal structure of iron aluminide.

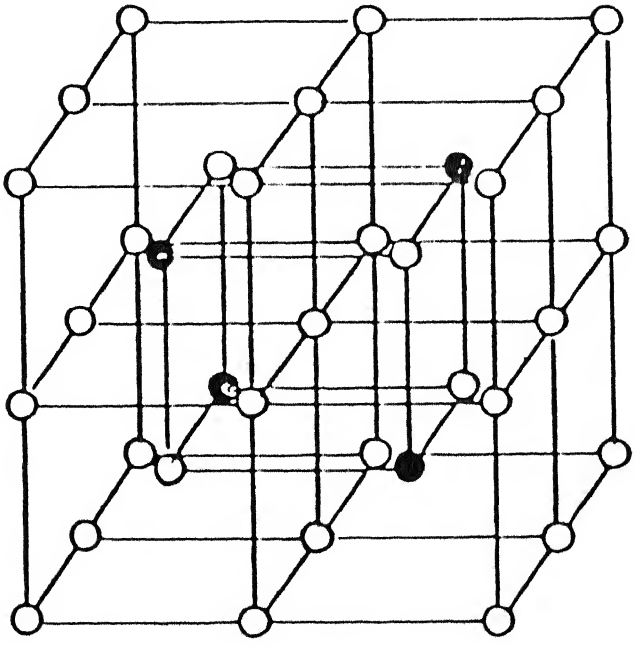

Figure 2.3 The DO_3 ordered crystal structure of iron aluminide.

Apart from these phases which are of technological importance, the other intermetallic phases that exist in the Fe-Al system are $FeAl_2$, $FeAl_3$ and Fe_2Al_5.

2.1.2 Microstructural Characteristics

Iron aluminides have complex point defect structures, consisting of antistructure (substitutional) atoms, vacancies or both [12-15]. The vacancies play an important role in the mechanical deformation because of the importance of defect hardening at low temperatures and of diffusion processes at high temperatures [16].

In view of the inadequate strengths of the binary alloys at temperatures of interest, ternary additions have been affected to modify properties by introducing point defects. Furthermore, the ordering temperature T_c of Fe_3Al should be high for increased high temperature strength [17]. Ternary additions are therefore also added for significantly increasing T_c. Additions ranging from 3 to 10 % Ti, Cr, Mn, Ni, Mo and Si to Fe_3Al raise T_c [18-20]. Ti and Si additions increase T_c significantly [19]. Si atoms substitute at the Al sublattice sites and result in an increase in T_c with increasing Si content. Ti substitutes at specific Fe sites and T_c increases [19].

Alloying additions change the microstructure of iron aluminides in three different ways, viz, by going into solid solution, by causing the precipitation of ternary intermetallic compounds due to the limited solubility and thirdly by exhibiting limited solubility without precipitation of ternary compounds. Addition of 1, 2 or 4 at% Ti, Cr, V or Ni and addition of 1 or 2 at% Nb, Mo, Ta, W or Si all produce significant solid solution strengthening at 873 and 973K [19]. Addition of 1 to 5 at% Mn and Co result in the additions going into solid solution. Iron aluminides with 1 to 5 at % Cr, Ti, Mn and Co exhibit a single phase microstructure [18-20]. Moreover, Cr also refines the grain size [21]. The grain size of Fe_3Al with about 5 at% Cr is quite fine and equiaxed.

Addition of 0.8 to 5 at% B, Zr, Ta, Nb, Re and Hf additions result in solid solution strengthening and precipitation of ternary intermetallic compounds due to their limited solubility [18-20]. It has been reported that 2 at% Nb addition to iron aluminides (Fe-25Al-2Nb) results in the precipitation of coherent precipitates of Fe_2Nb [19]. These precipitates are thermally unstable. Therefore such alloyed iron aluminides are unsuitable for long-term elevated-temperature applications. In case of TiB_2, Hf and Zr additions, TiB_2, Hf-rich and Zr-rich particles refine the grain size to 1μm and produce a high density of subgrains and a fine dispersion of incoherent particles [19,22]. Moreover, small amounts of ZrB_2 produce a fairly stable fine microstructure [22].

W and Mo have very limited solubilities and no ternary compound formation have been reported yet in iron aluminides alloyed with W and Mo [11].

2.1.3 MECHANICAL PROPERTIES

The following discussion focuses briefly on the mechanical properties of iron aluminides. The typical room temperature properties of base iron aluminides are given in Table 2.1. The tensile properties that are of great importance are ductility, yield strength and ultimate tensile strength.

Ductility (or % elongation) of iron aluminides is low at room temperature. The effect of environment on room temperature ductility (Table 2.2) shows that whenever there is atomic or molecular hydrogen present in the atmosphere the ductility is very low due to hydrogen embrittlement [5,23]. At temperature upto 400°C, the ductility shows a general trend of decreasing with increasing aluminium level [2]. At higher temperatures, the alloys exhibit a maximum ductilities around 35-38 at % Al. The decrease in tensile elongation of the alloys with higher aluminium concentration is due to grain boundary cavitation during deformation at elevated temperatures. Smaller grain size improve ductility [24]. Increasing the annealing temperature increases the ductility when only some recrystalization is evident at the

Alloy	Crystal Structure	Temp. (^{o}C)		Density (gm/cc)	Room Temp. Y.Strength (MPa)	Room Temp Elongatic (%)
		order -ing	M.P.			
Fe_3Al	DO_3	540	1540	6.72	300	3.7
Fe_3Al	B2	760	1540	6.72	380	4.1
FeAl	B2	1250	1250	5.56	360	2.2

Table 2.1 Typical room temperature properties of iro aluminides.

Environment	Yield Strength (MPa)	UTS (MPa)	Ductility (%)
	Heat Treated for 2 hr at 700°C (B2 Structure)		
Vacuum	387	851	12.8
Oxygen	392	867	12.0
Ar + 4% H_2	385	371	8.4
Air	387	559	4.1
H_2O vapour	387	475	2.1
	Heat Treated for 120 hr at 500°C(DO_3 Structure)		
Vacuum	316	813	12.4
Oxygen	298	888	11.7
Air	279	514	3.7
H_2O vapour	322	439	2.1

Table 2.2 Room temperature tensile properties of Fe_3Al in different test environments [37].

surface of the specimen (Table 2.3). Increasing the degree of recrystalization resulted in a decrease in tensile ductility [25]. The completely recrytallized microstructures produced the least desirable properties (Table 2.4). Therefore, a partially recrystallized microstructure is desired minimizing HE and obtain higher ductilities [25].

Cr addition increases the ductilities from less than 4% in the base Fe_3Al intermetallic to 8.2-9.4 % in the intermetallics with 2-6 % Cr [26]. By furnace cooling from 850°C to 500°C the % elongation of Fe-28%Al-4%Cr can be increased upto 13% [26]. Boron addition increases ductility by alleviating intrinsic brittleness [24,27,28]. Mn additions also improve ductility [29]. Recently it has been shown that microalloying with Ce increases ductility at ambient temperatures [9]. Finally, based on the passivity alloy development philosophy [8], the intermetallics that are alloyed with Cr and Ti in Fe_3Al show enhanced ductilities compared to base Fe Al [10].
3

Yield strength of alloys near the Fe_3Al composition increases with temperature above 673 K to a peak value just below T_c [11,30]. These alloys are age hardenable above 673 K owing to precipitation of α from ordered DO_3. Consequently, the yield strength of DO_3 increases with temperature since the kinetics of age hardening increases with temperature [31-33]. The yield peaks were caused by a combination of α and B2 precipitation [31-33]. Yield strength drops rapidly with increasing temperatures at about T_c [11]. Therefore, the low T_c adversely affects high temperature strength of iron aluminides due to transition from DO_3 to the more simply ordered B2 phase formed at high temperature. Low annealing temperature also decreases yield strength [25]. Increasing the annealing time decreases the yield strength. The yield strength is insensitive to test environment [23]. Iron aluminides show a general increase in yield strength with aluminium at temperatures upto 400°C. The strength becomes insensitive to the aluminium concentration at 600°C and generally decreases with aluminium content at 700°C [2]. Increasing strain rate increases yield

Structure	Temperature (°C)	Elongation (%)	Strength (MPa)	
			Yield	Ultimate
DO_3 Procedure	--	8.4	227.54	517.13
B_2	700	19.28	523.81	1038.39
B_2	750	16.74	465.34	936.27
B_2	800	11.24	392.26	723.08
B_2	900	11.64	351.16	695.02

Table 2.3 Effect of annealing temperature on tensile properties [25].

Heat treatment[b] (h/°C)	Fraction recrystallized (%) (grain size, μm)	Yield stress (MPa)	Fracture stress (MPa)	Elongat (%)
1/550	0	550	760	5.4
1/650	0	543	807	8.1
1/750	10	479	736	8.0
1/850	20	453	670	6.4
1/1000	100 (41)	280	413	3.0
1/1100	100 (68)	279	450	4.0
0.5/750	<5	481	736	8.2
1/750	10	466	710	7.8
4/750	25	438	665	7.8
24/750	50 (20-30)	369	577	5.2
48/750	80 (20-60)	328	492	4.4
0.17/1000	100 (34)	288	439	3.6
0.5/1000	100 (36)	287	425	3.0
1/1000	100 (43)	274	436	3.2
4/1000	100 (45)	277	422	3.0

[a]Alloy composition, Fe-28Al-5Cr-0.1Zr-0.05B (at.%).
[b]All alloys were heat treated 1 h at 700°C before punching test specimens. After the recrystallization heat treatment, all specimens were annealed for 3 d at 500°C to establish DO_3 order.

Table 2.4 Effect of recrystallization on room temperature tensile properties [25].

strength [29]. The grain size dependence of yield strength of iron aluminides with various aluminium concentration follows the standard Hall-Petch equation [11]. Increasing the degree of recrystalization decreases yield strength and completely recrytallized microstructures produces the least desirable properties.

Yield strength of up to 4 at % Cr addition ranges between 256 and 192 MPa. The yield strength decreases on Cr addition because of solid solution softening (easy movement of dislocations) effect produced by chromium [7]. Similarly upto 2 at % Mn addition increases yield strength because of solid solution strengthening [11]. Microalloying with Ce enhances yield strengths at ambient temperatures [9]. At a high temperature of 600 ^{o}C, the combined addition of Ce with Mo, Zr or Nb also increases yield strength [9].

The ultimate tensile strength (UTS) is generally correlated with tensile ductility and it increases with decreasing temperature [23]. Temperature rise therefore increases UTS. If the environmental embrittlement does not occur, then the UTS is higher in that condition [23]. Increasing Al content increases UTS upto 400^{o}C [2]. Above this temperature, Al contents do not affect UTS upto 600^{o}C. However, UTS generally decreases with Al percentage after 700^{o}C [2]. Addition of some alloying elements that increase ductility (like Cr [26], Ce [9], Mn [29]) also increases UTS.

2.2. HYDROGEN EMBRITTLEMENT OF IRON ALUMINIDES

A major drawback of iron aluminides is their poor ductility and low fracture toughness at ambient temperatures. It is established that poor room temperature ductility in iron aluminides is due to hydrogen embrittlement [1-6].

The mechanism of hydrogen embrittlement is also known. The environmental embrittlement essentially occurs due to the following reaction:

$$2Al + 3H_2O = Al_2O_3 + 6H \qquad (2.2)$$

The reaction of moisture in air with Al at crack tips results in the generation of high fugacity atomic hydrogen that rapidly penetrates into the crack tips and causes severe embrittlement. The very low ductility in H_2O vapour, air and in hydrogen containing environments [5,23] stablishes the validity of the above explanation. The maximum degree of moisture-induced hydrogen embrittlement occurs around ambient temperatures. At higher temperatures less hydrogen is concentrated at crack tips, and in-situ protective oxide film can form more rapidly on specimen surfaces. At lower temperatures, the rate of the Al-moisture reaction is lowered, and the equilibrium moisture in air also is lowered. The highest ductility is generally obtained in a dry O_2 atmosphere (rather than in vacuum) because O_2 reacts with the aluminium oxide directly, thereby suppressing the aluminium-moisture reaction and the generation of atomic hydrogen as in Equation (1.2).

There is no single mechanism which has been fully accepted in understanding the mechanism of hydrogen embrittlement in iron aluminides.

Birbaum *et al.* have proposed a mechanism known as hydrogen enhanced localized plasticity (HELP) [34]. This mechanism suggests that hydrogen increases plasticity at the crack tip in many metals and alloys, leading to brittle fracture. There is a controversy about this mechanism that whether hydrogen induces plasticity through the volume or the surface. But there are enough evidences to prove slip localization due to hydrogen near a crack tip in several fcc and bcc metals [34]. Another mechanism of embrittlement is one in which hydrogen facilitates dislocation motion. This increased dislocation mobility throughout the lattice increases the crack growth rate and hence brittle fracture occurs.

Generally, the fracture appearance in this class of intermetallics is of the cleavage type, with facets of {100} type suggesting "decohesion" as the possible mechanism of hydrogen embrittlement. Evidence for decohesion mechanism is based upon the

brittle appearance of fracture surface and the propensity for cleavage on {001} planes in embrittled single crystals of intermetallic aluminides [9] and iron aluminides [35]. Moreover, the brittle appearance of hydrogen induced (or moisture induced) fatigue cracks in iron aluminides alloys also suggests decohesion as the likely mechanism of hydrogen embrittlement [1].

The environmental sensitivity of iron aluminides is markedly reduced when the Al concentration is higher than 38 at % [3,4]. This is because they are intrinsically brittle in these compositions.

Microalloying with boron alleviates intrinsic brittleness in iron aluminides [27,28]. Boron tends to segregate to the grain

boundaries and enhances their cohesive strength. As referred to in the first chapter, Cr addition prevents HE [26,35,38] possibly by modifying the surface protective oxide such that the hydrogen liberation rates are lowered, thereby reducing the environmental brittlement. Interestingly, Cr additions as low as 2 % can induce sufficient ductilities [26,35,38] and passivity to iron aluminides [36]. Optimum addition of Ni, Mo, W, V, Nb, Ta, Si, Ti, Zr and Al should also reduce HE by inducing passivity [8]. The effect of passive layer on the HE of iron aluminides has been recently reviewed [37]. Morever, the iron aluminides are strain rate sensitive indicating the role of hydrogen in their embritllement [38].

2.3 ELECTROCHEMICAL CHARACTERISTICS

Ordered intermetallics are primarily intended for high temperature service. They may also be advantageous for applications where ambient-temperature aqueous corrosion resistance is also of importance. The Fe_3Al-type iron aluminides are of interest for many years because of their potential oxidation and corrosion properties at relatively low cost. Their relatively lower corrosion/oxidation rates compared to stainless steels and Ni-Cr alloys (including coating materials) is borne out by Figure 2.4. Note that the oxidation was monitored in a severe sulfidizing environment at $800^{O}C$ [1].

There have been only a few published studies on the corrosion behavior of iron aluminides. Janavicus and Payer have shown that iron aluminide FeAl corrodes in NaOH solution with aluminium preferentially dissolving from the surface of the aluminide, thereby resulting in the formation of an iron-rich surface layer (iron oxide) which passivates the alloy [39]. They have also observed that related the corrosion behavior of iron aluminide FeAl is directly related to the corrosion behavior of pure iron and aluminium in NaOH and Na_2SO_4 electrolytes of pH 10, 6 and 4. In the NaOH solution of pH 10, the aluminide is passive and corrodes in a uniform manner. In the 1N Na_2SO_4 solution, the

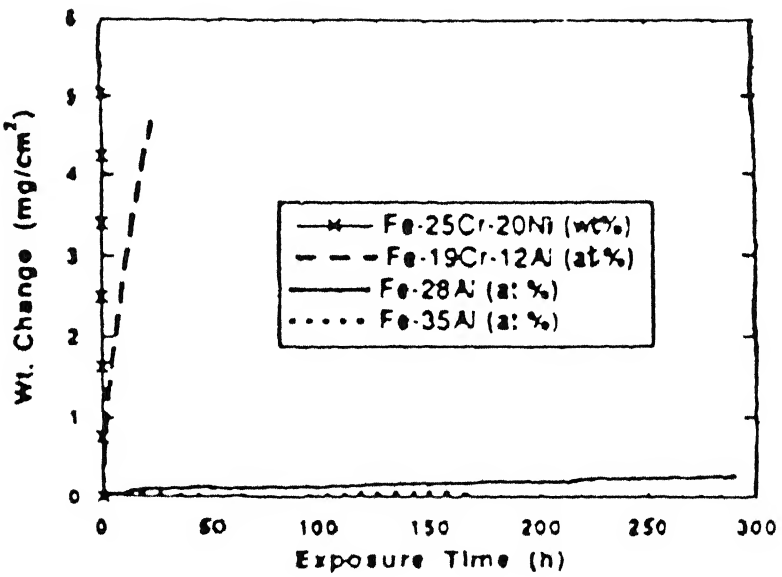

Figure 2.4 Weight gain curves for Fe based alloys and other high temperature alloys in sulfidizing environment at high temperature [1].

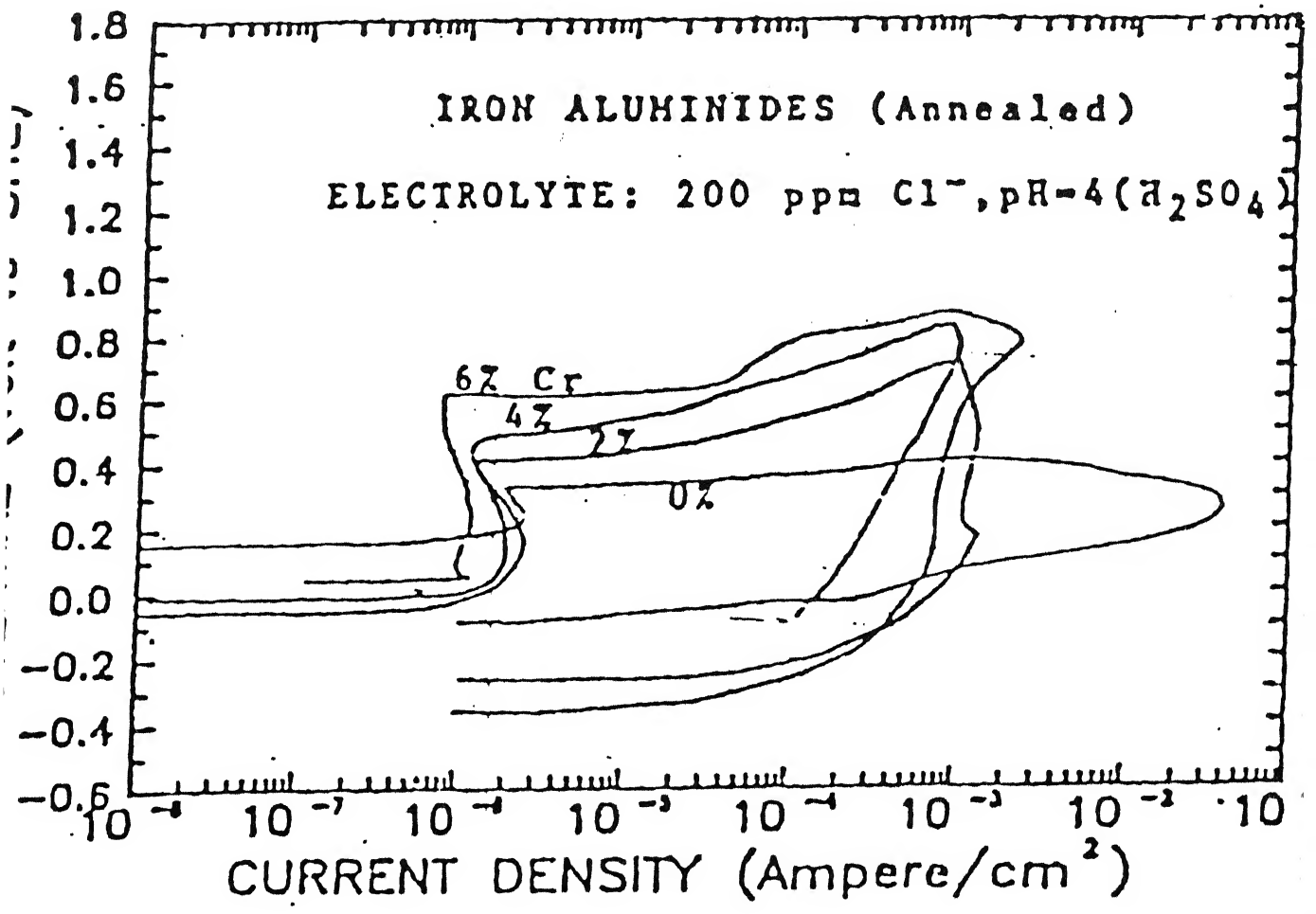

Figure 2.5 Cyclic anodic polarization behavior of iron aluminide in aqueous H_2SO_4 solution of pH 4 with 200 ppm Cl^- [40].

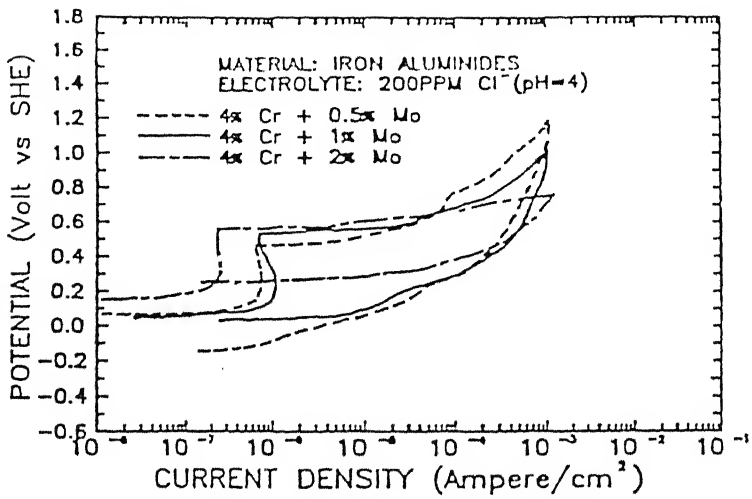

Figure 4. Effects of Mo on the Cyclic Anodic Polarization Behavior of 4% Cr Iron Aluminide.

Figure 2.6 Effect of Mo on the cyclic anodic polarization behavior of Fe-28Al-4Cr in aqueous H_2SO_4 solution of pH 4 containing 200 ppm Cl^- [40].

Alloy	Al	Cr	Mo	Nb	Zr	Y	C	B	Fe
FA-84	28	2	—	—	—	—	—	0.05	bal
FA-129	28	5	—	0.5	—	—	0.2	—	bal
FAL-Mo	28	5	1	—	0.08	—	—	0.04	bal
FAP-Y	16.1	5.4	1.1	—	0.1	0.06	0.1	—	bal
CM-Mo	15.8	4.9	1.6	—	0.15	0.06	0.05	—	bal

Table 2.5 Designations and chemical compositions of iron aluminides (in at %) developed by Oak Ridge National Laboratory, Oak Ridge, USA.

e_3Al base iron aluminides show excellent resistance to uniform queous corrosion in basic (sodium hydroxide) and neutral chloride olutions. They are susceptible to localized pitting/crevice orrosion in chloride solutions, but alloys containing both Cr and lo are relatively better having higher resistance to localized ttack, nearly of the order of that of 304L stainless steel. The lloys corrode rapidly in acid environments (hydrochloric, ulfuric and nitric acids) [40]. In sulphur-bearing thiosulphate nd tetrathionate solutions, the FA-84 and FA-129 corrode rapidly. he Cr and Mo containing FAL-Mo passivate with significantly lower orrosion rates. The iron aluminides are susceptible to hydrogen mbrittlement through interactions with water vapour in air or ater in aqueous solutions. However, slow-strain-rate tests for Cr ontaining iron aluminides in a mild acid-chloride solution ndicate that the embrittlement is not enhanced by the aqueous olution over that observed in air of normal humidity [40]. Low Al lloys (16 at% Al) containing Cr and Mo are comparable in queous-corrosion properties to the Fe_3Al-based iron aluminides. lso, their ductilities during slow-strain rate testing in an queous solution are significantly higher than that of the Fe_3Al-based alloys.

The experiments previously conducted in our laboratory on Fe_3Al were performed in pH 1.5, 4 (H_2SO_4) and 8 and 12 (NaOH) solutions, with and without chloride additions [41]. Experiments were also conducted on Fe_3Al-5M (M=Cr, Mo, Ta, Ti) intermetallics in pH 1.5, 4 (H_2SO_4) and 8 and 12 (NaOH) solutions, with and without chloride additions [10]. The base iron aluminide exhibited passive behavior in pH 4, 8 and 12. It exhibited active behavior in electrolyte of pH 1.4. In electrolyte of pH 1.5, it exhibited passivity, with the presence of cathodic loops. The corrosion characteristics of Fe_3Al is better (where also the passivity range is larger) in electrolyte of pH 8 than in that of pH 4. The corrosion behavior of Fe_3Al is better than stainless steel in electrolyte of pH 8. But in the presence of chlorides, the passivation behavior and pitting resistance of stainless steel is

Sample	Free corrosion potential (mV vs SCE)	Complete passivation potential (mV vs SCE)	Pitting potential (mV vs SCE)	Passivity range (mV)
Fe_3Al	-272	-750	850	1600
Fe_3Al-Cr	-180	-1381	634	2015
Fe_3Al-Ti	-180	-1357	664	2021
Fe_3Al-Mo	-187	-1435	690	2125
Fe_3Al-Ta	-141	-1480	700	2180

Table 2.6 Corrosion characteristics of Fe_3Al-5M and Fe_3Al in NaOH electrolyte of pH 8 [10].

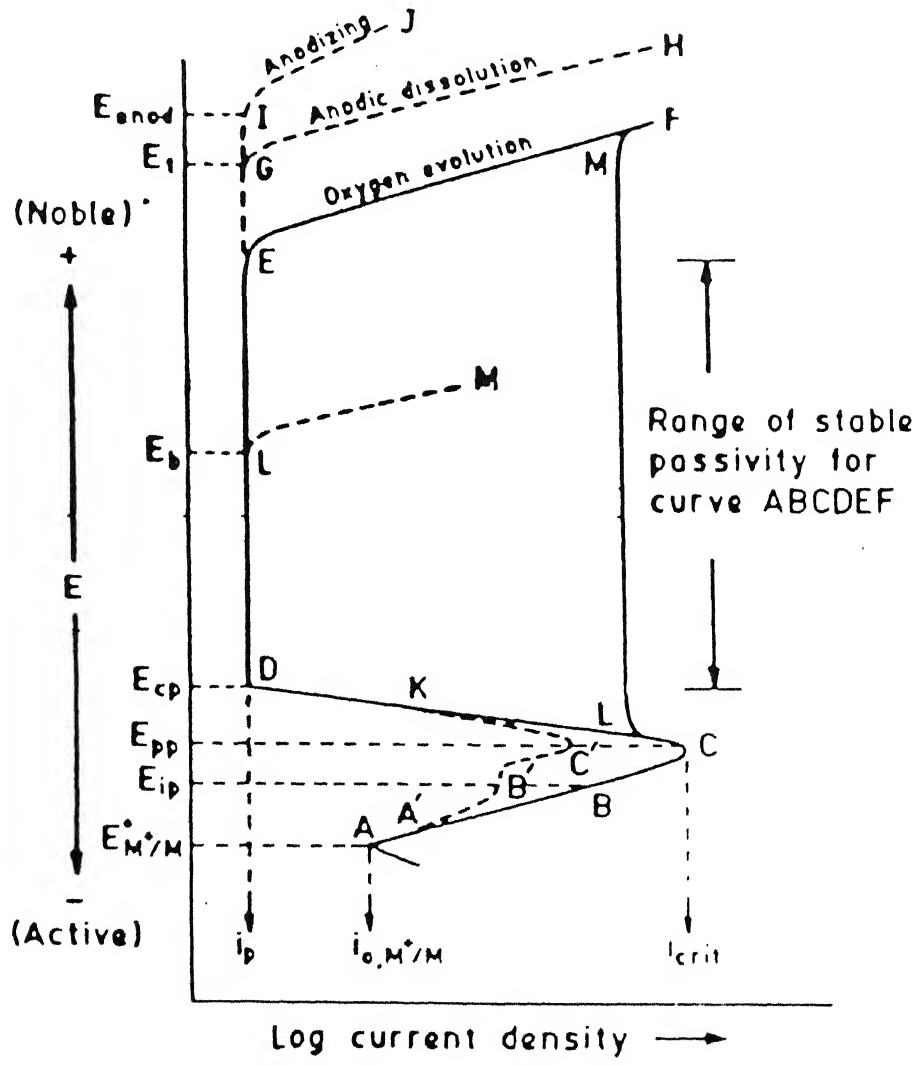

Figure 2.7 Anodic polarization curve of metal exhibiting passivity.

At potential E_{pp}, the rate of protective film growth already exceeds the rate of its chemical dissolution and the process of protective film formation begins.

D - at potential E_{cp} where formation of continuous protective film is completed and complete passivation is obtained.

DE - metal dissolution occurs at a constant rate through the passivating oxide film.

E - end of passivity range and beginning of transpassivity.

2.5.1 EXPERIMENTAL POLARIZATION CURVES

The experimental polarization curves can be understood based on the theoretical anodic and cathodic polarization curves [42]. Material will passivate spontaneously when theoretical cathodic polarization curve intersects the theoretical anodic polarization curve at passive region only as shown in Figure 2.8. This is the condition, when specimen passivates easily on immersion in the electrolyte. This situation is most desirable for material construction.

The experimental polarization curve shows a typical peak shaped curve, as shown in Figure 2.9, when theoretical cathodic curve intersects the anodic curve in the active region. Metals exhibiting this behavior corrode under given environment conditions. but they can be protected by application of anodic protection.

The experimental anodic polarization curve can also exhibit a cathodic current loop after the peak-shaped active to passive transition, as shown in Figure 2.10. This results when the cathodic curve intersects the theoretical anodic polarization curve in each of the active, partially passive and passive region. Metals exhibit either high corrosion rates or low corrosion rates, and are undesirable since a surface supposed to be passive is rendered active by even a slight damage to the passive film. Once the surface becomes active it may not passivate again and corrosion can proceed to complete destruction of the material.

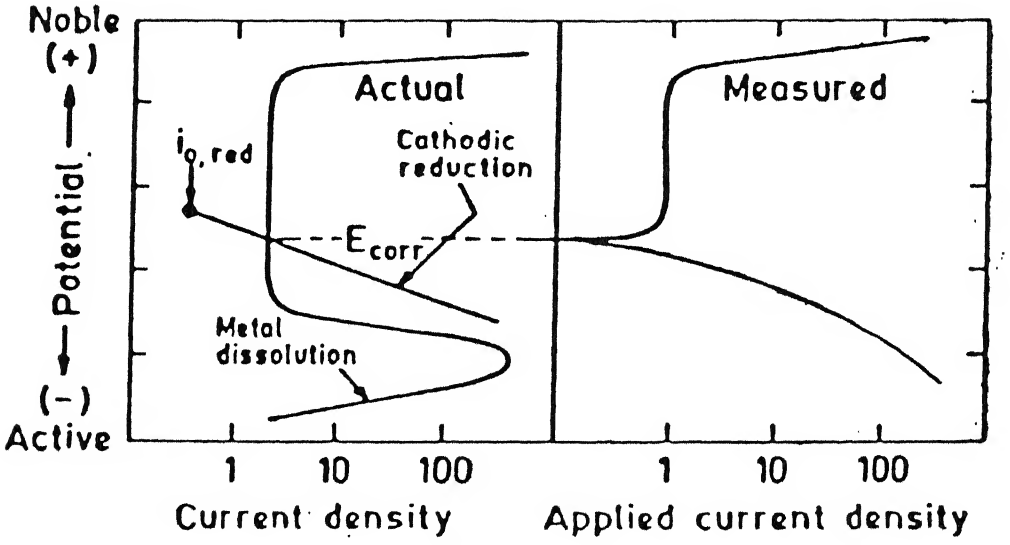

Figure 2.8 Theoretical and measured anodic polarization curves of a metal exhibiting passivity when passive state is stable.

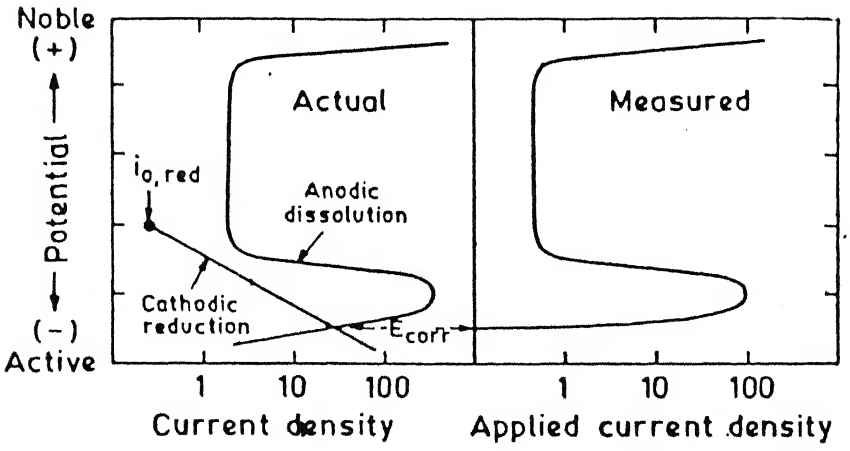

Figure 2.9 Theoretical and measured anodic polarization curves of a metal exhibiting passivity when only active state is stable.

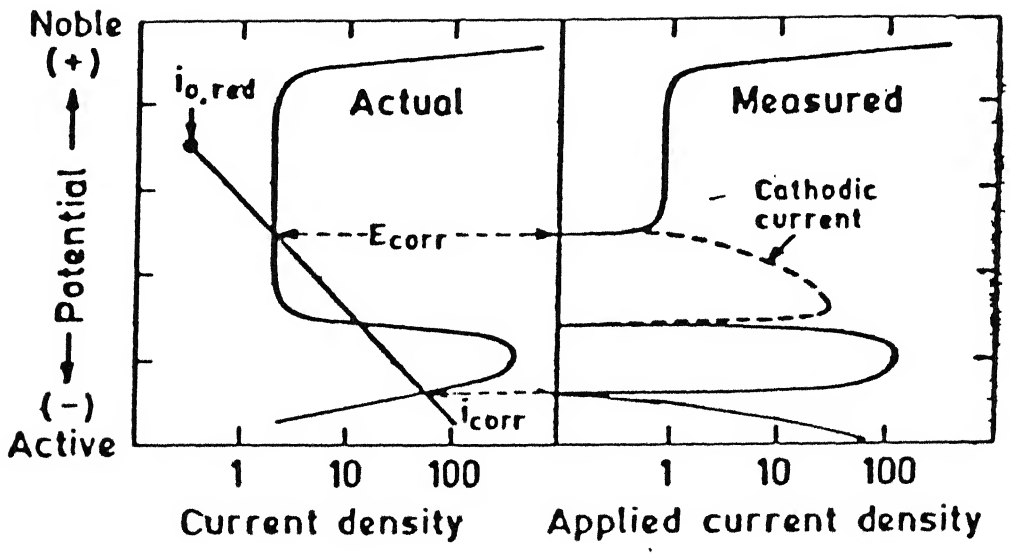

Figure 2.10 Theoretical and measured anodic polarization curves of a metal exhibiting passivity when both active and passive states are stable.

2.5.2. CRITERION FOR SELECTION OF ACTIVE-PASSIVE METALS

Potentiostatic/dynamic anodic polarization is a widely used method to compare the corrosion resistance of different metals and alloys in a specific environment [43]. A schematic representation of various comparing parameters is given in Figure 2.11 and a schematic comparison of the hypothetical alloys is given in Figure 2.12. For reducing conditions, as in number 1, either the non-passivating alloy A or the partially passivating alloy B is superior to the other two because A and B have lower corrosion rates (or current densities, $i_{corr,1A}$ and $i_{corr,1B}$) in the active condition without oxidizers. The alloying elements, for example chromium, needed to produce strong passivity make C and D far more expensive and thus unjustifiable for service in condition 1.

For moderately oxidizing conditions, number 2, the recommended alloy would be C because the reduction curve exceeds the critical current density for passivation and it is the only alloy in the stable passive condition. Although the reduction curve also exceeds the critical passivation current density for alloy B, the passivation current at 2B is not low enough and the passive region is not broad enough to ensure good resistance in the passive state. Alloy D is in a state of borderline passivity with both active, 2D, and passive state possible. The active state is generally chosen as the most likely in cases of borderline passivity. The corrosion rate of the non-passive alloy, A, is predictably high at 2A in oxidizing conditions of any degree.

The recommended alloy in highly oxidizing condition (number 3)is D, since now the reduction curve exceeds the critical current density for passivation, and the corrosion rate is low at 3D. Passivity breaks down for alloy C at E_c, and corrosion rate is increased at 3C, which is above the passive current density at 2C. Alloys A and B are not resistant to highly oxidizing conditions.

The breakdown of the alloy C, at E_c, may occur due to initiation of localized corrosion in pits or crevices. With no breakdown ether of the alloys C or D may be chosen because

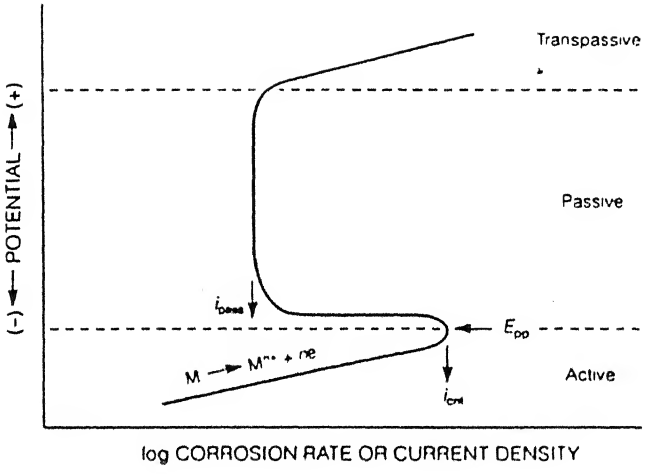

Figure 2.11 Schematic active-passive polarization behavior.

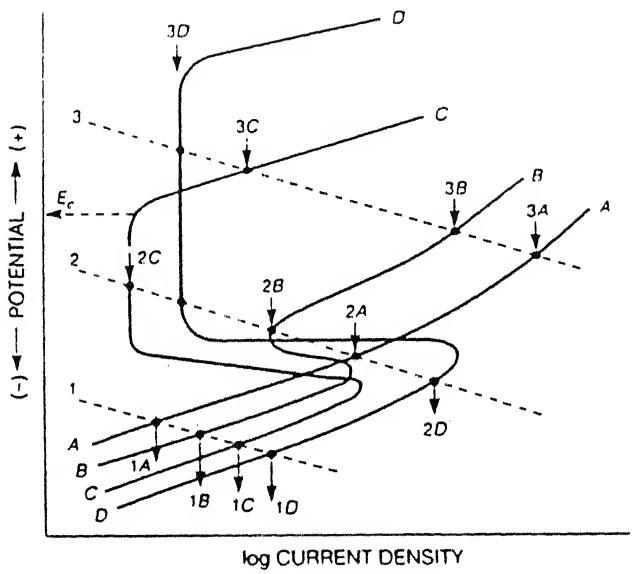

Figure 2.12 Schematic anodic polarization curves for hypothetical alloys A, B, C and D, illustrating evaluation in various chemical conditions: 1, reducing; 2, moderately oxidizing; 3, highly oxidizing.

The above Fe_3Al-5M intermetallics were obtained in the form f buttons of about 2cm diameter. These buttons were homogenized t 1000^{o}C for 4 hours, before processing, to furthur minimize egregation. The buttons of Fe_3Al-5M (M = Cr, Mo, Ta, Ti, Nb, V nd Si) were thermomechanically processed before preparing orrosion specimen according to the following procedure. The uttons were soaked at 1000 ^{o}C in a furnace and immediately rolled n multiple passes to obtain thin strips. The buttons of Fe_3Al-5M M = Nb, V and Si) cracked extensively while rolling and therefore pecimens for corrosion studies could not be obtained from the olled strips. Although the buttons of Fe_3Al-5M (M = Mo and Ta) lso cracked after deformation, 1cm square specimens could be btained from them as the rolled strips contained sections without racks [10].

In the second round of specimen preparation, fresh buttons of Fe_3Al-5M (M = Si, Nb, Zr, V and W) were melted according to the rocedure mentioned above and homogenized at 1000^{o}C for 4 hours. s the previous experience with the Nb and V containing ntermetallic indicated that they would crack during rolling, the lloyed intermetallics prepared in the second round were not rocessed thermomechanically. The interesting aspect aspect about pecimen preparation during the second time was that the Fe_3Al-5Si ntermetallic cracked heavily even after melting, while it did not rack when it was melted the first time. Therefore they could not e used for preparing the polarization specimens for the xperimental study. The alloyed buttons were sectioned midway cross the thickness with the aid of a diamond saw and these ections (of surface area between 1.5 to 2.9 sq. cm.) were used or preparing the polarization specimens.

The compositions of the intermetallics used in the study have been analyzed thoroughly using a electron microproble analyzer and hese are tablulated in Table 3.1.

3.2 SPECIMEN PREPARTION

After obtaining the materials, electric contact between

Table 3.1 : COMPOSITION OF THE INTERMETALLICS

Intermetallic	Atom %		
	Fe	Al	M
Fe_3Al	74.6 ±0.25	25.4 ±0.25	---
Fe_3Al + Ti	65.65	28.41	5.93
Fe_3Al + Zr	64.63±0.68	29.28±0.53	6.12±0.44
Fe_3Al + V	67.56±1.55	28.00±1.51	4.41±0.23
Fe_3Al + Nb	70.20±0.62	23.15±0.45	6.65±2.65
Fe_3Al + Ta**			
Fe_3Al + Cr	67.2±0.22	27.94±0.38	4.84±224
Fe_3Al + Mo	69.17±0.82	25.84±0.84	4.99±0.14
Fe_3Al + W**			
Fe_3Al + Si	73.15±1.29	22.22±1.13	4.64±0.302

** Not Done

sample and a (sealed) wire was established by using a cello tape and immediately mounted by cold mounting using a thermosetting resin which acted as an insulator for the other sides. Each mounted specimen was coarseground initially with the help of an abrading belt and later polished with degreasing grit size of emery paper (1/0 through 4/0) and degreased with acetone before experiment. In case the specimen had to be used for other studies, the surface was polished with emery paper to a 4/0 finish and degreased with acetone before each experiment.

One of the problems faced during the mounting procedure was the loss of contact between the conducting wire and the specimens. In order to obtain a better contact, the conducting copper wire was tried to be soldered to the intermetallics. However, it was not possible to solder the copper wire on to the alloyed intermetallics because the solder did not wet the surface. Therefore, some of the alloyed intermetallics (alloyed with Nb, Zr and W) were cemented with copper and later the conductive wire was soldered to the the copper layer. For this purpuse, the half buttons of the alloyed intermetallics were painted on the flat surface and immersed in $CuSO_4$ solution for cementation. The Cu deposited on the curved surface was then soldered with (sealed) wire and was then immediately mounted by cold mounting using a thermosetting resin which acted as an insulator for the other sides. After mounting, the paint on the flat surface was removed and the polarization samples were surfaced finished as mentioned earlier.

3.3 APPARATUS FOR POLARIZATION STUDIES

The main apparatus used for the polarization experiments were a polarization cell and a potentiostat (Vibrant Potentiostat/Galvanostat VSM/PG/ mention number here) interfaced to a personal computer (NEC PC 80386) attached with a printer (EPSON FX-80). The potentiostat used in the study was capable of performing a wide variety of potentio and galvano function required for basic and applied studies in the field of corrosion

Repeatable results were obtained as long as studies did not require a compliance voltage beyond ±30V (d.c.). The cell potential would be controlled within +4V. However, one limitation of the potentiostat was that it would not measure currents below 1 microamperes and therefore the instrument sensitivity limit is indicated in some of the experimental polarization diagrams to be presented later. In order to acquire polarization curves by the computer system, current and potential measurements had to be converted to digital form by a two channel analog-digit converter. Two digit digital display meters (one for potential and the other for current) were fixed on the front panel to visually aid noting down of readings manually during simply steady state experiments or with slow ramping rates. The experimental arrangement is schematically illustrated in Figure 3.1.

The polarization cell used in the study is shown in Figure 3.2. A round-bottom flask was modified by the addition of various necks to permit the introduction of electrodes, gas inlet and outlet tubes, and a thermometer. The Luggin probe connected with KCL salt bridge seperated the bulk solution from the saturated calomel reference electrode (SCE). The probe tip could be easily adjusted to bring in close proximity with the working electrode. The three electrodes used are the working electrode (mounted specimen connected with a wire), the counter electrode (high-purity platinum flat stock wire), and the reference electrode (satured calomel electrode with E^{O}= + 0.242 V vs standard hydrogen electrode), as per the ASTM recommendations [44]. The potential of the calomel electrode was checked at periodic intervals to ensure the accuracy of the potential of the electrode.

3.4 ELECTROLYTES

The following electrolytes were used in the present study to evaluate the corrosion behavior of Fe_3Al and Fe_3Al-5M (M = Cr, Mo, Ta, Ti, Nb, Zr, V, W) intermetallics.

(a) 0.05 mol/lit H_2SO_4 with and without 200 ppm of Cl^-

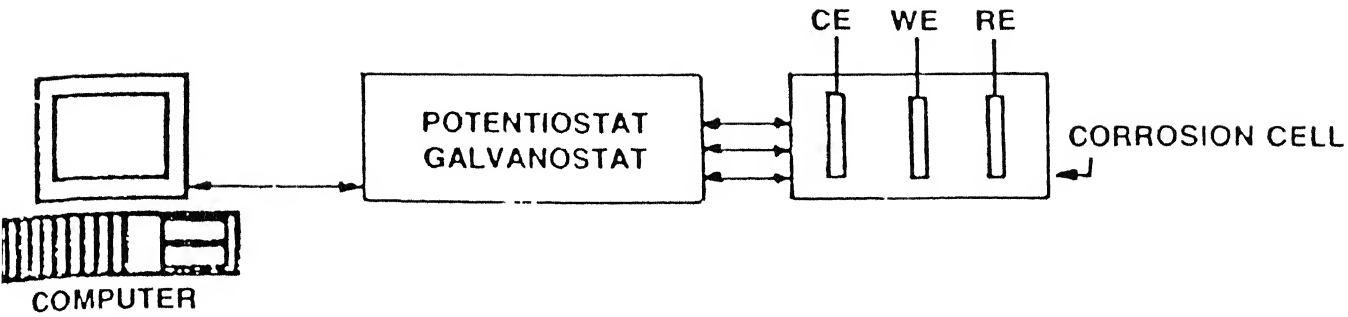

Figure 3.1 Computer assisted instrumentation employed for the polarization studies.

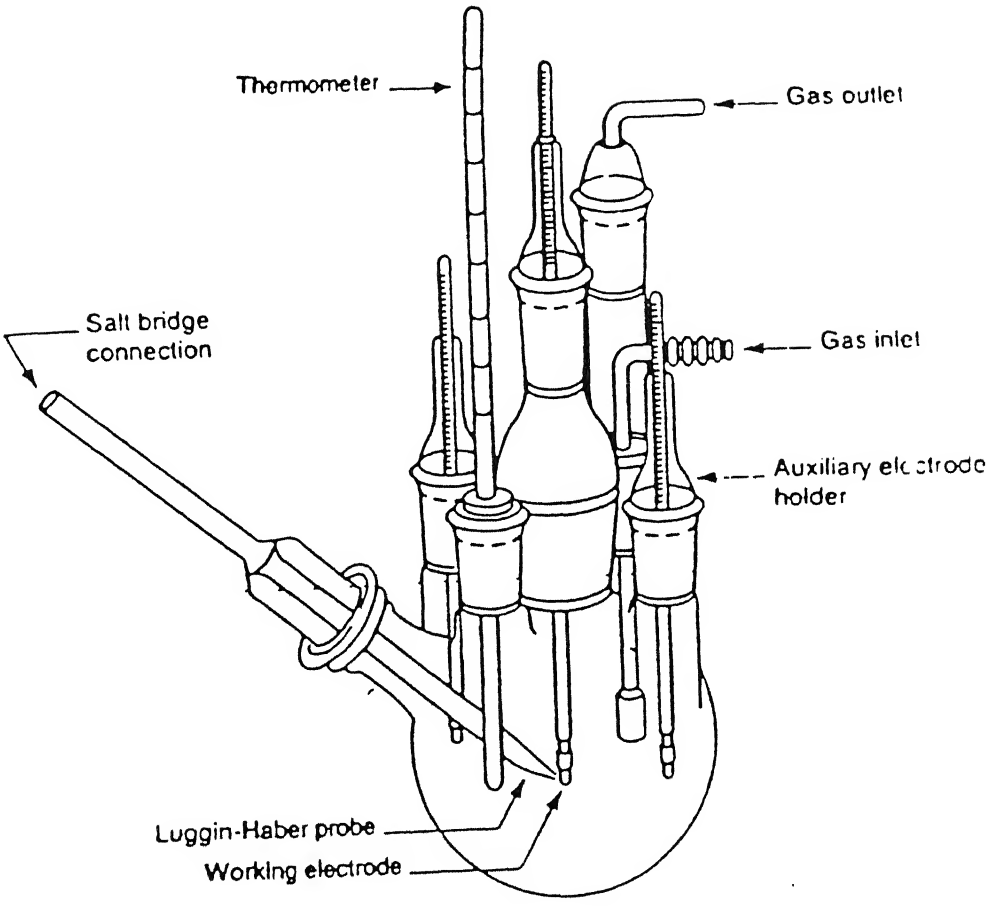

Figure 3.2 Electrochemical polarization cell used for conducting polarization studies.

(b) 0.1 mol/lit NaOH with and without 200 ppm of Cl^-

Electrolytes of different pH (1.4, 13) were made with distilled water and reagent grade chemicals. The solutions of 0.05 mol/lit H_2SO_4 and 0.1 mol/lit NaOH had the pH of 1.5 and 13 respectively. 200 ppm of Cl^- was maintained in the solution by adding 0.316 gm NaCl to one litre of the solutions.

A fixed volume of 1000 ml of test solution was used for all the tests. Although ASTM recommends 40 ml of test solution to every 1 cm^2 area of test surface [44], it is also recommended to keep the ratio of the solution volume to specimen surface area high in order to avoid any appreciable change in the corrosivity of the solution during the test, especially since the solution would not be recirculated [44]. Only test solutions that were less than 24 hours old were used in order to minimize contamination of the electrolyte. Additional care was taken to stir the solution thoroughly before starting each test.

The temperature of the electrolytes could not be controlled using a water bath due to the shape of the polarization cell. The experiments were conducted between August 1995 (temperature 33°C) and January 1996 (temperature 20°C). The major difference in the solution condition between the two extremes in temperature is that the concentration of dissolved oxygen would have been lower when the solution was at a higher temperature compared to that when it was a lower temperature.

3.5 TEST PROCEDURE FOR POLARIZATION STUDIES

The electrolyte solution (1000 ml) was transferred to corrosion cell. The electrodes were immersed in the electrolyte and secured in a place using a retort stand. Precaution was taken that the specimens were dipped to the same depth and the luggin probe was adjusted so that its tip was consistently as close to the working electrode as possible. It is well known in polarization measurements that the portion of the electrolyte between the working electrode and the capillary tip of the reference electrode also contributes towards the electrical

resistance. Since resistanec is a function of the distance between the electrodes, better accountability for the measured values was achieved by keeping the gap as small as possible to minimize the extra resistance.

The corrosion potential of the working electrode was continuously recorded starting immediately after immersion until a constant potential was obtained. Potentiodynamic polarization studies were conducted immediately after stabilized corrosion values were obtained. The period for stabilization depended upon the specimen, its surface finish, and the electrolyte. Generally, it took 1-2 hours for obtaining a constant potential. All the tests were conducted with a potential scan rate of 1 mV/sec. In an earlier study of the electrochemical behavior of Fe_3Al [41], the effect of scan rate on polarization behavior was studied and it was found that this scan rate was suitable for reliable measurement of equilibrium electrochemical charateristics. Data were collected at every 30 sec interval until breakdown occured or until the potential of 2V was reached, whichever was earlier. Generally the total duration of the test was 3 hours.The data was processed by the computer and stored digitally. The specimen area was taken into account during the processing of data.

3.6 MATERIAL CHRATERIZATION

3.6.1. COMPOSITION

The compositions of the base intermetallic and the alloyed intermetallics were analysed in a JEOL electron probe microanalyzer (JXA-8600MX). Several composition analysis were obtained from each specimen and the average of the values have been reported in Table 3.1 along with the standard deviation obtained. However, the composition of the Ta- and W-containing intermetallics could not be obtained as the EPMA was not able to standardize the Ta and W pure standard that was mounted along with the intermetallics that was used for the analysis. Therefore, their compositions have not been provided but it is expected to conform to the composition Fe_3Al-5M.

peak of Fe_3Al [35,45] and therefore it can be concluded that the ordered intermetallic was in the state of order and the intermetallic after rolling at 1000°C did not contain the DO_3 ordered phase it does not exhibit line broadening of the (440) peak. Moreover, as the rolling was performed at a temperature above the critical temperature of the base Fe_3Al, the presence of the ordered DO_3 phase is not expected.

The Cr- and Ti-alloyed intermetallics did not exhibit any additional diffraction peaks (Figure A3 and A4) apart from the peaks that were obtained earlier in the case of the base intermetallic. Therefore, it can be concluded that Cr and Ti additions essentially enter into solid solution in the Fe_3Al matrix. However, additional peaks could be clearly identified in the other alloyed intermetallics (Figures A5 through A10) and the phase(s) due to which these additional peaks arise have been identified with the aid of JCPDS X-ray diffraction files. Note that some peaks in the alloyed intermetallics have not been identified as the lines do not correspond to lines obtained from the JCPDC files. The additional phases that form in the alloyed intermetallics that have been identified are as follows: Fe_2Nb, FeNb, $AlNb_2$ and Al_3Nb in Fe_3Al-5Nb, Fe_5Ta_3, Ta_2Al_3 and FeTa in Fe_3Al-5Ta, $Fe_{63}Mo_{37}$ and $Al_{17}Mo_4$ in Fe_3Al-5Mo, FeV in Fe_3Al-5V, Fe_2W and Fe_7W_6 in Fe_3Al-5W, Fe_2Zr in Fe_3Al-5Zr and Al_8Fe_2Si in Fe_3Al-5Si. The presence of these phases can also be predicted from the binary phase diagrams of Fe-M and Al-M.

4.2 STABILIZATION OF FREE CORROSION POTENTIALS

The nature of stabilization of the free corrosion potentials (FCP) provide some information about the nature of the film that forms on the surface of materials under free corrosion conditions [46]. If the FCP moves from an active to noble potential during stabilization, it implies the dissolution of the film that forms under free corrosion conditions and equilibrium FCP is attained when the dissolution rate equals the growth rate of the film. In case the FCP moves from an active to noble potential during

stabilization, it again implies that the equilibrium potential is attained when the dissolution rate equals the film growth rate with the major difference from the earlier case being that the film that forms in this case is more protective as it moves the potential towards the noble direction. In case the FCP stabilizes immediately upon immersion, it implies that the equilibrium dissolution is attained relatively fast and that the nature of the film that forms is protective.

The stabilization of the free corrosion potentials for the intermetallics used in the present study are presented in Figure 4.1 and 4.2 in the acidic solution without and with chloride ions, respectively. The FCP of the intermetallics stabilize around -0.50 V vs SCE in almost all the cases except in the case of the Fe_3Al-5V intermetallic which stabilizes at a nobler potential. The nature of the stabilization curves are similar for all the cases and the potentials move from noble to active potentials on stabilization. The time for stabilization is relatively fast for all the intermetallics except the Fe_3Al-5V intermetallic. In the case of the acidic solution with the presence of chlorides (Figure 4.2), the FCP stabilizes around -0.50 V vs SCE for the intermetallics alloyed with Cr, Ta, Ti, Nb and W and this similar to that obtained in the case without the presence of chloride ions. The Fe_3Al-5V intermetallic also stabilizes at a potential around 0.0 V vs SCE similar to that found earlier in the acidic solution without chlorides. However, the FCPs of the Fe_3Al-5Zr, Fe_3Al-Ta and Fe_3Al-5Mo intermetallics stabilize at a more noble potential compared to the earlier case. The nature of the stabilization curve for the Zr alloyed intermetallic is unusual, although the general trend that is seen is that the potential moves from a noble to active potential. The nature of the stabilization curve for the other intermetallics is similar to that seen in the acidic solution without chlorides. However, the exception to this is the Fe_3Al-5Mo intermetallic whose FCP moves from an active to noble value during stabilization. The free corrosion potentials for the intermetallics in acidic medium are

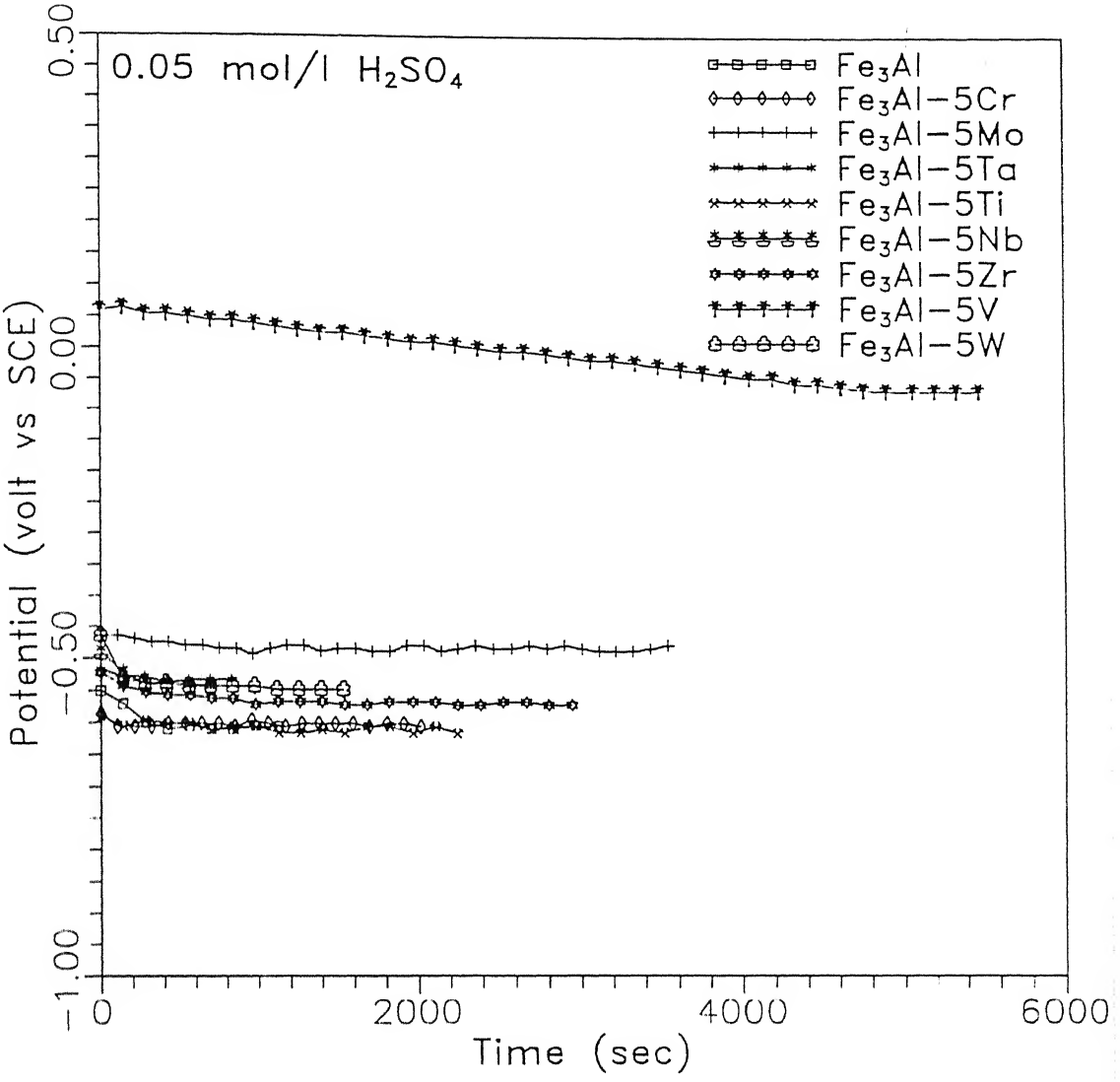

Figure 4.1 Variation of free corrosion potential as a function of time for the intermetallics in 0.05 mol/l H_2SO_4 solution.

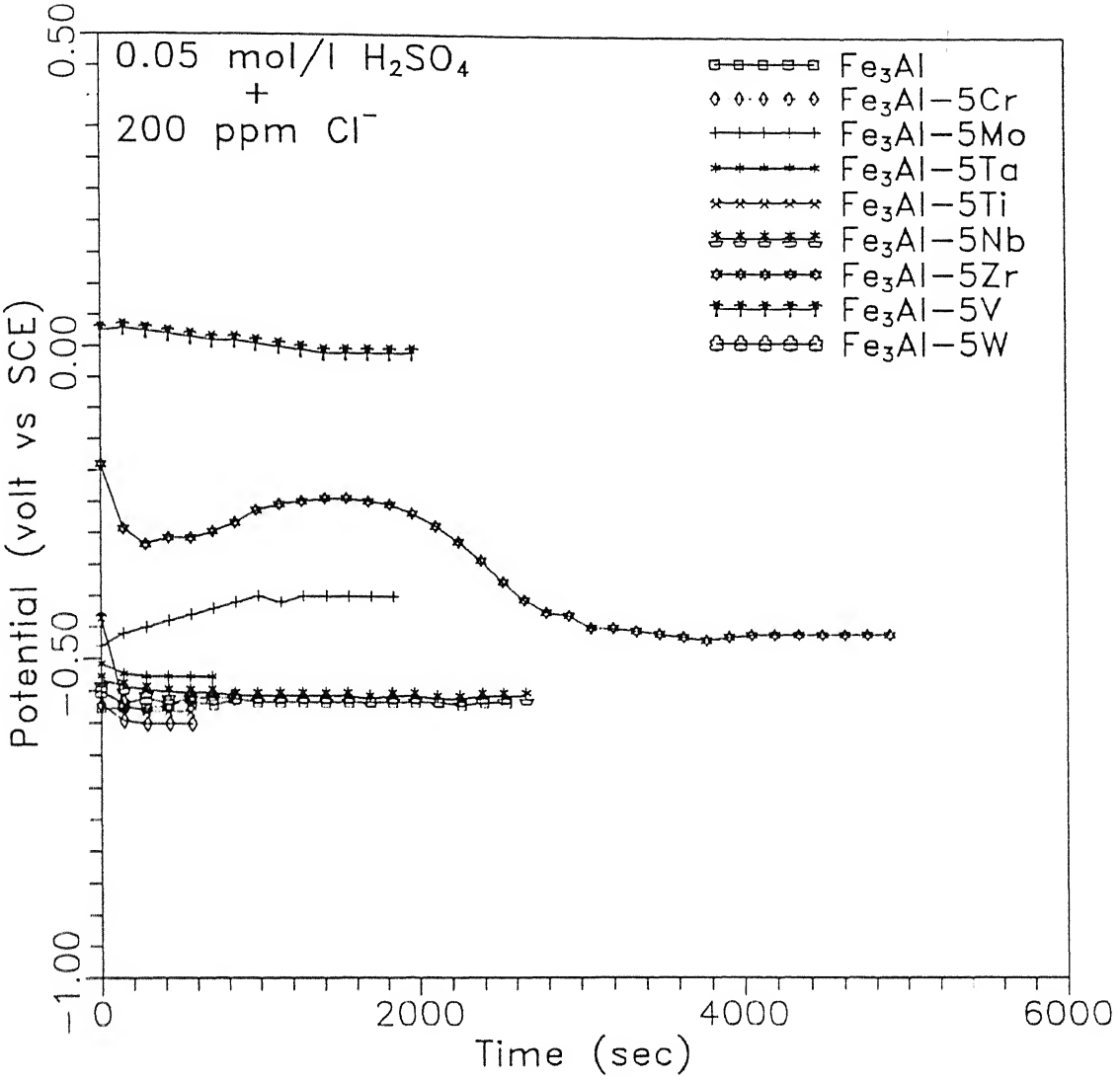

Figure 4.2 Variation of free corrosion potentials as a function of time for the intermetallics in 0.05 mol/l H_2SO_4 solution with 200ppm Cl^-.

Table 4.1

Free Corrosion Potential (E_{corr}) and Zero Current Potential (ZCP) of the Intermetallics in 0.05 mol/l H_2SO_4, without and with 200 ppm chloride ions. All the potentials are in volt versus SCE.

INTERMETALLIC	Acid		Acid + Cl^-	
	E_{corr}	ZCP	E_{corr}	ZCP
Fe_3Al	-0.61	-0.40	-0.58	-0.35
Fe_3Al-5Ti	-0.61	-0.52	-0.58	-0.50
Fe_3Al-5Zr	-0.57	-0.50	-0.46	-0.45
Fe_3Al-5V	-0.08	0.0	-0.02	0.0
Fe_3Al-5Nb	-0.54	-0.50	-0.56	-0.50
Fe_3Al-5Ta	-0.60	-0.45	-0.48	-0.50
Fe_3Al-5Cr	-0.60	-0.55	-0.60	-0.55
Fe_3Al-5Mo	-0.48	-0.40	-0.40	-0.45
Fe_3Al-5W	-0.55	-0.50	-0.54	-0.50

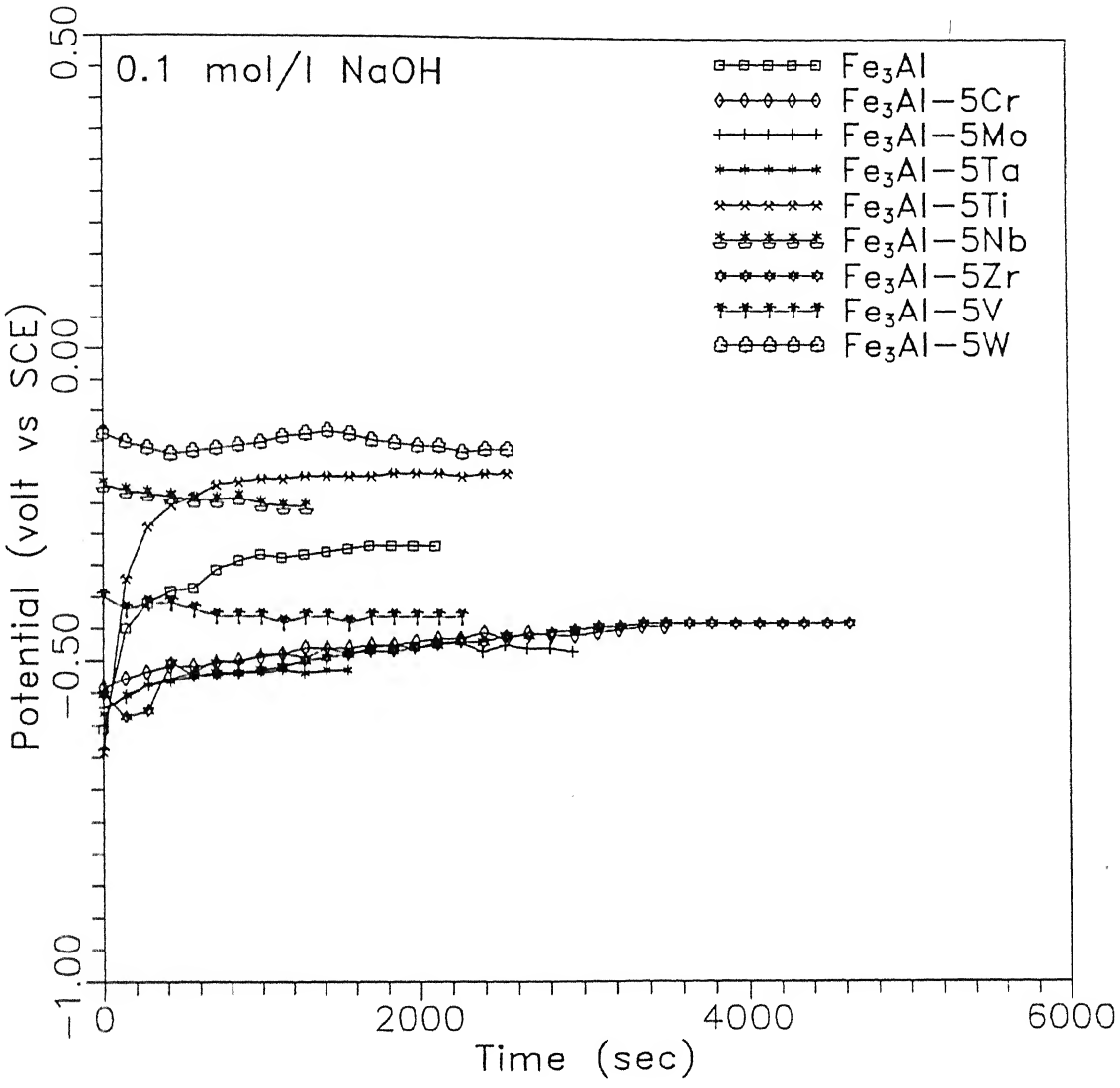

Figure 4.3 Variation of free corrosion potentials as a function of time for the intermetallics in 0.1 mol/l NaOH solution.

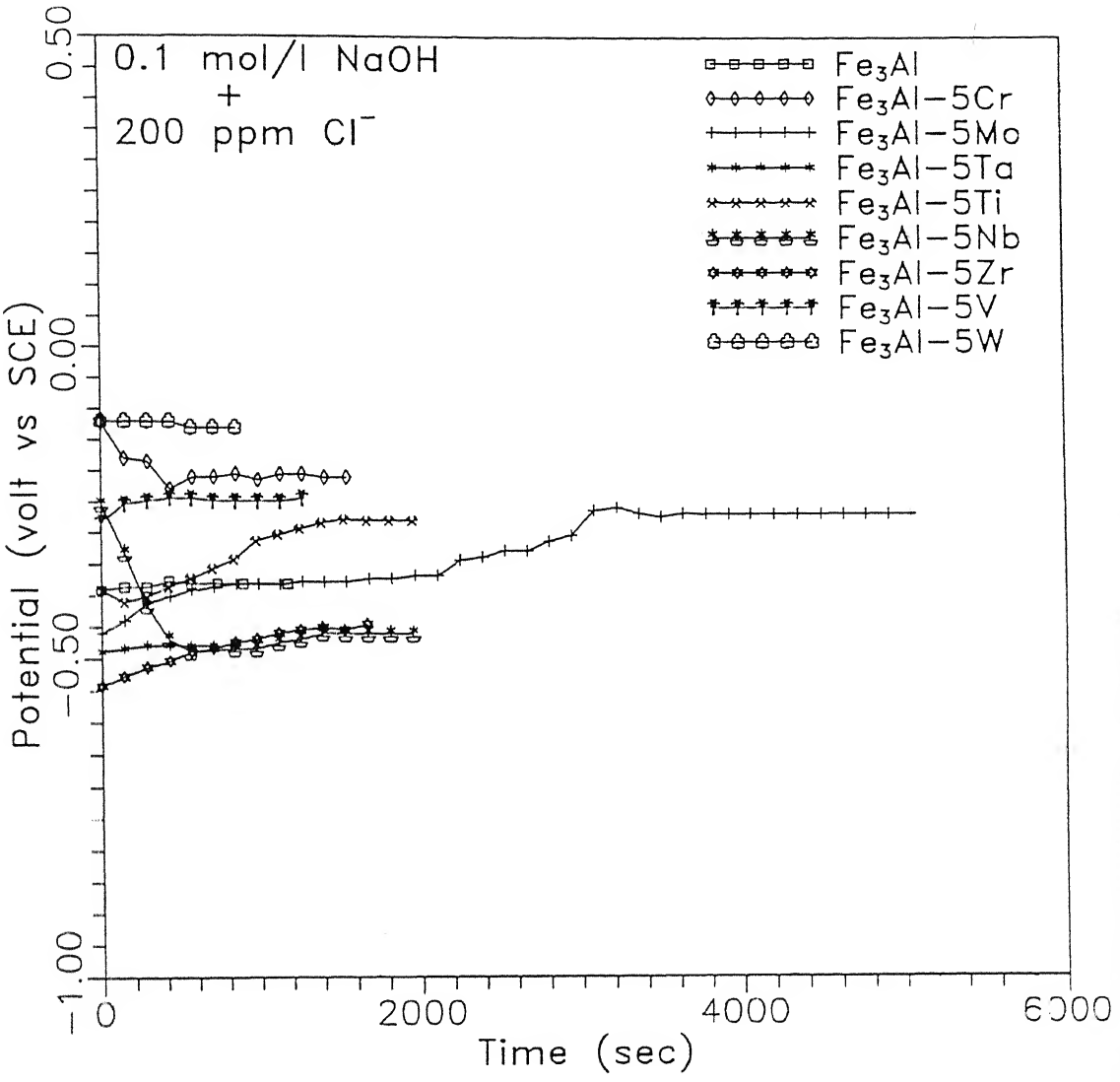

Figure 4.4 Variation of free corrosion potentials as a function of time for the intermetallics in 0.1 mol/l NaOH solution with 200ppm Cl^-.

tabulated in Table 4.1.

The stabilization of the FCP for the intermetallics in the alkaline solution without and with chloride ions are presented in Figures 4.3 and 4.4, respectively. In the case of the alkaline solution without chlorides, the FCP of the intermetallics alloyed with Zr, V, Ta, Cr and Mo stabilize around -0.50 V vs SCE while the FCP of the intermetallic base Fe_3Al, and those alloyed with Nb, Ti and W are higher (in the ascending order of magnitude). The nature of the stabilization curve is also different from that seen in the acidic solution. The FCP moves from an active potential towards a noble value in the case of all the intermetallics, except the Nb, V and W alloyed intermetallics. Normally, the FCP stabilizes within 2000 sec for the intermetallics in this solution. In contrast to the behavior observed in the alkaline solution without the chlorides, the nature of the stabilization curves in the alkaline solution with chloride ions is different in that the potential moves from a noble value to an active value during stabilization for all the intermetallics except the one containing V. The FCP in the chloride-containing electrolyte stabilizes at a nobler value of potentials for the intermetallics except the base, Ti- and Nb-containing intermetallics compared to the earlier case without chloride ions. The stabilized FCP of the intermetallics in the alkaline solution, without and with chloride ions, are tabulated in Table 4.2.

4.3 ELECTROCHEMICAL BEHAVIOR IN ACIDIC MEDIUM

The cyclic potentiodynamic polarization behavior of the intermetallics in the acidic solution (with and without chloride ions) are discussed individually in the following sub-sections. An overall comparison of their behavior in the acidic solution is discussed at the end of this section.

4.3.1 Fe_3Al

The potentiodynamic polarization curves (forward and reverse scans) for Fe_3Al in the acidic H_2SO_4 solution without chloride

ions are presented in Figure 4.5. The intermetallic exhibited active behavior in this electrolyte as can be seen from the forward scan. This is consistent with the behavior of Fe_3Al in the electrolyte which was also determined in an earlier study [41]. However, on the reverse scan, the existence of passivity can be discerned. The stabilized FCP for this intermetallic was -0.61 V vs SCE and the zero current potential (ZCP) on scanning from the cathodic to the anodic (active to noble) direction is -0.40 V vs SCE. The value of the critical current density for passivation (i_{crit}) obtained from the reverse scan is 19.95 mA/cm^2.The passive range is very small and extends to about 0.1 V. No distinct breakdown potential can be identified from the forward polarization curve. However, it was noticed that the intermetallic pits once anodic potentials are attained and a large current density is drawn because of this reason. The nature of the curve on reverse scanning indicates the good re-passivation behavior of this intermetallic as the lower current densities are obtained during the initial stage of the reverse scan compared to that obtained in the forward scan. It is interesting to note that the ZCP on reverse scanning is nearly the same as that on forward scanning indicating the active nature of the surface during the reverse scan.

The potentiodynamic polarization curves (forward and reverse scans) for Fe_3Al in the acidic H_2SO_4 solution with 200 ppm chloride ions are presented in Figure 4.6. The polarization curve exhibits active behavior in the forward scan. Similar to the behavior in the solution without chloride ions, the ZCP (-0.35 V vs SCE) on forward scanning is noble to the stabilized FCP (-0.50 V vs SCE). The unstable nature of the passive film in the presence of chloride ions is further reflected in the very high current densities drawn and the active value of ZCP on reversing the scan. Moreover, the ZCP is similar during the reverse scan as the ZCP on forward scanning and this again is indicative of the active nature of the surface in the presence of chloride ions.

The anodic polarization curve for Fe in 1N H_2SO_4 has been

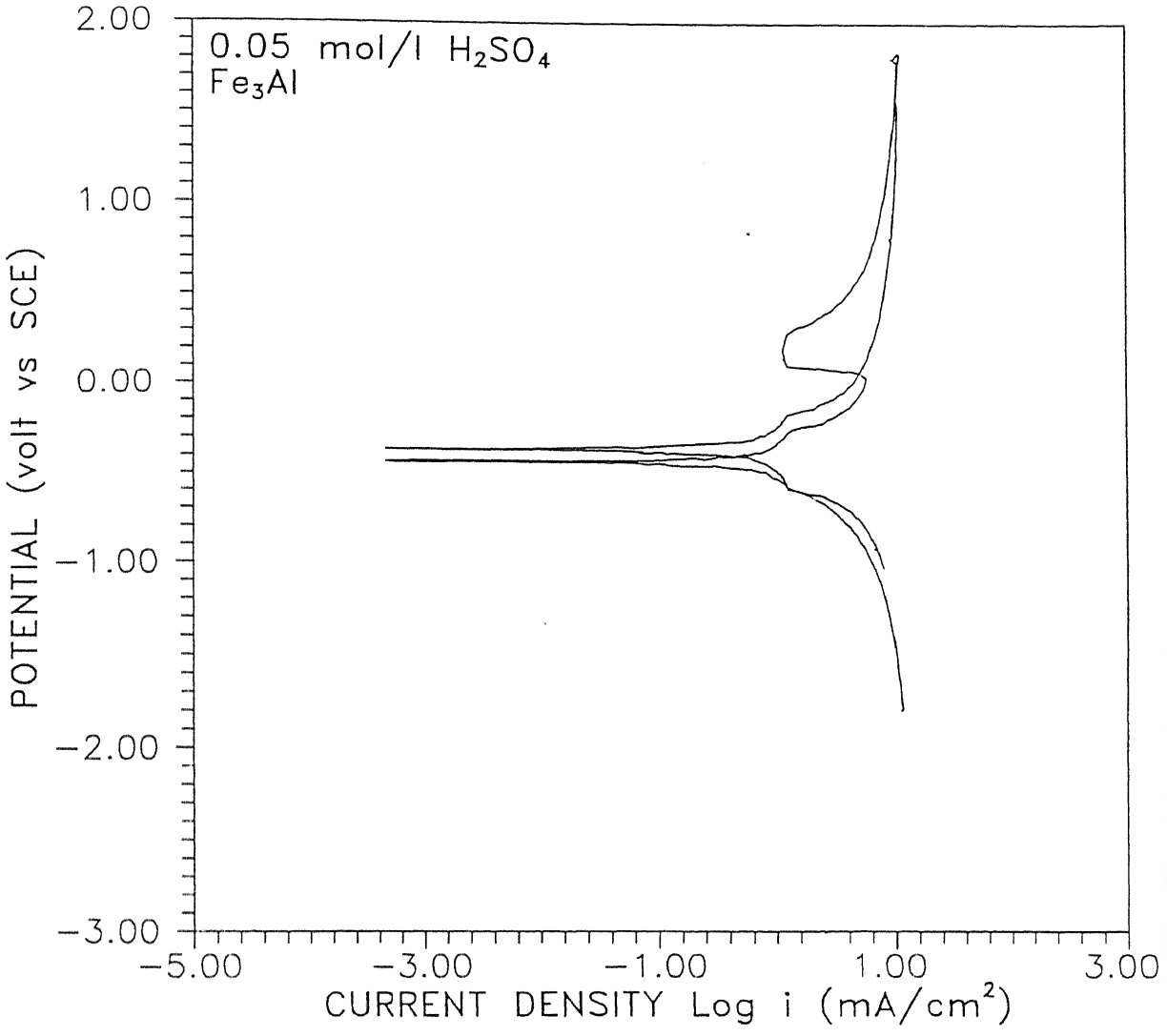

Figure 4.5 Cyclic polarization curve of base Fe_3Al intermetallic in 0.05 mol/l H_2SO_4.

determined earlier [47] and it exhibits active-passive behavior in this electrolyte. The region where the i_{crit} is obtained in the case of pure Fe is very similar to that observed for Fe_3Al in the acidic solution without chlorides on the reverse scan (Figure 4.5). Therefore, it can be concluded that the passivity that obtains in Fe_3Al primarily arises due to Fe. This has also been noted by Janavicius and Payer [39] who noted that the polarization behavior of FeAl resembled that of Fe in a wide variety of solutions and they hypothesized that the passive layer that forms on the FeAl intermetallic is a hydrated oxide of Fe which forms due to the selective dissolution of Al. The present study also confirms this for the Fe_3Al intermetallic where the probability of forming the iron oxide is higher due to the higher concentration of Fe in the base intermetallic.

4.3.2 Fe_3Al-5Ti

The potentiodynamic polarization curve (both forward and reverse scans) for Fe_3Al-5Ti in the acidic H_2SO_4 solution without chloride ions are presented in Figure 4.7. The intermetallic exhibited active-passive behavior in this electrolyte as can be seen from the forward scan and this is in contrast to the active behavior observed earlier for the base Fe_3Al intermetallic. The stabilized FCP for this intermetallic was -0.61 V vs SCE and the ZCP on scanning from the cathodic to the anodic (active to noble) direction is -0.52 V vs SCE. The value of the critical current density for passivation (i_{crit}) is 1.99 mA/cm^2 and this is lower than the i_{crit} of unalloyed Fe_3Al (obtained during the reverse scan) in the same electrolyte. The passive range extends to about 0.6 V and this is higher than the passive range obtained in unalloyed Fe_3Al in the reverse scan. Two breakdown potentials can be identified from the forward polarization curve (namely at 0.6 V and 1.5 V). The appearance of the secondary passivation could most probably be due to the selective dissolution of Ti, similar to the dissolution of Cr in Fe-Cr alloys [47]. This intermetallic also pits heavily once the second breakdown potential is attained and a large current density is drawn because of this reason. The passive

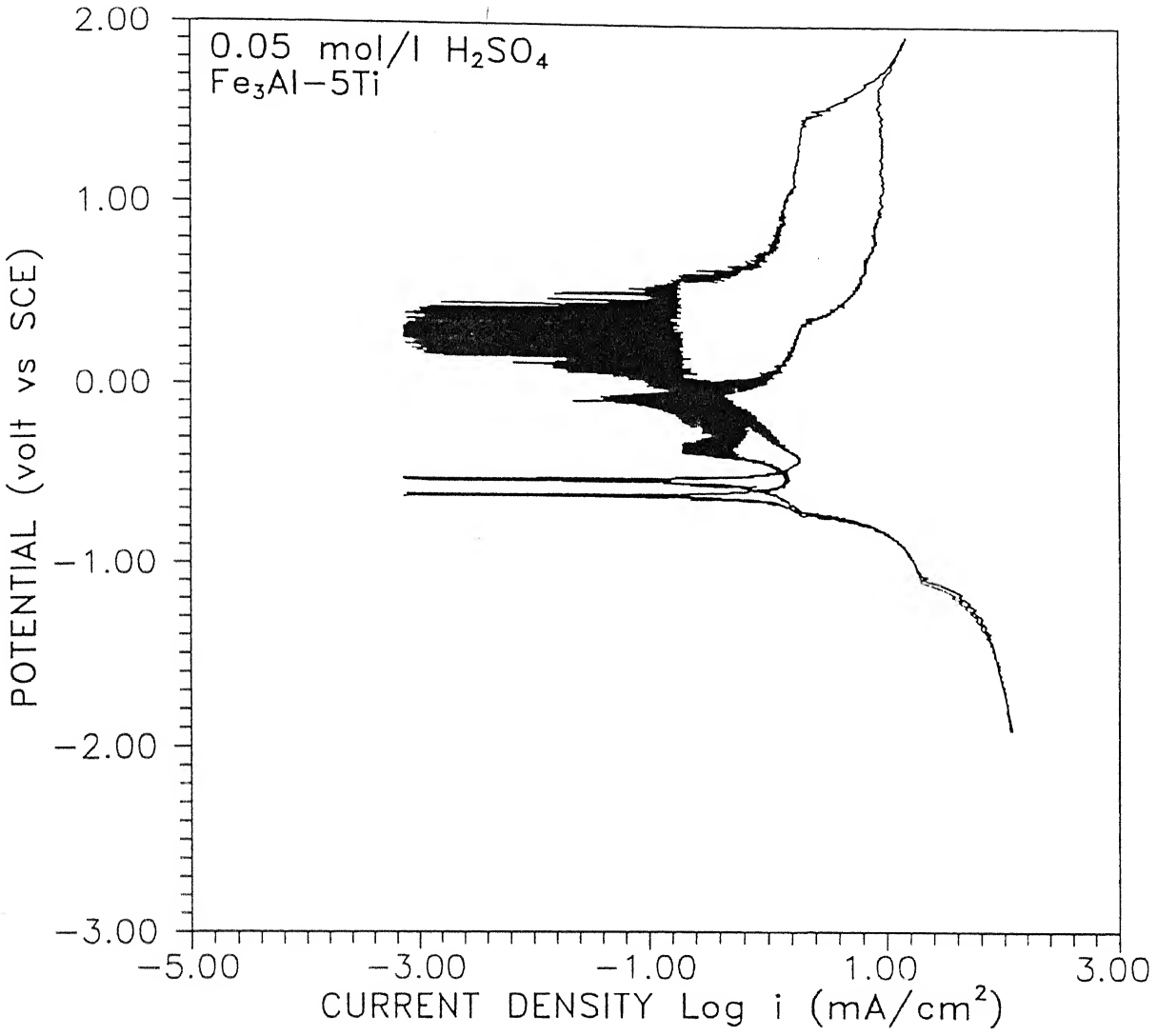

Figure 4.7 Cyclic polarization curve of Fe_3Al-5Ti intermetallic in 0.05 mol/l H_2SO_4.

range is lower on reverse scanning from the noble to active potential. The nature of the curve on reverse scanning indicates the moderate re-passivation characteristics of the Ti-alloyed intermetallic as the reverse scan does not trace the original forward scan in the initial period of the scan and the forward scan is intersected at a much lower value of potential (in the transition region between active and passive behavior). Higher currents are drawn between the potential at which the scan is reversed and the potential at which it intersects the forward scan curve. It is interesting to note that the ZCP on reverse scanning occurs at nearly the same potential as in the forward scan, similar to that observed for the base intermetallic.

The potentiodynamic polarization curves (forward and reverse scans) for Fe_3Al-5Ti in the acidic H_2SO_4 solution with 200 ppm chloride ions are presented in Figure 4.8. The polarization curve exhibits active-passive behavior in the forward scan. Similar to the behavior in the solution without chloride ions, the zero current potential (-0.50 V vs SCE) on forward scanning is nearly the same as the stabilized free corrosion potential (-0.58 V vs SCE). Note that the i_{crit} in the chloride containing solution (1.41 mA/cm^2) is slightly lower than that obtained in the earlier case without chloride ions. The passive current density (i_{pass}) is nearly the same in the presence of chloride ions (0.16 mA/cm^2) compared to the earlier case without chloride ions. The passive range (0.4 V) in this case is slightly lower than in the earlier case (0.6 V) and this is because the passivity breaks down at a lower value of potential in the chloride-containing solution. This indicates that the chloride ions destabilize the passive layer on the surface of Fe_3Al-5Ti in acidic solutions. The unstable nature of the passive film in the presence of chloride ions is further reflected in the very high current densities drawn and the active value of zero current potential on reversing the scan. Moreover, the range of passivity is lower on reversing the scan in the presence of chlorides when compared to the case without chlorides.

It has been previously reported that addition of Ti to iron

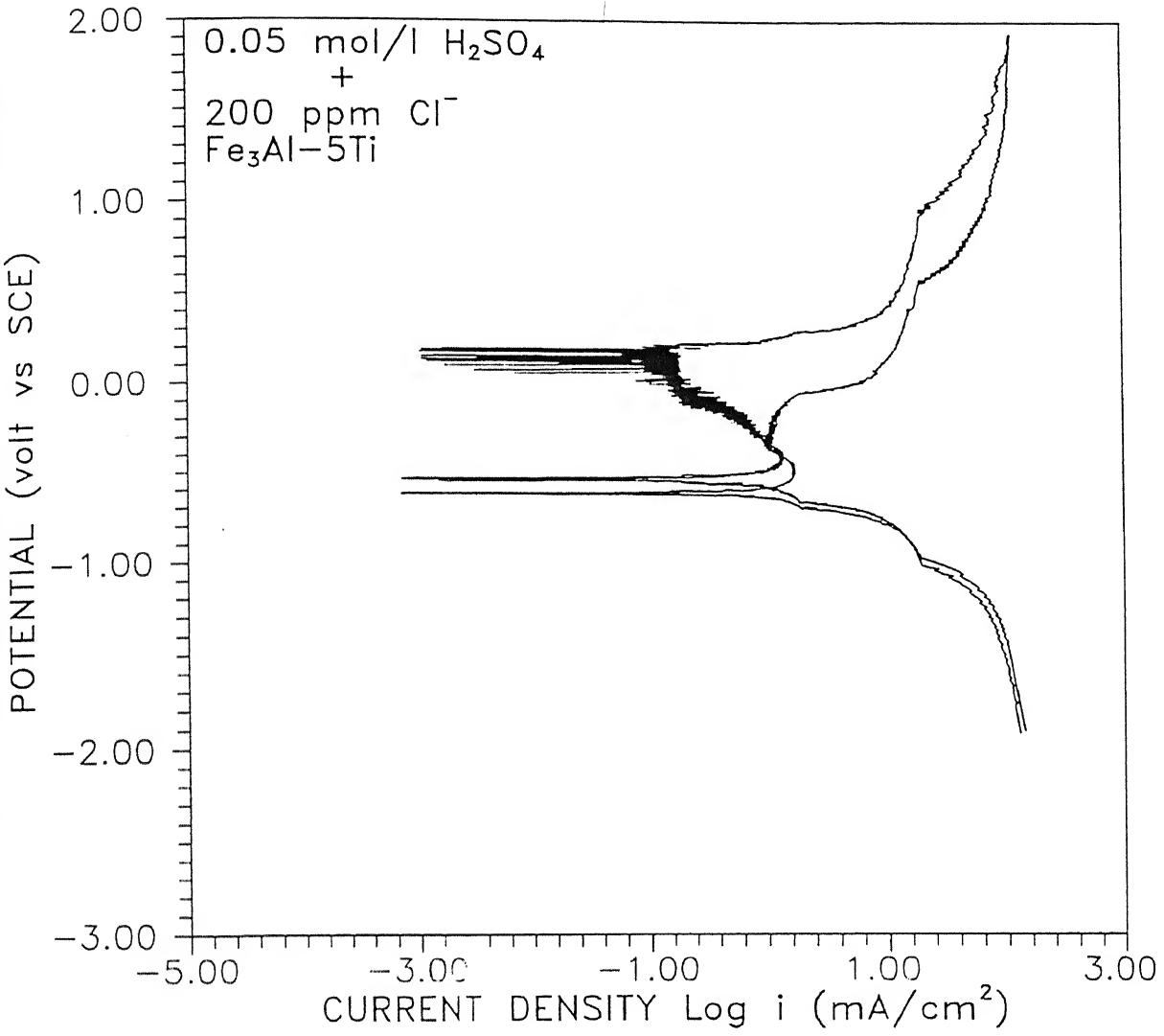

Figure 4.8 Cyclic polarization curve of Fe_3Al-5Ti intermetallic in 0.05 mol/l H_2SO_4 with 200ppm of Cl^-.

based alloys, for example stainless steels, are retained in solid solution by annealing at a high temperature (1250^{o}C) Ti strongly enhances the passivity [48]. This occurs also in the case of Cr-steel and the passivity is acheived much faster with Fe-28Cr-3Ti than Fe-28Cr in 10% H_2SO_4 solution [49]. Moreover, Ti addition is also reported to promote enhancement in passivity of Fe alloys where it strongly lowers the i_{crit} [49]. The polarization behavior of the Ti-alloyed intermetallic is, therefore, similar to that obtained when Ti is alloyed to Fe. Therefore the addition of Ti to Fe_3Al generally enhances the passive behavior of the base intermetallic by decreasing i_{crit}, E_{pp}, E_{cp} and increasing E_b. In an earlier study, the enhanced passivity due to Ti addition was also observed in H_2SO_4 solution of pH 4 and in NaOH solution of pH 8 [10]. It must be also mentioned that addition of Ti to the base intermetallic provides sufficient ductilities to the intermetallic at ambient temperatures [10] and superplastic behavior at high temperatures [50]. The present study further validates the argument that higher ductilities could be obtained when there is an enhancement in passivity due to Ti addition.

4.3.3 Fe_3Al-5Zr

The potentiodynamic polarization curve (both forward and reverse scans) for Fe_3Al-5Zr in the acidic H_2SO_4 solution without chloride ions are presented in Figure 4.9. The intermetallic exhibited active-passive behavior in this electrolyte as can be seen from the forward scan and this is in contrast to the active behavior observed earlier for the base Fe_3Al intermetallic. The stabilized FCP for this intermetallic was -0.57 V vs SCE and the ZCP on scanning from the cathodic to the anodic (active to noble) direction is -0.50 V vs SCE. The value of the critical current density for passivation (i_{crit}) is 3.98 mA/cm^2 and this is lower than the i_{crit} of unalloyed Fe_3Al during the reverse scan in the same electrolyte. The passive range extends to about 0.70 V and this is higher than the passive range obtained in unalloyed Fe_3Al in the reverse scan. Two breakdown potentials can be identified

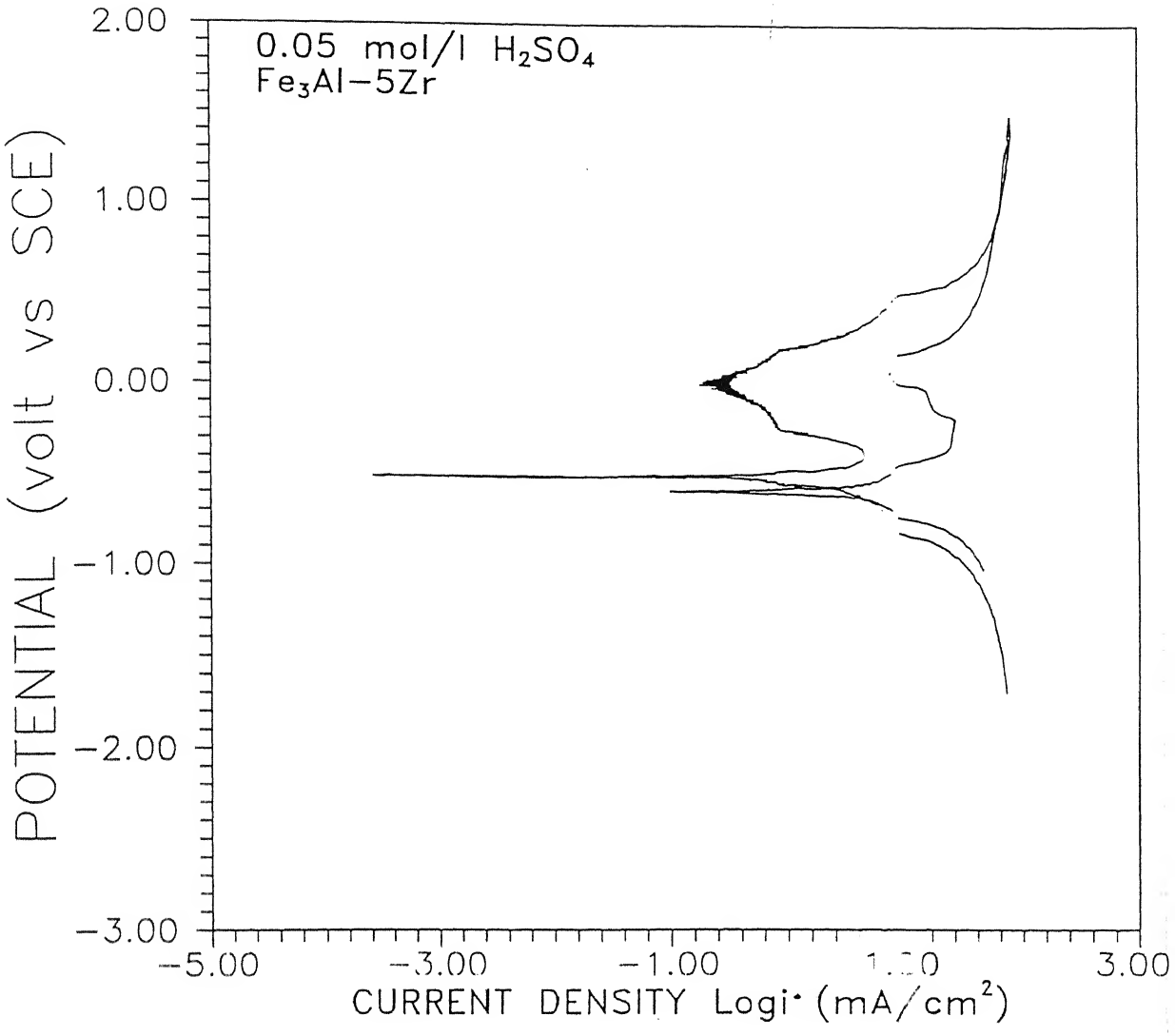

Figure 4.9 Cyclic polarization curve of Fe_3Al-5Zr intermetallic in 0.05 mol/l H_2SO_4.

breakdown potential in this case is 0.05 V compared to 0.2 V in the earlier case. Interestingly, the reverse scan traces the forward scan until the passive region is reached and this implies that the re-passivation in the presence of chlorides is relatively better than in the case without chlorides. Much higher currents are drawn in the passive region during the reverse scan than in the forward scan and the forward scan is intersected at a potential very close to the ZCP on forward scan indicating that the material is not very resistant to chloride-induced pitting.

The effect of Zr addition on the passivation behavior of iron is not known. However, it is established that pure Zr is resistant up to 60% H_2SO_4 at room temperature [51]. Therefore, it appears that the addition of Zr results in the enhancement of passivity of the base intermetallic due to the inherent passive nature of Zr in sulfuric acid.

4.3.4 Fe_3Al-5V

The potentiodynamic polarization curves (forward and reverse scans) for Fe_3Al-5V in the acidic H_2SO_4 solution without chloride ions are presented in Figure 4.11. The intermetallic exhibited active behavior in this electrolyte as can be seen from the forward scan, similar to the behavior obtained for the base intermetallic. Interestingly, the reverse scan exactly traces the forward scan indicating that active behavior is also exhibited on reversal of scan. The stabilized FCP for this intermetallic was -0.08 V vs SCE and the ZCP on scanning from the cathodic to the anodic (active to noble) direction is -0.0 V vs SCE. This intermetallic also pits heavily once anodic potentials are attained. Moreover, the polarization curve and ZCP on reverse scanning are nearly the same as that on forward scanning indicating the active nature of the surface during the reverse scan.

The potentiodynamic polarization curves (forward and reverse scans) for Fe_3Al-5V in the acidic H_2SO_4 solution with 200 ppm chloride ions are presented in Figure 4.12. The intermetallic

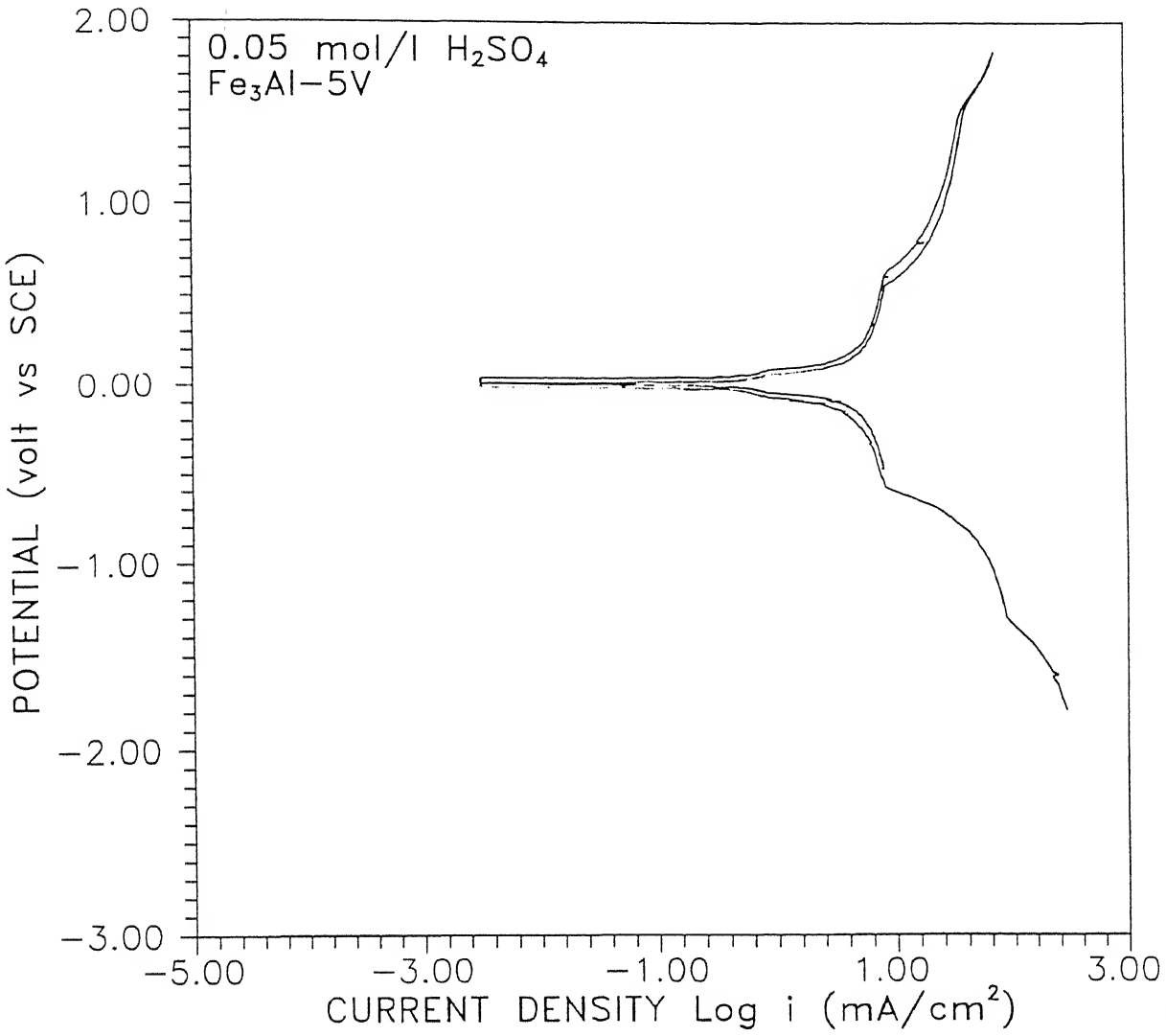

Figure 4.11 Cyclic polarization curve of Fe_3Al-5V intermetallic in 0.05 mol/l H_2SO_4.

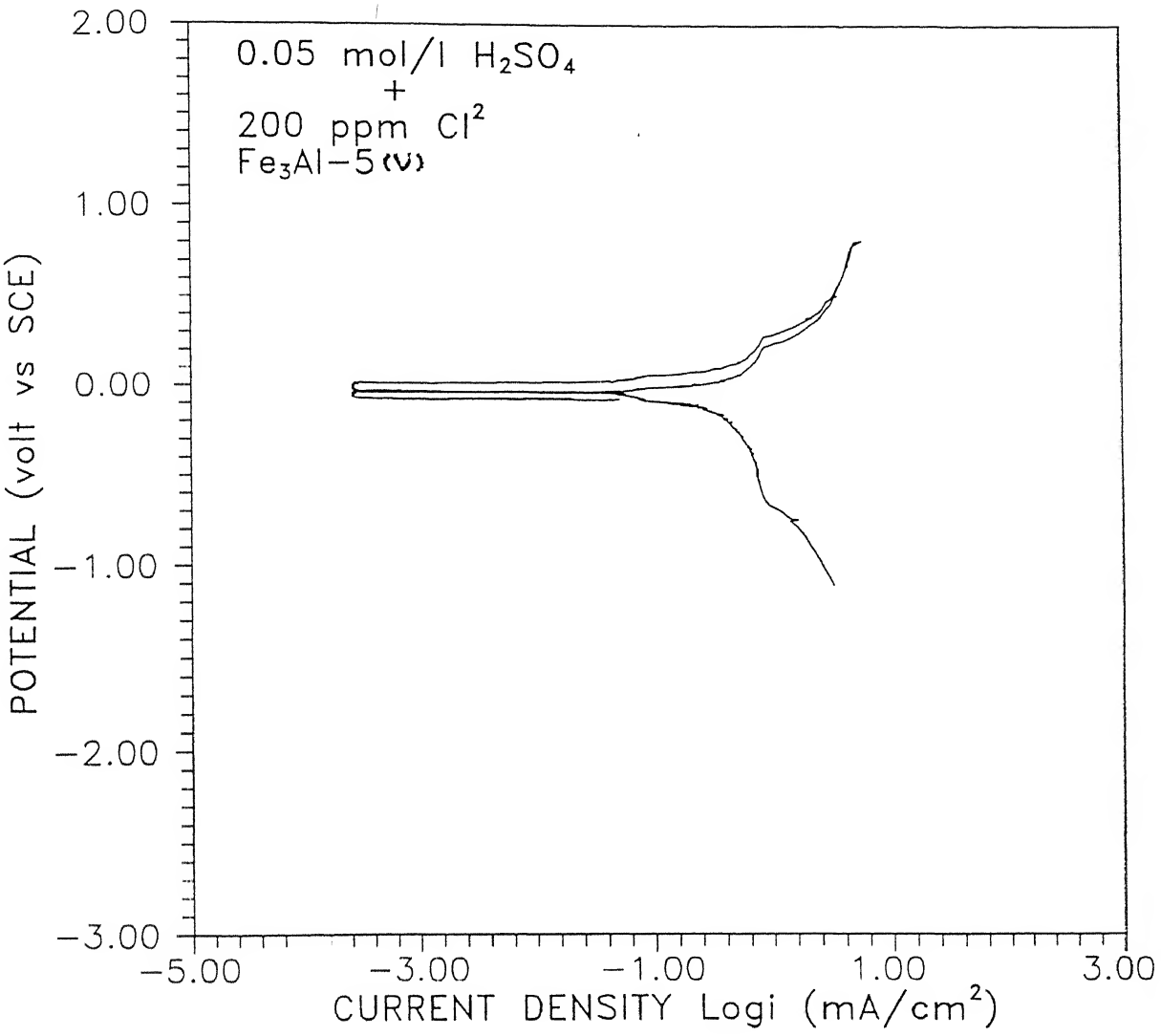

Figure 4.12 Cyclic polarization curve of Fe_3Al-5V intermetallic in 0.05 mol/l H_2SO_4 with 200ppm of Cl^-.

exhibits active behavior in the electrolyte, very similar to the behavior of the intermetallic in the solution without chloride ions. The zero current potential (0.0 V) on forward scanning is nearly the same as the stabilized free corrosion potential (-0.02). Moreover, the ZCP and E_{corr} are similar in acidic electrolyte, with and without chloride ions.

It has been reported that addition of 5% V enhances passivity in Fe-14Ni-18Cr steel in 0.1N HCl [52] by lowering i_{crit} and increasing the passive region breakdown potential, but it had practically no effect on passivity of the same alloy in 30% H_2SO_4 [52]. However, the present study shows that addition of V to Fe_3Al does not change the active nature of the base intermetallic and this could be due to the absence of Cr in the intermetallic. Moreover, it has should be mentioned that The Fe-14Ni-18Cr is an alloy with good inherent passive properties and addition of V relatively changes the passive behavior only marginally as mentioned above. However, the base intermetallic to which V was alloyed in this study exhibits active behavior in the acidic medium and the addition of V does not alter this behavior. Therefore, the addition of V does not induce passivity in Fe_3Al.

4.3.5 Fe_3Al-5Nb

The forward and reverse potentiodynamic polarization curves for Fe_3Al-5Nb in the acidic H_2SO_4 solution without chloride ions are presented in Figures 4.13 and 4.14, respectively. The intermetallic exhibited active-passive behavior in this electrolyte as can be seen from the forward scan and this is in contrast to the active behavior observed earlier for the base Fe_3Al intermetallic. The stabilized FCP for this intermetallic was -0.54 V vs SCE and the zero current potential (ZCP) on scanning from the cathodic to the anodic (active to noble) direction is -0.50 V vs SCE. The value of i_{crit} is 0.4 mA/cm^2 and this is lower than the i_{crit} of unalloyed Fe_3Al during the reverse scan in the same electrolyte. The passive range extends to about 0.3 V and this is higher than the passive range obtained in unalloyed Fe_3Al

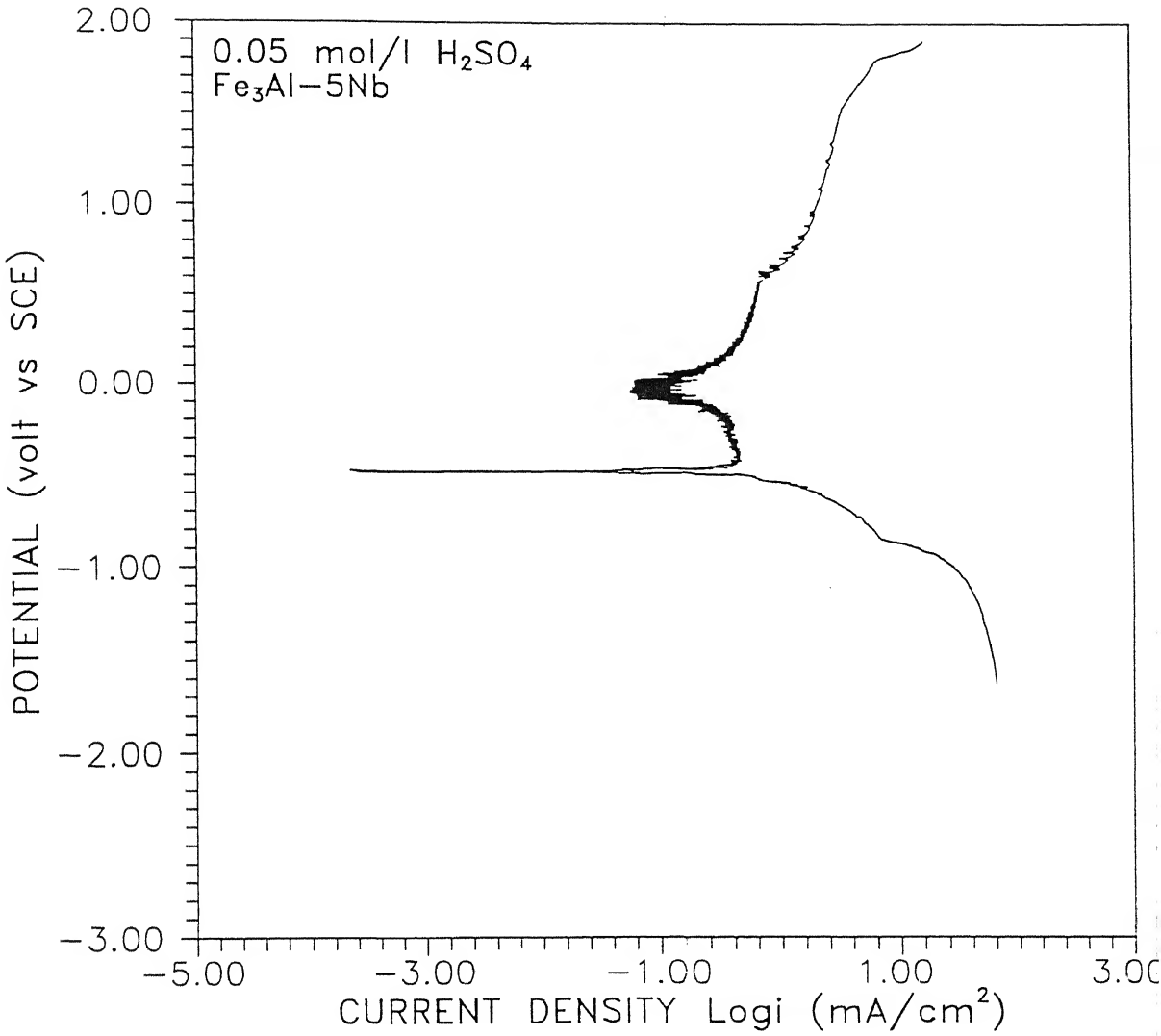

Figure 4.13 Forward polarization curve of Fe_3Al-5Nb intermetallic in 0.05 mol/l H_2SO_4.

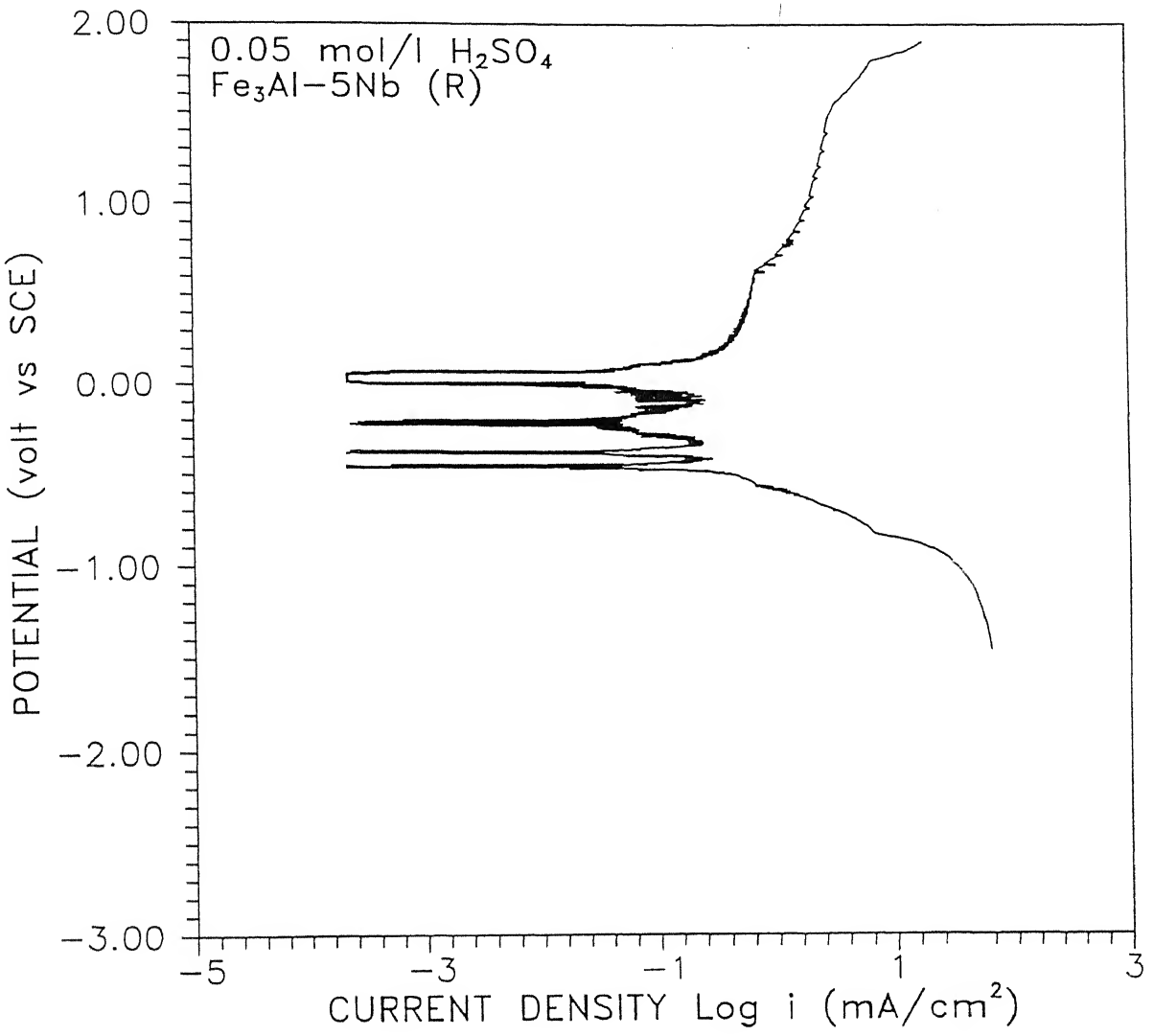

Figure 4.14 Reverse polarization curve of Fe_3Al-5Nb intermetallic in 0.05 mol/l H_2SO_4.

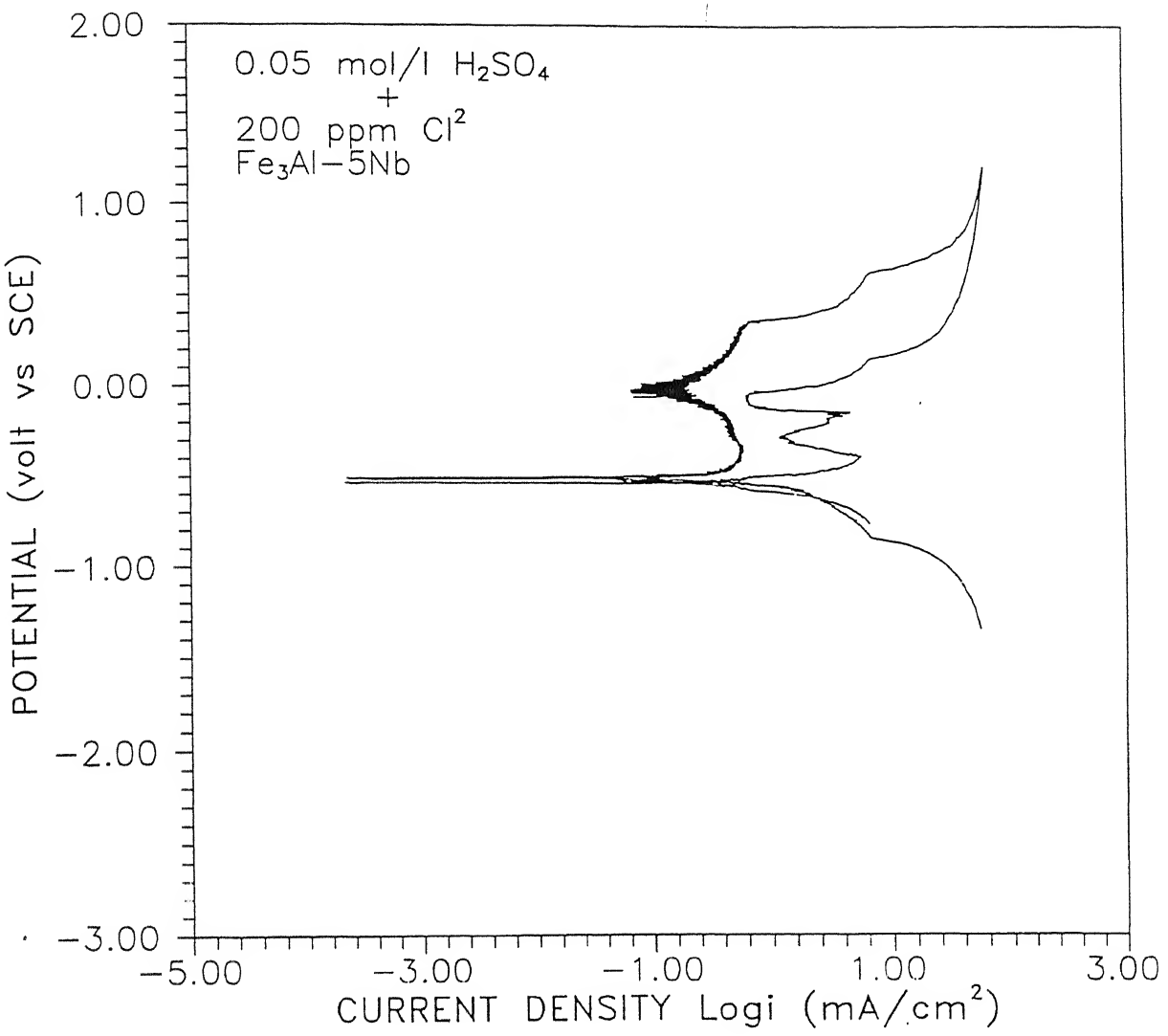

Figure 4.15 Cyclic polarization curve of Fe_3Al-5Nb intermetallic in 0.05 mol/l H_2SO_4 with 200ppm of Cl^-.

in the reverse scan. Two breakdown potentials can be identified from the forward polarization curve (namely at 0.2 V and 0.7 V). The nature of the curve on reverse scanning indicates the relatively good re-passivation characteristics of the Nb-alloyed intermetallic as the reverse scan closely traces the original forward scan all the way to the passive region. This indicates the relatively good pitting resistance of the Nb-alloyed intermetallic. However, the reverse scan exhibits a cathodic loop which could most probably due to the cathodic polarization curve intersecting the passive region during the reverse scan because of the shift in the polarization curve to the left due to the low value of i_{pass} obtained on reversing the scan. The ZCP on reverse scanning occurs at a lower potential than the ZCP on forward scanning.

The potentiodynamic polarization curves (forward and reverse scans) for Fe_3Al-5Nb in the acidic H_2SO_4 solution with 200 ppm chloride ions are presented in Figure 4.15. The polarization curve exhibits active-passive behavior in the forward scan. Similar to the behavior in the solution without chloride ions, the zero current potential (-0.50 V vs SCE) on forward scanning is nearly the same as the stabilized free corrosion potential (-0.56 V vs SCE). Note that the i_{crit} in the chloride containing solution (1.25 mA/cm^2) is slightly higher than that obtained in the earlier case without chloride ions (0.63 mA/cm^2) and this is the expected behavior when chloride ions are present in the environment [46]. The i_{pass} is slightly lower in the presence of chloride ions (0.12 mA/cm^2) compared to the earlier case without chloride ions (0.16 mA/cm^2). The passive range (0.2 V) in this case is lower than in the earlier case without chlorides (0.3 V). The passive region breaks down at a potential of 0.1 V compared to 0.2 V in the earlier case (without chloride ions). In contrast to the good repassivation behavior observed in the solution without chlorides, the reverse scan does not trace the forward scan and this implies that the re-passivation in the presence of chlorides is altered and that it is now poorer than in the case without chlorides. Much

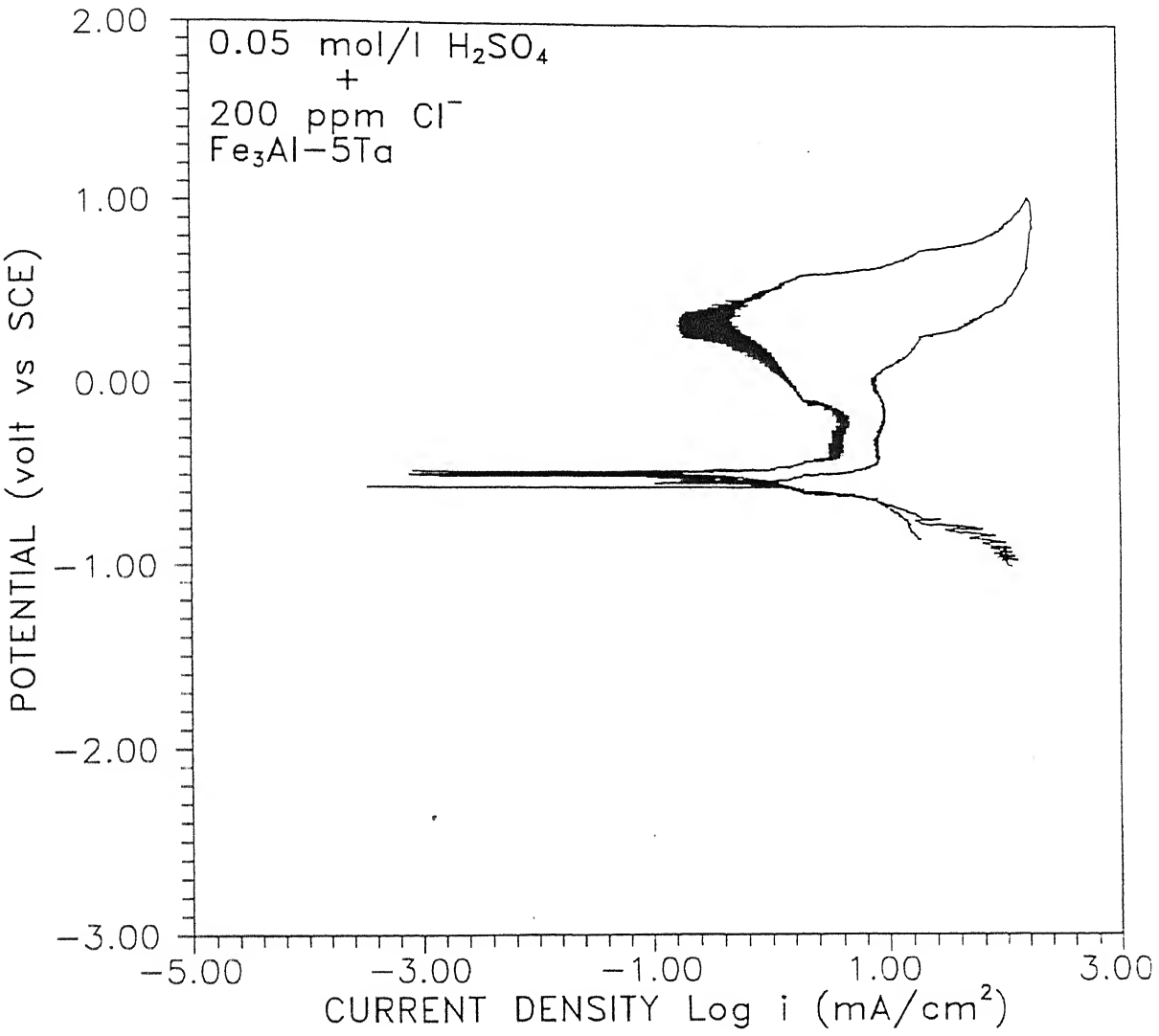

Figure 4.17 Cyclic polarization curve of Fe_3Al-5Ta intermetallic in 0.05 mol/l H_2SO_4 with 200ppm of Cl^-.

and the large passive range also indicate the relatively good pitting resistance of the Ta-alloyed intermetallic.

The potentiodynamic polarization curves (forward and reverse scans) for Fe_3Al-5Ta in the acidic H_2SO_4 solution with 200 ppm chloride ions are presented in Figure 4.17. The polarization curve exhibits active-passive behavior in the forward scan. Similar to the behavior in the solution without chloride ions, the zero current potential (-0.50) on forward scanning is nearly the same as the stabilized free corrosion potential (-0.48). Note that the i_{crit} in the chloride containing solution (5.01 mA/cm^2) is slightly higher than that obtained in the earlier case without chloride ions (3.98 mA/cm^2) and this is the expected behavior when chloride ions are present in the environment [46]. However, the i_{pass} is slightly lower in the presence of chloride ions (0.63 mA/cm^2) compared to the earlier case without chloride ions (1.26 mA/cm^2). The passive range (0.65 V) in this case is lower than in the earlier case without chlorides (1.0 V). The passive region breaks down at a potential of 0.6 V compared to 1.0 V in the earlier case (without chloride ions). In contrast to the good repassivation behavior observed in the solution without chlorides, the reverse scan does not trace the forward scan and this implies that the re-passivation in the presence of chlorides is altered and that it is now poorer than in the case without chlorides. Much higher currents are drawn during the reverse scan than in the forward scan and the forward scan is intersected at a potential very close to the ZCP on forward scan indicating that the material is not very resistant to chloride-induced pitting.

The effect of Ta on the passivity of Fe is not known. However, it has been reported that pure Ta at room temperature is resistant to up to 60% H_2SO_4 [51]. Therefore, it appears that the addition of Ta results in the enhancement of passivity of the base intermetallic due to the inherent passive nature of Ta in sulfuric acid, similar to that observed for Zr addition discussed earlier.

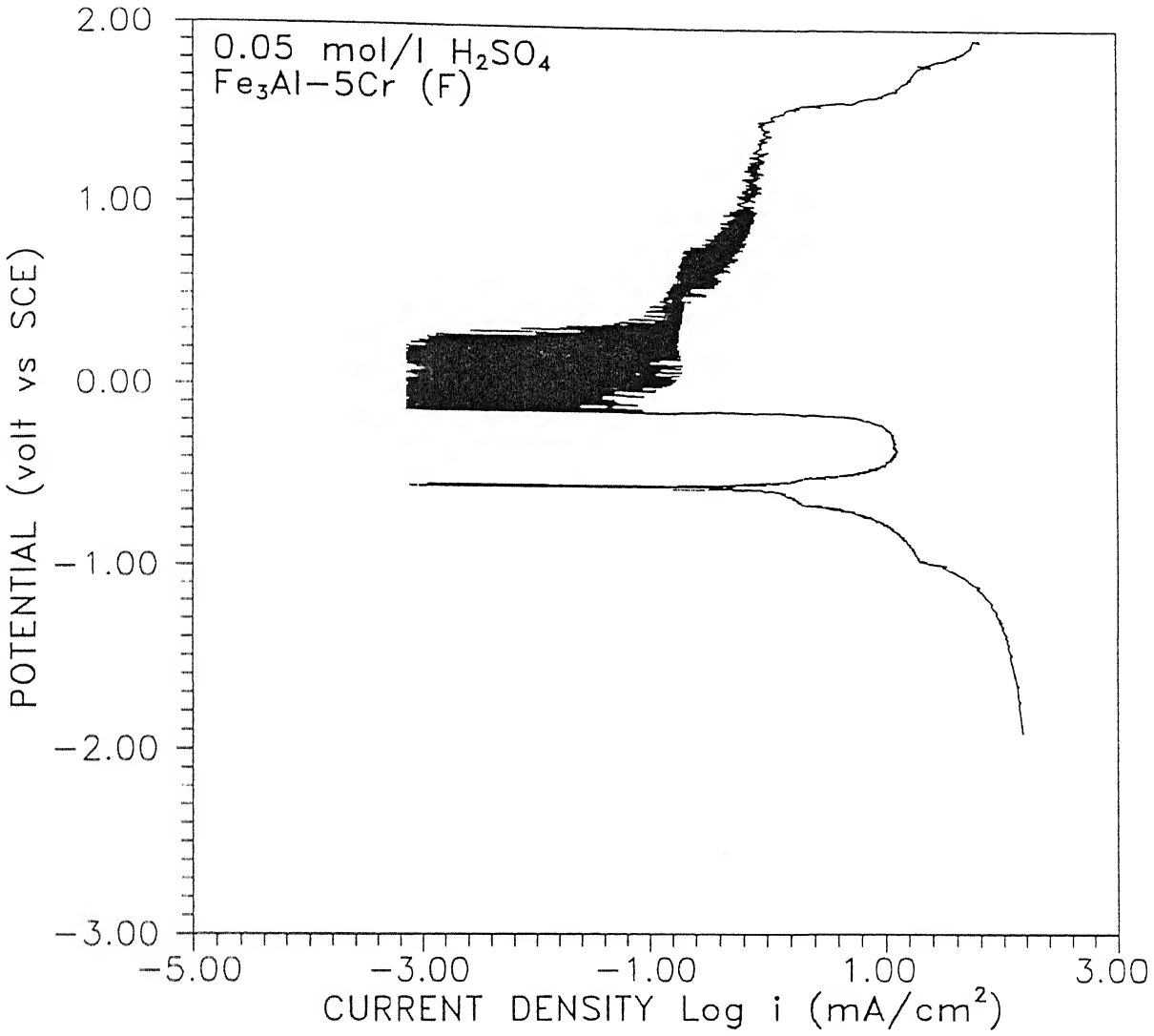

Figure 4.18 Forward polarization curve of Fe_3Al-5Cr intermetallic in 0.05 mol/l H_2SO_4.

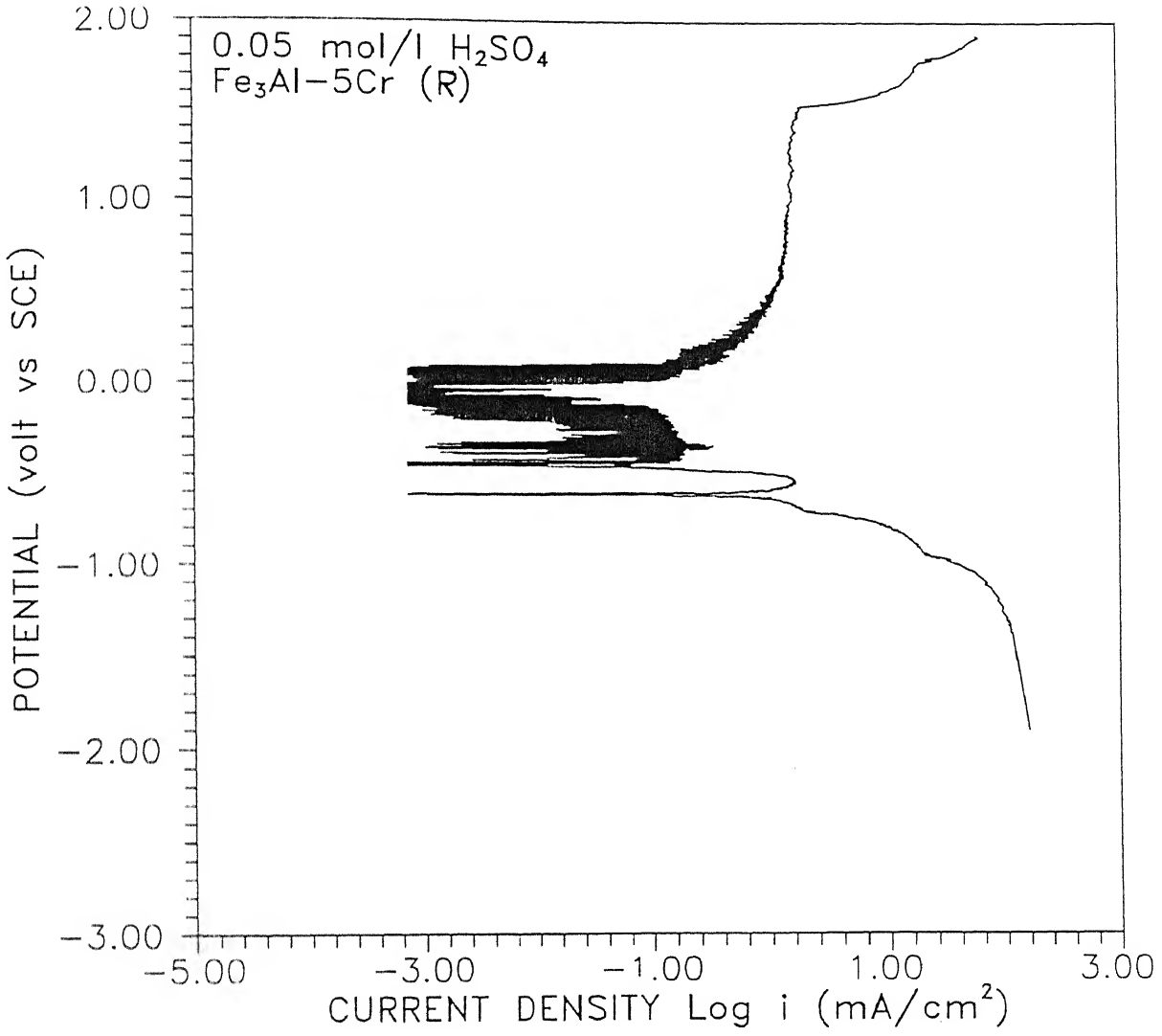

Figure 4.19 Reverse polarization curve of Fe_3Al-5Cr intermetallic in 0.05 mol/l H_2SO_4.

4.3.7 Fe_3Al-5Cr

The potentiodynamic forward and reverse polarization curves for Fe_3Al-5Cr in the acidic H_2SO_4 solution without chloride ions are presented in Figure 4.18 and Figure 4.19, respectively. The intermetallic exhibited active-passive behavior in this electrolyte as can be seen from the forward scan and this is in contrast to the active behavior observed earlier for the base Fe_3Al intermetallic. The stabilized FCP for this intermetallic was -0.60 V vs SCE and the zero current potential (ZCP) on scanning from the cathodic to the anodic (active to noble) direction is -0.55 V vs SCE. The value of the critical current density for passivation (i_{crit}) is 11.2 mA/cm^2 and this is lower than the i_{crit} of unalloyed Fe_3Al during the reverse scan in the same electrolyte. The passive range extends to about 0.7 V and this is higher than the passive range obtained in unalloyed Fe_3Al in the reverse scan. Two breakdown potentials can be identified from the forward polarization curve (namely at 0.5 V and 1.5 V). The appearance of the secondary passivation could most probably be due to the selective dissolution of Cr as this has been reported for the case of Cr-containing steels [47]. The intermetallic pits heavily once the second breakdown potential is attained and a large current density is drawn because of this reason. The passive range is lower on reverse scanning from the noble to active potential. The nature of the curve on reverse scanning indicates the relatively good re-passivation characteristics of the Cr-alloyed intermetallic as the reverse scan nearly traces the original forward scan and intersects the forward scan curve in the passive region. Higher currents are drawn between the potential at which the scan is reversed and the potential at which it intersects the forward scan curve. The breakdown potentials occur at nearly the same values during the reverse scans. It is interesting to note that the ZCP on reverse scanning occurs at nearly the same potential as in the forward scan.

The potentiodynamic polarization curves (forward and reverse

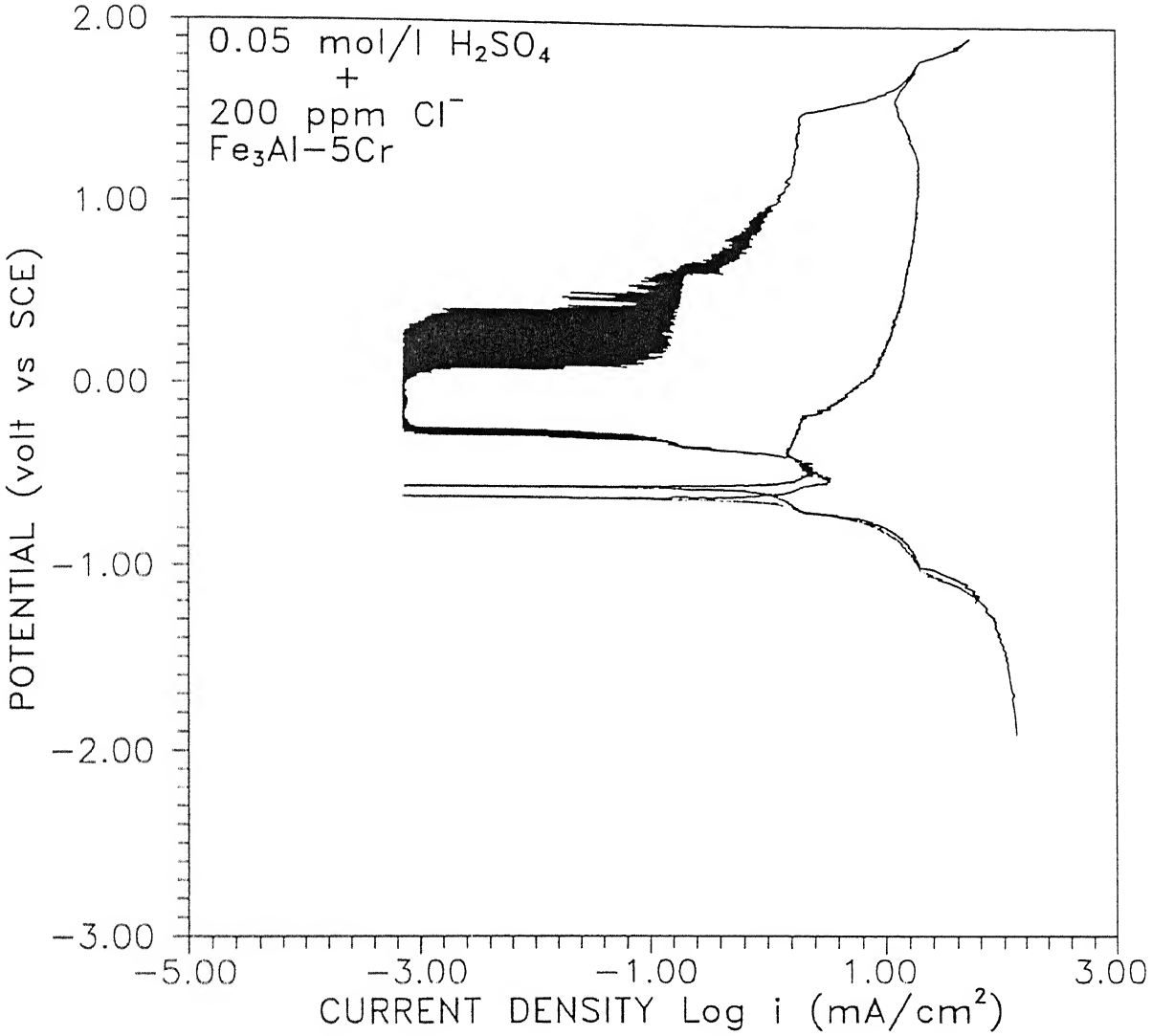

Figure 4.20 Cyclic polarization curve of Fe_3Al-5Cr intermetallic in 0.05 mol/l H_2SO_4 with 200ppm of Cl^-.

scans) for Fe_3Al-5Cr in the acidic H_2SO_4 solution with 200 ppm chloride ions are presented in Figure 4.20. The polarization curve exhibits active-passive behavior in the forward scan. Similar to the behavior in the solution without chloride ions, the zero current potential (-0.55 V) on forward scanning is nearly the same as the stabilized free corrosion potential (-0.6 V SCE). Note that the i_{crit} in the chloride containing solution (2.5 mA/cm^2) is lower than that obtained in the earlier case without chloride ions (11.2 mA/cm^2) and this may be due to the formation of metallic chlorides on the surface of the intermetallic which should lower the apparent surface area and result in a lower value of i_{crit}, as observed experimentally. However, this is in contrast to the behavior in Cr containing steels where the presence of chloride ions generally results in increased i_{crit}. The passive range (0.45 V) in this case is lower than in the earlier case (0.7 V) and this due to the fact that the first breakdown potential is lower in this case compared to the earlier case. This indicates that the chloride ions destabilize the passive layer on the surface of Fe_3Al-5Cr in acidic solutions. The unstable nature of the passive film in the presence of chloride ions is further reflected in the very high current densities drawn and the active value of zero current potential on reversing the scan.

The cyclic polarization behavior of Cr-alloyed Fe-28Al has been studied by Kim and Buchanan [36] and they have observed that increasing amounts of chromium additions increased the passive range and the presence of chloride ions in the solution resulted in lower breakdown potentials. Addition of Mo in addition to Cr enhanced the pitting resistance in the presence of chloride ions [36]. In the present study , it was observed that the addition of Cr to Fe_3Al increased the passive range and also resulted in a lower i_{crit}. Moreover, the potential at which complete passivity and primary passivity is established is also lowered with Cr addition. These behaviors are similar to that obtained when Cr is alloyed to Fe as has been extensively reported in the literature [46,47,53]. Therefore the addition of Cr to Fe_3Al generally

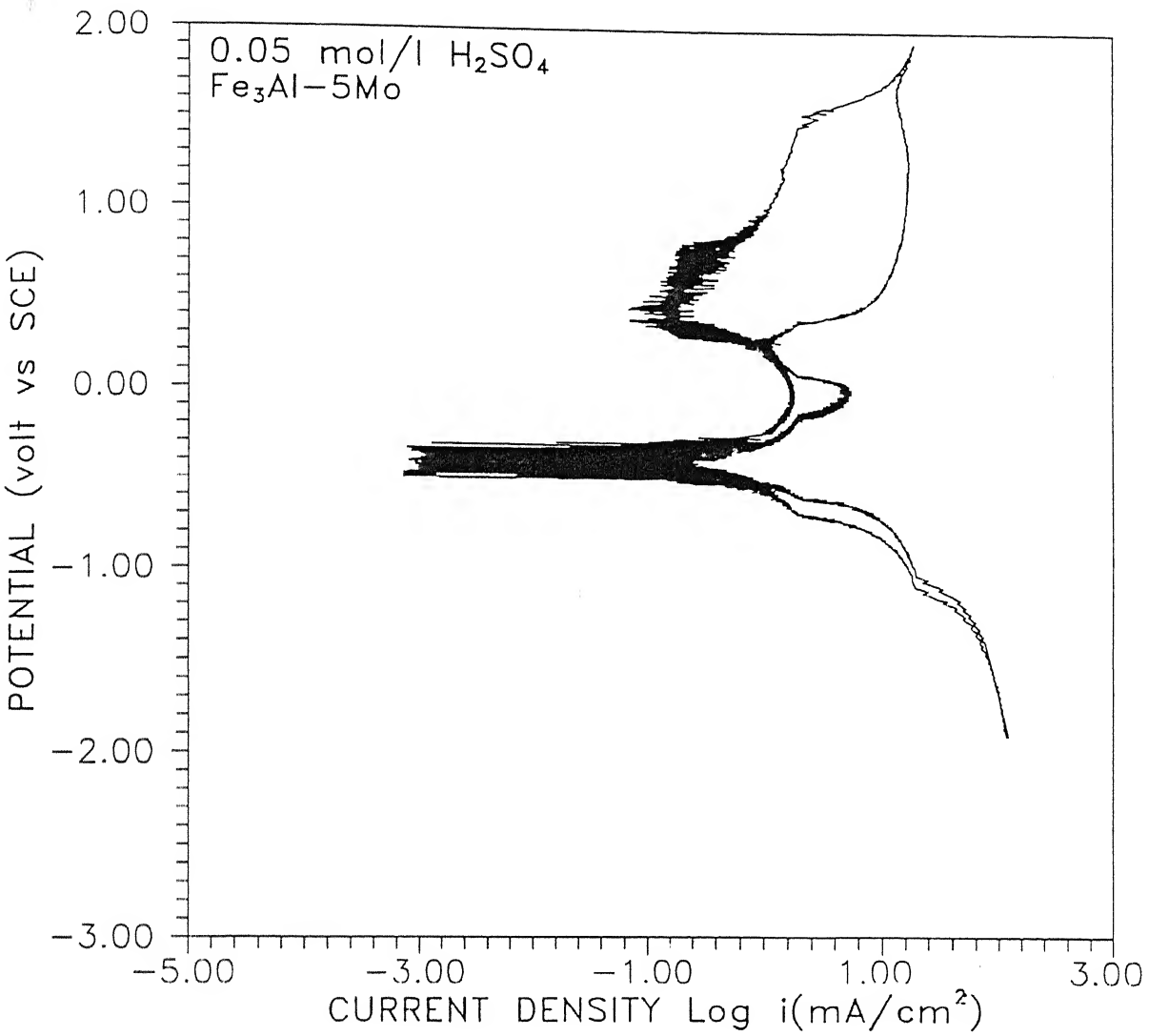

Figure 4.21 Cyclic polarization curve of Fe_3Al-5Mo intermetallic in 0.05 mol/l H_2SO_4.

lower value of potential (in the transition region between active and passive behavior) than in the case of the Cr-alloyed intermetallic. Higher currents are drawn between the potential at which the scan is reversed and the potential at which it intersects the forward scan curve. It is interesting to note that the ZCP on reverse scanning occurs at nearly the same potential as in the forward scan, similar to that obtained with the Cr-alloyed intermetallic.

The potentiodynamic polarization curves (forward and reverse scans) for Fe_3Al-5Mo in the acidic H_2SO_4 solution with 200 ppm chloride ions are presented in Figure 4.22. The polarization curve exhibits active-passive behavior in the forward scan. Similar to the behavior in the solution without chloride ions, the zero current potential (-0.45 V vs SCE) on forward scanning is similar to the the stabilized free corrosion potential (-0.40V vs SCE). Note that the i_{crit} in the chloride containing solution (6.3 mA/cm^2) is higher than that obtained in the earlier case without chloride ions (1.99 mA/cm^2). Moreover, the passive current density (i_{pass}) is much higher in the presence of chloride ions (1.58 mA/cm^2) compared to the earlier case without chloride ions (0.39 mA/cm^2). The passive range (0.3 V) in this case is lower than in the earlier case (0.5 V). This indicates that the chloride ions destabilize the passive layer on the surface of Fe_3Al-5Mo in acidic solutions. The unstable nature of the passive film in the presence of chloride ions is further reflected in the very high current densities drawn and the active value of zero current potential on reversing the scan.

It is well known that addition of Mo enhances the passivity of stainless steels by increasing the pitting potential [46,51,54]. Moreover, Mo increases the passivity of Fe-alloys.For example, addition of Mo (1 to 3%) in Fe-23Cr alloy enhances passivity by decreasing E_{pp} and i_{crit} in 1N H_2SO_4 [55]. It is well known that addition of small amount (2%) of Mo Type 304 stainless steel to produce 18-8SMo (type 316) increases the pitting potential, decreases i_{crit}, reduces i_{pass} (with slight changes in

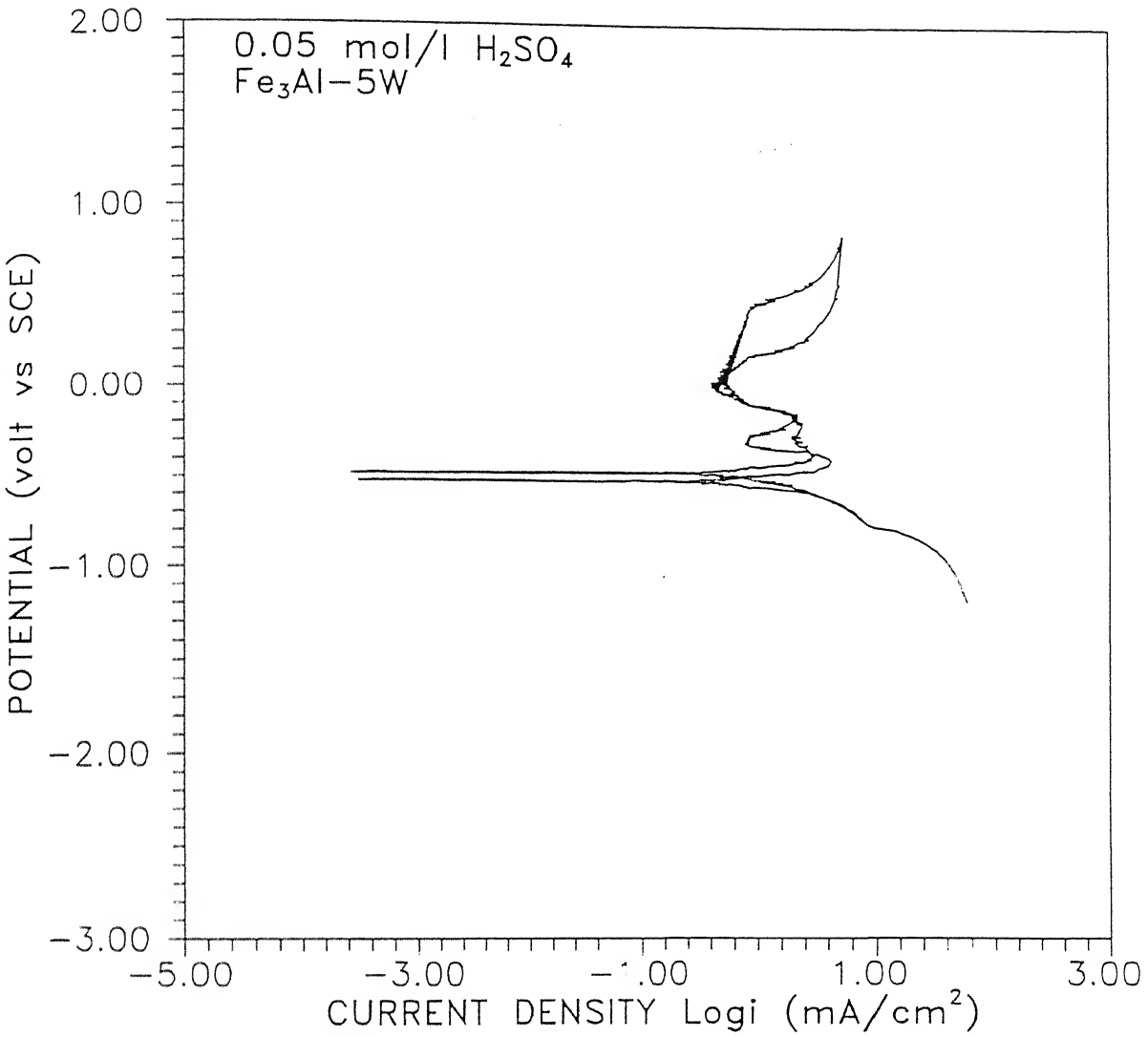

Figure 4.23 Cyclic polarization curve of Fe_3Al-5W intermetallic in 0.05 mol/l H_2SO_4.

the primary passivation potential but decrease in the complete passivation potential), increases stability in the passive region by increasing the film breakdown potential and also shifts the transition potential in the positive direction, thereby delaying the transition into the transpassive state [46]. These also seem to apply when Mo is added to Fe_3Al. Therefore the addition of Mo to Fe_3Al generally enhances the passive behavior of the base intermetallic. In an earlier study, the enhanced passivity due to Mo addition was also observed in H_2SO_4 solution of pH 4 [10].

Kim and Buchanan [36] have shown that the pitting resistance of Cr-alloyed Fe_3Al was poor. Addition of 2% Mo was found to be sufficient to provide resistance to chloride-induced pitting to the Fe-28Al-4Cr intermetallic. Therefore, the addition of Mo along with Cr enhances passivity by resisting breakdown of the passive film even in the presence of chloride. The present study also shows that plain Mo addition also enhances the passive behavior of the base Fe_3Al intermetallic.

It must be mentioned that the addition of Mo did not result in significant ductilities although there is an enhancement in passivity with the alloying addition. This could be most probably due to the formation of the ternary intermetallics in this intermetallic with the addition of Mo (see section 4.1) which most probably embrittles the material.

4.3.9 Fe_3Al-5W

The potentiodynamic polarization curve (both forward and reverse scans) for Fe_3Al-5W in the acidic H_2SO_4 solution without chloride ions are presented in Figure 4.23. The intermetallic exhibited active-passive behavior in this electrolyte as can be seen from the forward scan and this is in contrast to the active behavior observed earlier for the base Fe_3Al intermetallic. It appears that there are two passive regions present with both the passive regions showing distinct bumps. This becomes apparent during the reverse scanning, to be discussed below. The stabilized FCP for this intermetallic was -0.55 V vs SCE and the ZCP on

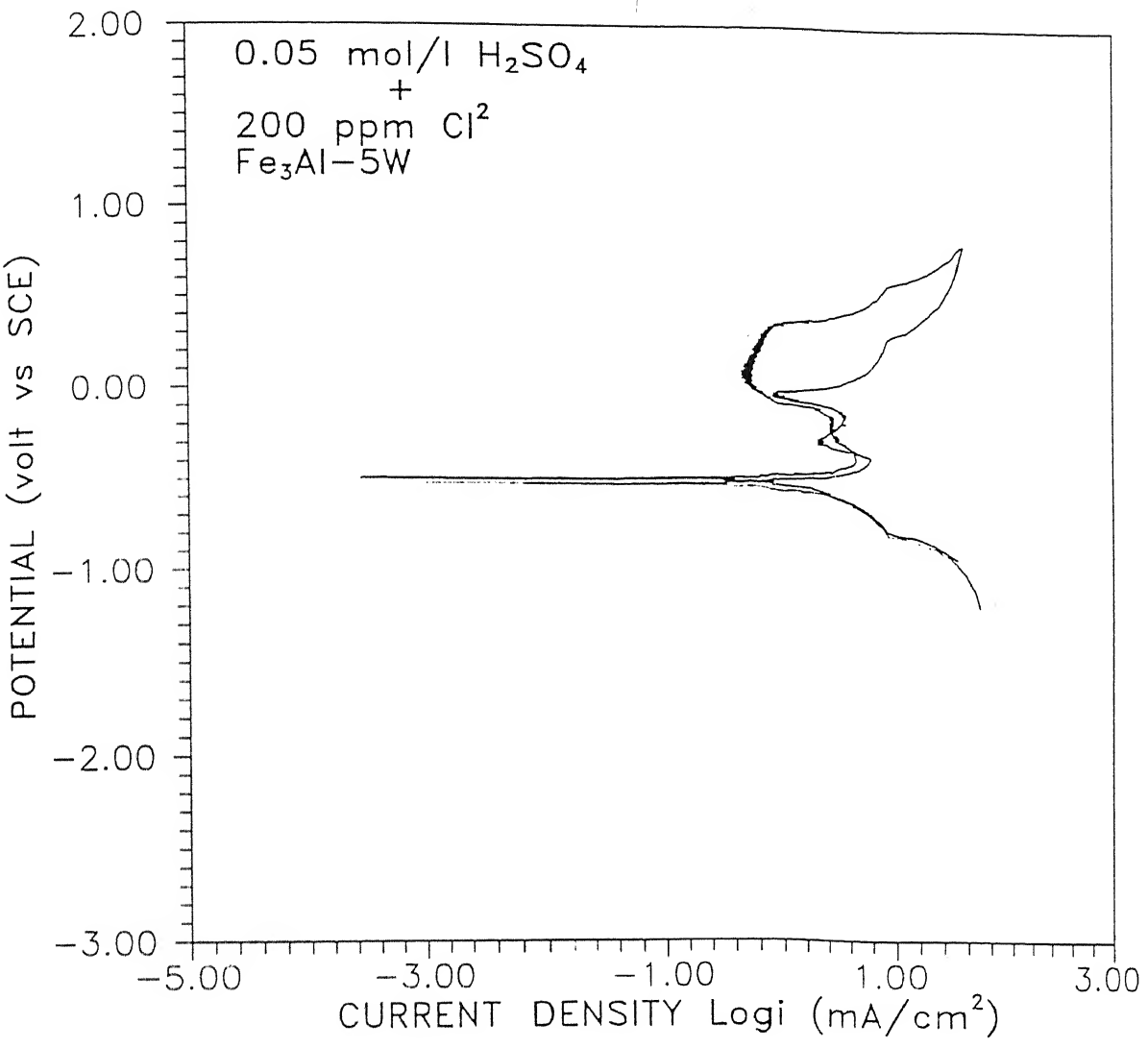

Figure 4.24 Cyclic polarization curve of Fe_3Al-5W intermetallic in 0.05 mol/l H_2SO_4 with 200ppm of Cl^-.

scanning from the cathodic to the anodic (active to noble) direction is -0.50 V vs SCE. The value of the critical current density for passivation (i_{crit}) is 3.55 mA/cm^2 and this is lower than the i_{crit} of unalloyed Fe_3Al during the reverse scan in the same electrolyte. The passive range extends to about 0.6 V and this is higher than the passive range obtained in unalloyed Fe_3Al in the reverse scan. The breakdown potential (0.45 V) can be identified from the forward polarization curve. The passive range is lower on reverse scanning from the noble to active potential. The nature of the curve on reverse scanning indicates the moderate re-passivation characteristics of the W-alloyed intermetallic as the reverse scan does not trace the original forward scan in the initial period of the scan and the forward scan is intersected in the passive region. Higher currents are drawn between the potential at which the scan is reversed and the potential at which it intersects the forward scan curve. It is interesting to note that the ZCP on reverse scanning occurs at nearly the same potential as in the forward scan, similar to that obtained with the Cr-alloyed intermetallic. Another interesting feature of the reverse polarization curve is that the existence of two passive regions is indicated. The first passive region that obtains on reverse scanning is most probably due to the alloyed element W and the second passive region (that occurs just above the ZCP) could be due to Al as passivity was exhibited by Fe_3Al during reverse scanning around the same potentials see(Figure 4.5).

The potentiodynamic polarization curves (forward and reverse scans) for Fe_3Al-5W in the acidic H_2SO_4 solution with 200 ppm chloride ions are presented in Figure 4.24. The polarization curve exhibits active-passive behavior in the forward scan. Similar to the behavior in the solution without chloride ions, the zero current potential (-0.50 V vs SCE) on forward scanning is nearly the same as the stabilized free corrosion potential (-0.54 V vs SCE). Note that the i_{crit} in the chloride containing solution (3.98 mA/cm^2) is higher than that obtained in the earlier case without chloride ions. Moreover, the passive current density

Table 4.3

Potential for Primary Passivation (E_{pp}) and Potential for Complete Passivation (E_{cp}) of the Intermetallics in 0.05 mol/l H_2SO_4, without and with 200 ppm chloride ions. All the potentials are in volt versus SCE.

INTERMETALLICS	Acid		Acid + Cl^-	
	E_{pp}	E_{cp}	E_{pp}	E_{cp}
Fe_3Al	-0.0	+0.1	---active--	
Fe_3Al-5Ti	-0.4	0.0	-0.4	0.0
Fe_3Al-5Zr	-0.4	-0.3	-0.3	-0.1
Fe_3Al-5V	----active----		----active---	
Fe_3Al-5Nb	-0.3	-0.1	-0.3	-0.1
Fe_3Al-5Ta	-0.3	0.0	-0.3	-0.05
Fe_3Al-5Cr	-0.4	-0.2	-0.4	-0.3
Fe_3Al-5Mo	0.0	+0.3	-0.3	+0.4
Fe_3Al-5W	-0.3	-0.1	-0.2	-0.0

(i_{pass}) is similar both in the presence and absence of chloride ions (1.58 mA/cm^2). The passive range (0.4 V) in this case is slightly lower than in the earlier case (0.6 V). This indicates that the chloride ions destabilize the passive layer on the surface of Fe_3Al-5W in acidic solutions. The unstable nature of the passive film in the presence of chloride ions is further reflected in the higher current densities drawn on reversing the scan. Notice that similar to the polarization behavior in the acidic solution without the chloride, the reverse scan exhibits the presence of two passive regions. As mentioned earlier, the passive region occurring nearer to the ZCP could mostly arise due to Al.

It has been previously reported that addition of 5-6% W to Type 304 steel notably reduced i_{pass} [54]. W additions also shift the (primary and complete) passivation potentials in the positive direction [55]. In contrast, W addition to Fe_3Al decreases the E_{pp} and E_{cp}. However, the film breakdown potential also changes in the positive direction with W addition, similar to that reported for stainless steels [46,51]. In the case of Fe_3Al, the present study clearly shows that addition of W provides passivity to the base intermetallic and moreover aids the formation of passive layer due to Al on the surface.

4.3.10 COMPARISON OF INTERMETALLICS IN ACIDIC MEDIUM

It can be noted from the earlier sub-sections that the base intermetallic and the Fe_3Al-5V intermetallic exhibited active behavior in the acidic medium while all the other intermetallics exhibited active-passive behavior in this electrolyte. The polarization behavior of the active-passive intermetallics would be compared in the present section. In these discussions, it is assumed that the V-containing intermetallic is not referred while mention is made of passivity-inducing element alloyed intermetallic as it exhibits active behavior in the acidic medium.

The ZCP on forward scanning is generally similar to the stabilized free corrosion potential in the acidic medium (both

Table 4.4

Breakdown Potential of the Intermetallics in 0.05 mol/l H_2SO_4, without and with 200 ppm chloride ions. All the potentials are in volt versus SCE.

INTERMETALLIC	Acid		Acid + Cl^-	
	E_{bI}	E_{bII}	E_{bI}	E_{bII}
Fe_3Al	+0.2	+0.5	0.0	0.3
Fe_3Al-5Ti	+0.6	+1.5	+0.2	+1.0
Fe_3Al-5Zr	+0.2	--	+0.1	--
Fe_3Al-5V	----active----		----active----	
Fe_3Al-5Nb	+0.2	+0.7	+0.1	+0.7
Fe_3Al-5Ta	+1.0	+1.6	+0.6	--
Fe_3Al-5Cr	+0.5	+1.5	+0.2	+1.5
Fe_3Al-5Mo	+0.8	+1.6	+0.7	+1.4
Fe_3Al-5W	+0.5	--	+0.4	+0.6

materials and cause localized corrosion. It must be recollected that when the cyclic polarization behavior of the intermetallics was presented and discussed earlier, it was noticed that much larger current densities were obtained on reversing the scan in the case of chloride-containing solution and this indicates that the presence of chloride does not permit fast re-passivation of the pitted surface, thereby resulting in this behavior.

The passive ranges observed in the forward polarization of the alloyed intermetallics are presented in Table 4.5 from where it can be concluded that the passive region is larger in the case of the alloyed intermetallics when compared to the base intermetallic and secondly, the passive range is decreased in the presence of chloride ions. Interestingly, the passive range is maximum for the Fe_3Al-5Ta and Fe_3Al-5Mo intermetallics in the solution, without and with chlorides, respectively. The observations are consistent with the known effect of alloying with passivity-inducing elements [10] and chlorides on passivity [48,46].

The critical current density for passivation (i_{crit}) and the passive current density (i_{pass}) obtained from the forward polarization curves of the intermetallics are presented in Table 4.6. The i_{crit} of Fe_3Al is lowered upon alloying with passivity-inducing element and this is beneficial as passivity can be attained with a lower amount of imposed cathodic current (either imposed externally or by the cathodic reduction reactions). Moreover, the i_{crit} is higher in the presence of chloride ions except in the case of the Ti-, Cr- and Mo-containing intermetallic. The reason for the anomalous behavior for these two intermetallics has been addressed earlier in the subsection dealing with Fe_3Al-5Cr. The increase in i_{crit} in the presence of chloride has been observed for other active-passive alloys [46] and this appears to be the case also for the alloyed iron aluminides. As regards i_{pass}, it is lowered with alloying addition. This is the expected behavior on alloying passivity-inducing element to a metal as has been observed for

Table 4.6

Critical Current Density (i_{crit}) and Passivation Current Density (i_{pass}) of the intermetallics in 0.05 mol/l H_2SO_4 with and without 200 ppm chloride ions. All the currents are in mA/cm^2.

INTERMETALLIC	Acid		Acid + Cl^-	
	i_{crit}	i_{pass}	i_{crit}	i_{pass}
Fe_3Al	19.95	2.51	----active----	
Fe_3Al-5Ti	1.99	0.16	1.41	0.16
Fe_3Al-5Zr	3.98	0.4	1.0	0.03
Fe_3Al-5V	----active----		----active----	
Fe_3Al-5Nb	0.4	0.16	0.63	0.12
Fe_3Al-5Ta	3.98	1.26	5.01	0.63
Fe_3Al-5Cr	11.20	0.2	2.5	0.2
Fe_3Al-5Mo	1.99	0.39	6.3	1.58
Fe_3Al-5W	3.55	0.63	3.98	0.63

several Fe based alloys. Moreover, the i_{pass} does not significantly change in the presence of chloride ions for the Ti-, Cr-, and W-containing intermetallics whereas it increases in the case of Mo-containing intermetallic and decreases, surprisingly, in the case of the Zr- and Ta-containing intermetallics.

In summary, it is seen that the presence of chloride ions generally destabilize the passive layer on the surface of the intermetallics and the re-passiviation behavior is not fast. The addition of passivity-inducing elements in Fe_3Al results in the base Fe_3Al acquiring active-passive behavior and most of the electrochemical parameters change in the correct direction such that passivity is enhanced due to the alloying addition (for example, E_{pp} and E_{cp} decreases on alloying whereas the passive range increases with alloying).

The above observations on the effect of alloying on the polarization behavior of the base intermetallic could be explained as follows. Alloying with an element that readily passivates into a metal or alloy causes the metal or alloy to develop, either fully or partially , the passive properties of the introduced material [46]. Therefore, alloying Fe_3Al with passivity inducing components enhanced the passive behavior of binary Fe_3Al, as obtained in the present study. The passivating effect of such alloying elements can be attributed to the following reasons. Firstly, the enrichment of stable passive atoms in the surface of the alloy, by the formation of ordered structures with the alloying component, would result in enhanced passive behavior. This could be the case on alloying with Zr, Nb, Ta, Mo and W as the XRD patterns of the intermetallics containing these additions revealed the presence of additional phases (see section 4.1). Secondly, a change in the internal electronic structure of the atoms by the formation of solid solutions could result in enhanced passivity [56]. This could be the case on alloying with Cr and Ti as they exist in solid solution in Fe_3Al and, moreover, the vacancies in the 3d electron level of Ti and Cr allow electron transfer from iron and aluminum, thereby rendering them into

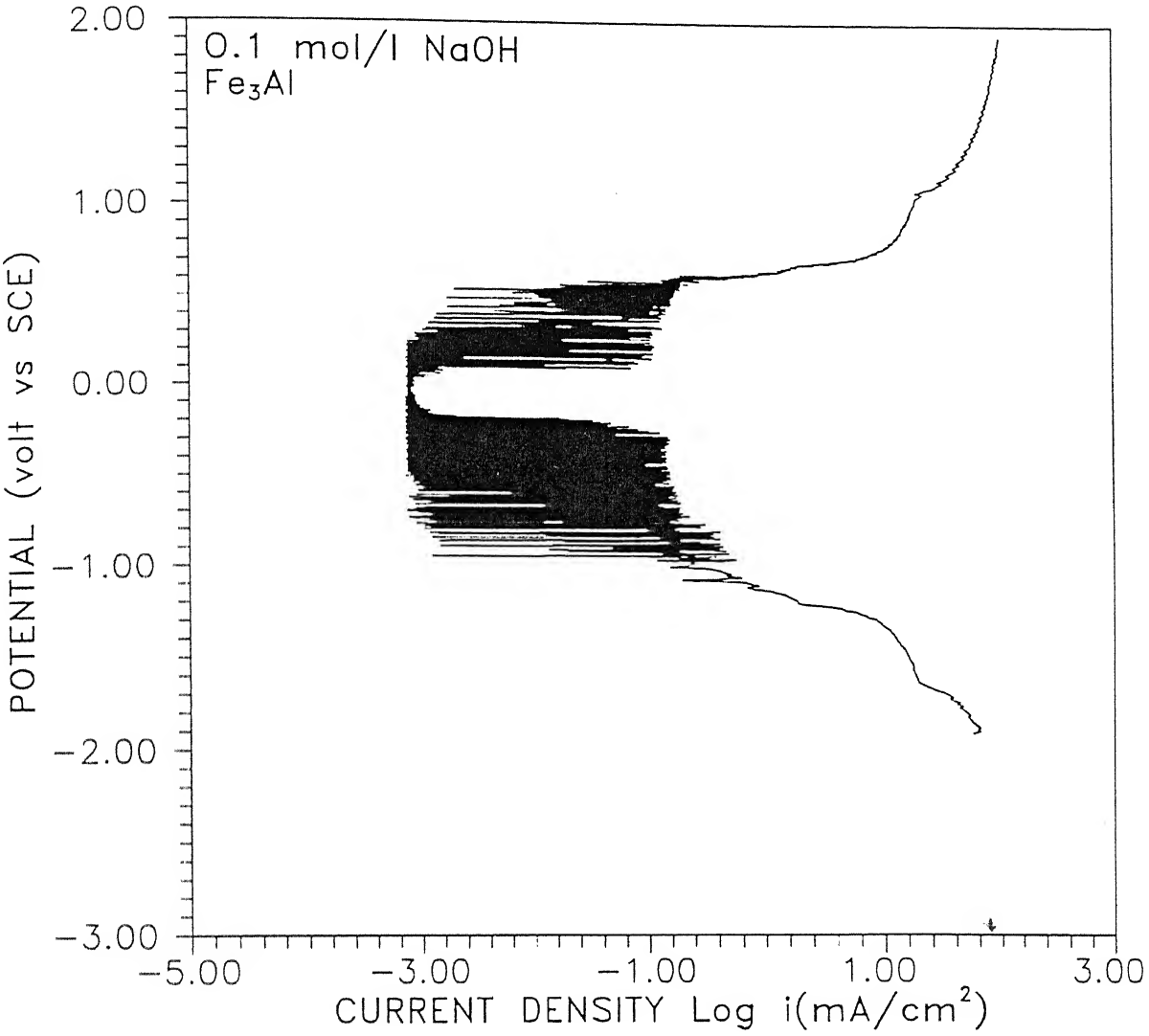

Figure 4.25 Forward polarization curve of Fe_3Al base intermetallic in 0.1 mol/l NaOH.

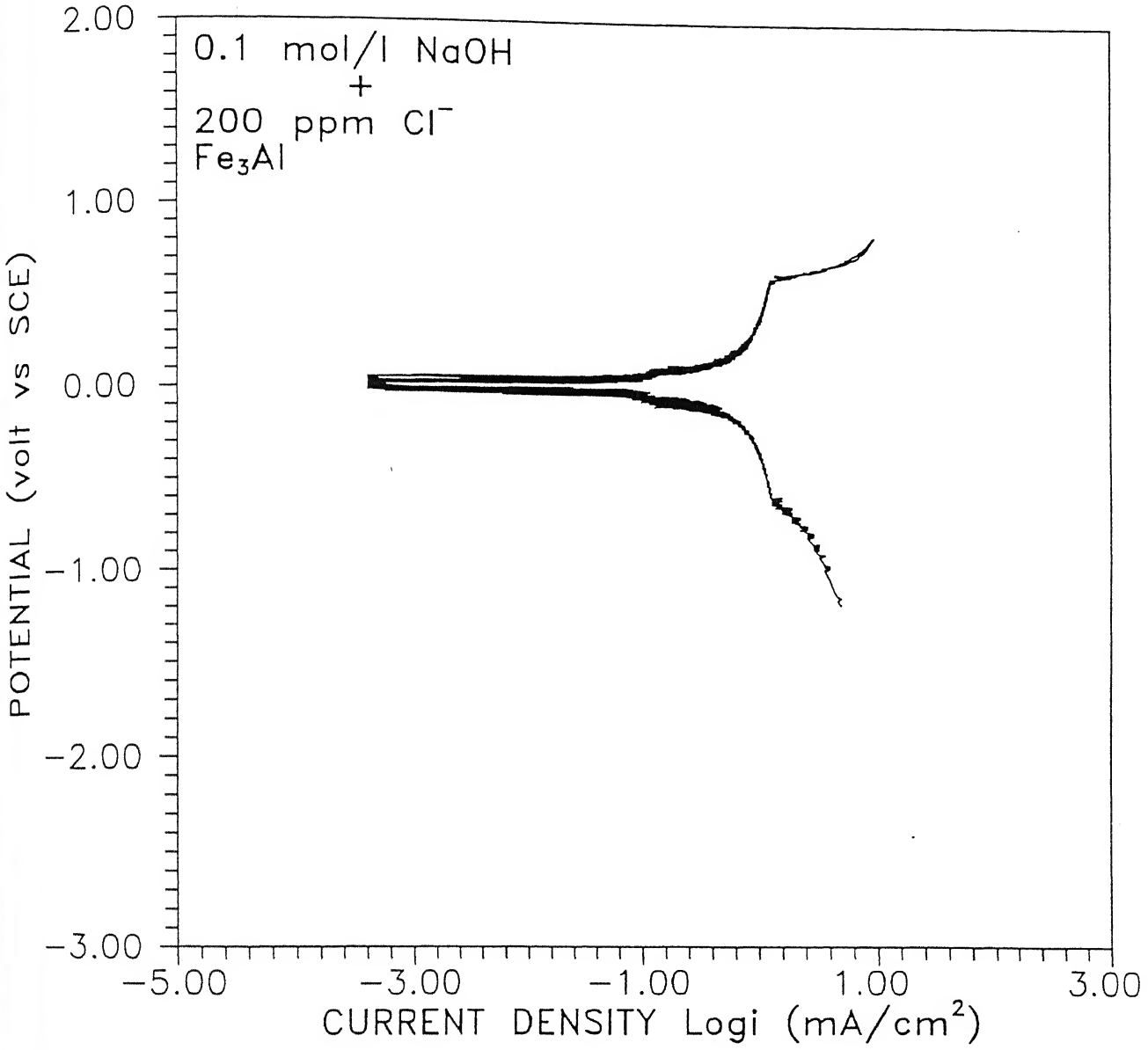

Figure 4.26 Forward polarization curve of Fe_3Al base intermetallic in 0.1 mol/l NaOH with 200 ppm Cl^-.

passive states, as has been shown for Cr alloyed to Fe [56]. Thirdly, it is possible that there is a gradual enrichment in the surface layer of the Fe_3Al-5M intermetallics with atoms of more stable/passive component due the corrosion process. This increase in the concentration of the passivity-inducing component of the alloy could lead to the formation of either new surface structures (intermetallic compounds) or even a surface layer of the alloyed component. This process should confer additional passivity. In this regard, it was earlier observed that the corrosion of FeAl in NaOH solution resulted in surface enrichment of Fe due to preferential dissolution of Al [39]. It is reasonable to assume that in the present intermetallics, the concentration of the passivity inducing elements (i.e, the alloying elements) would have been enhanced in the surface layers resulting in the superior passivation behavior of the alloyed Fe_3Al-5M intermetallics.

4.4 ELECTROCHEMICAL BEHAVIOR IN ALKALINE MEDIUM

Cyclic potentiodynamic polarization curves were also obtained for all the intermetallics in alkaline NaOH solution, both without and with chlorides. The potentiodynamic polarization scan for the base Fe_3Al intermetallic in 0.1 mol/l NaOH, without and with chlorides are presented in Figure 4.25 and 4.26, respectively. The polarization behavior were similar in the forward and reverse scans and only the forward scans are presented for experiments conducted in NaOH without chlorides. A small passive region is indicated in polarization curves obtained in the alkaline solution without the presence of chlorides. The polarization curves also indicate that the intermetallic attains stable passivity in this electrolyte as the polarization curve on forward scanning does not indicate the hump characteristic of i_{crit}. Moreover, the passivity is also exhibited even on reverse scanning from the noble potential. The behavior is similar to that obtained earlier with Fe_3Al [41]. The polarization curve in the alkaline solution with 200 ppm chloride ions indicate that the intermetallic exhibits active behavior. Incidentally, the ZCP in this electrolyte is

obtained in the same region of potential in which passive behavior was seen when the polarization scan was performed in the alkaline solution without the chlorides. This could possibly indicate that the passive region is lowered in this case compared to the case without the chloride ions. Interestingly, the polarization behavior in alkaline solution, without and with chloride ions, was similar for Fe_3Al alloyed with Ti (Figure 4.27 and 4.28), Ta (Figure 4.29 and 4.30), Cr (Figure 4.31 and 4.32) and Mo (Figure 4.33 and 4.34). These scans indicate that the nature of the surface of these alloyed intermetallics is very similar in the alkaline electrolyte. Moreover, it is interesting to note that in the case of the Fe_3Al-5Ta intermetallic, the polarization behavior on the forward scan indicated active-passive behavior in the solution without out the chloride ions. In the case of the intermetallics alloyed with Zr, Nb, V and W, the polarization behavior in the alkaline solution with and without chloride was very similar. They exhibit active behavior in the alkaline solution, both with and without chlorides. Typical polarization behavior for these intermetallis in the alkaline solution without and with chlorides are presented in Figures 4.35 and 4.36. The reason for the active behavior is improperly understood. It is quite probable that the nature of the surface in these intermetallics in the alkaline medium is very similar. It is to be noted that this characteristic behavior is observed for the alloys for which the polarization specimen were obtained after melting (without the thermomechanical processing) and that they were all obtained at a similar time in the experimental work later than that for the other intermetallics. Therefore, the systematic error due to malfunctioning of the potentiostat cannot be ruled out. This seems probable as the stabilized free corrosion potentials for these intermetallics in the alkaline solution is different from the ZCPs (a constant value of 0.0 V vs SCE) that obtain from the polarization curves. Although the results repeated in duplicate testing, further experiments have to be conducted preferably using another potentiostat to validate the results.

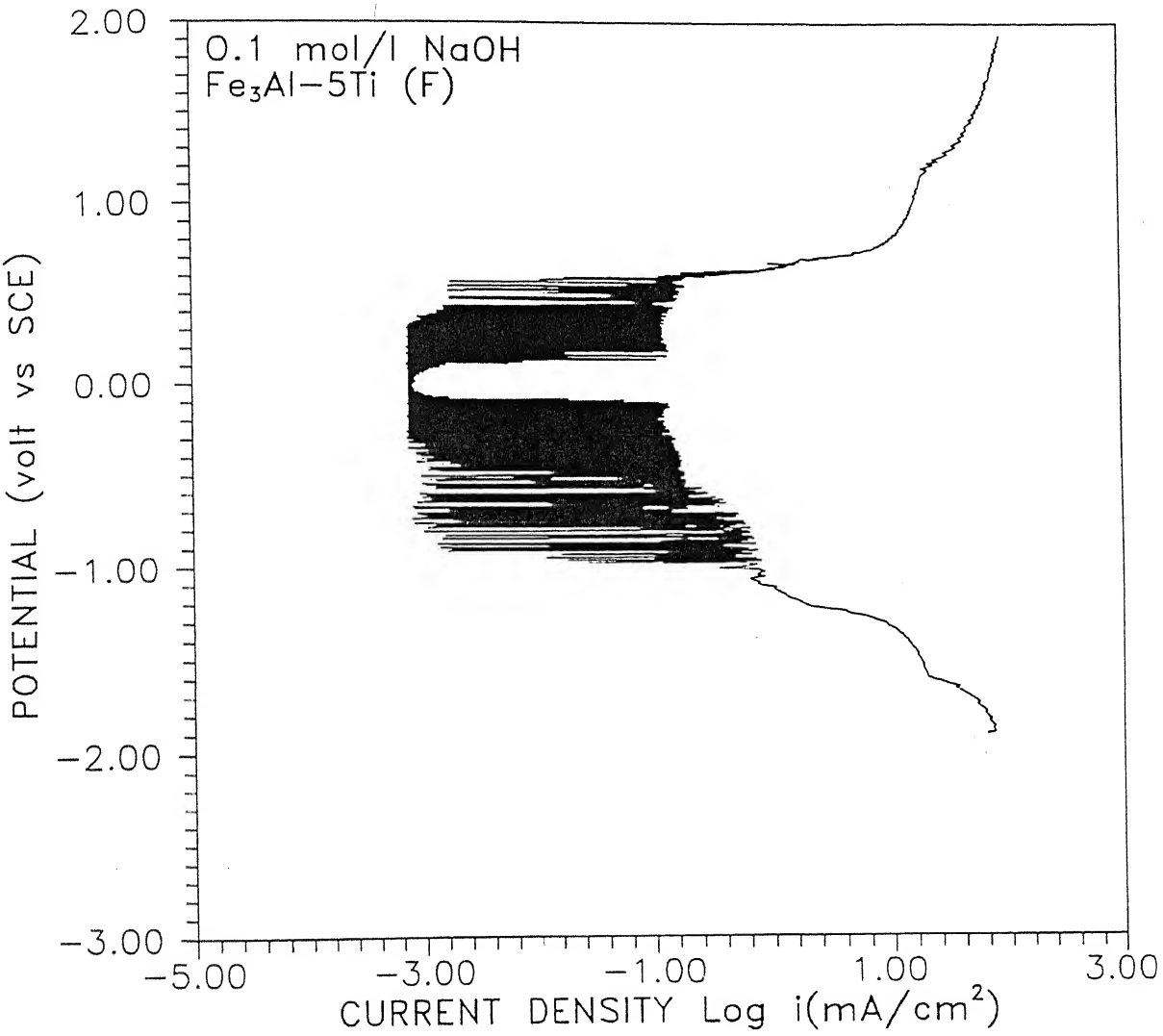

Figure 4.27 Forward polarization curve of Fe_3Al-5Ti intermetallic in 0.1 mol/l NaOH.

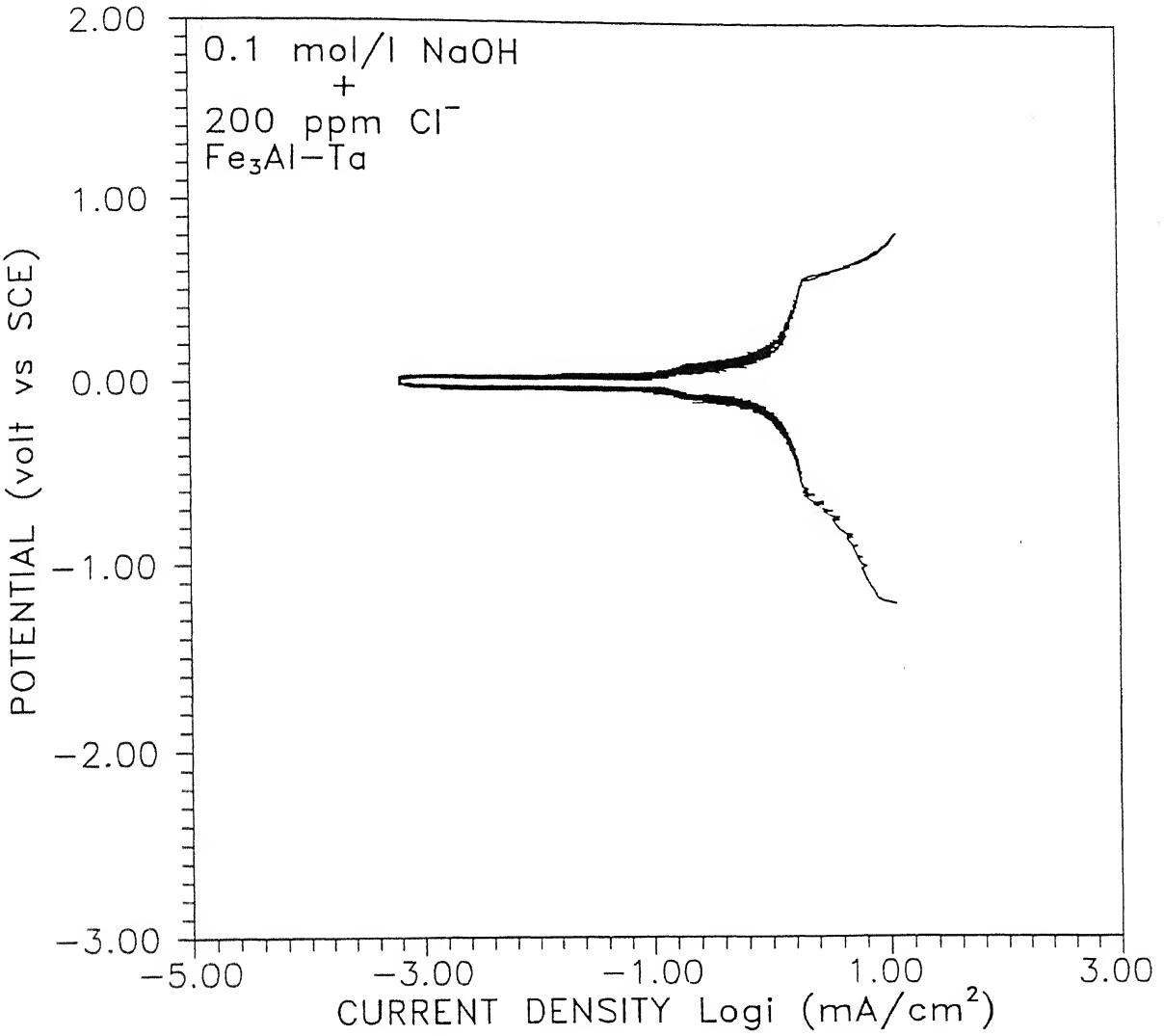

Figure 4.30 Forward polarization curve of Fe_3Al-5Ta intermetallic in 0.1 mol/l NaOH with 200 ppm Cl^-.

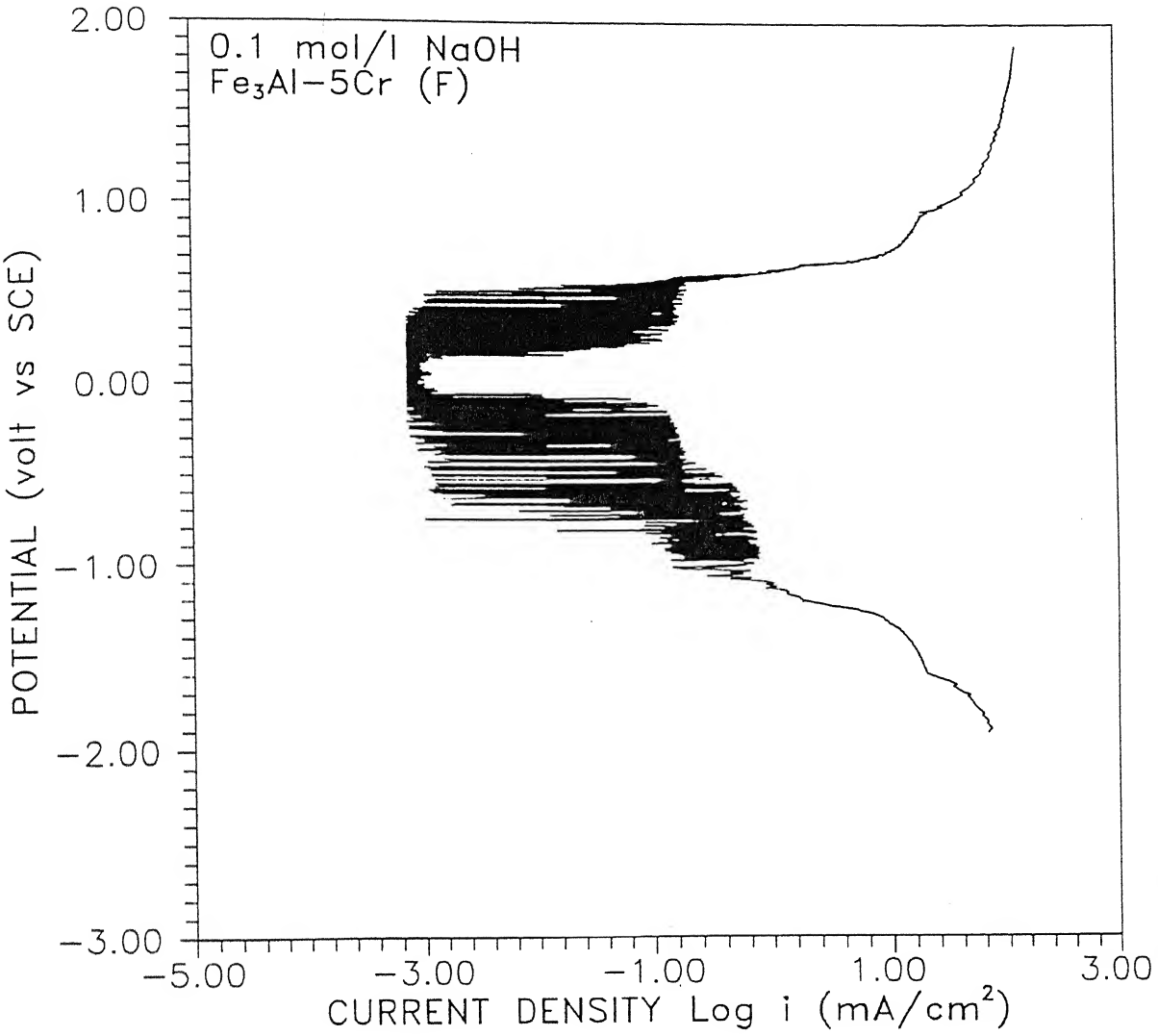

Figure 4.31 Forward polarization curve of Fe_3Al-5Cr intermetallic in 0.1 mol/l NaOH.

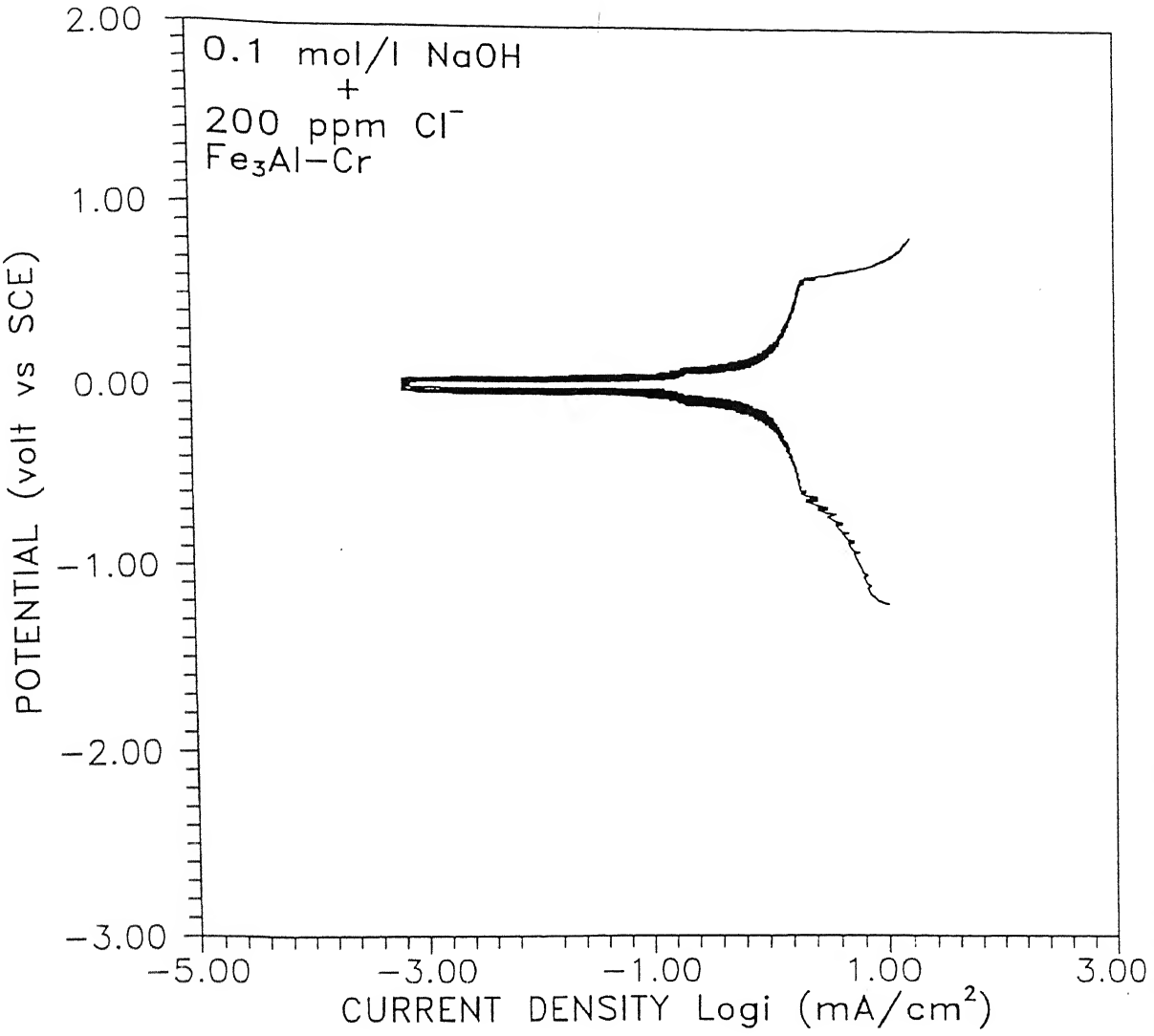

Figure 4.32 Forward polarization curve of Fe_3Al-5Cr intermetallic in 0.1 mol/l NaOH with 200 ppm Cl^-.

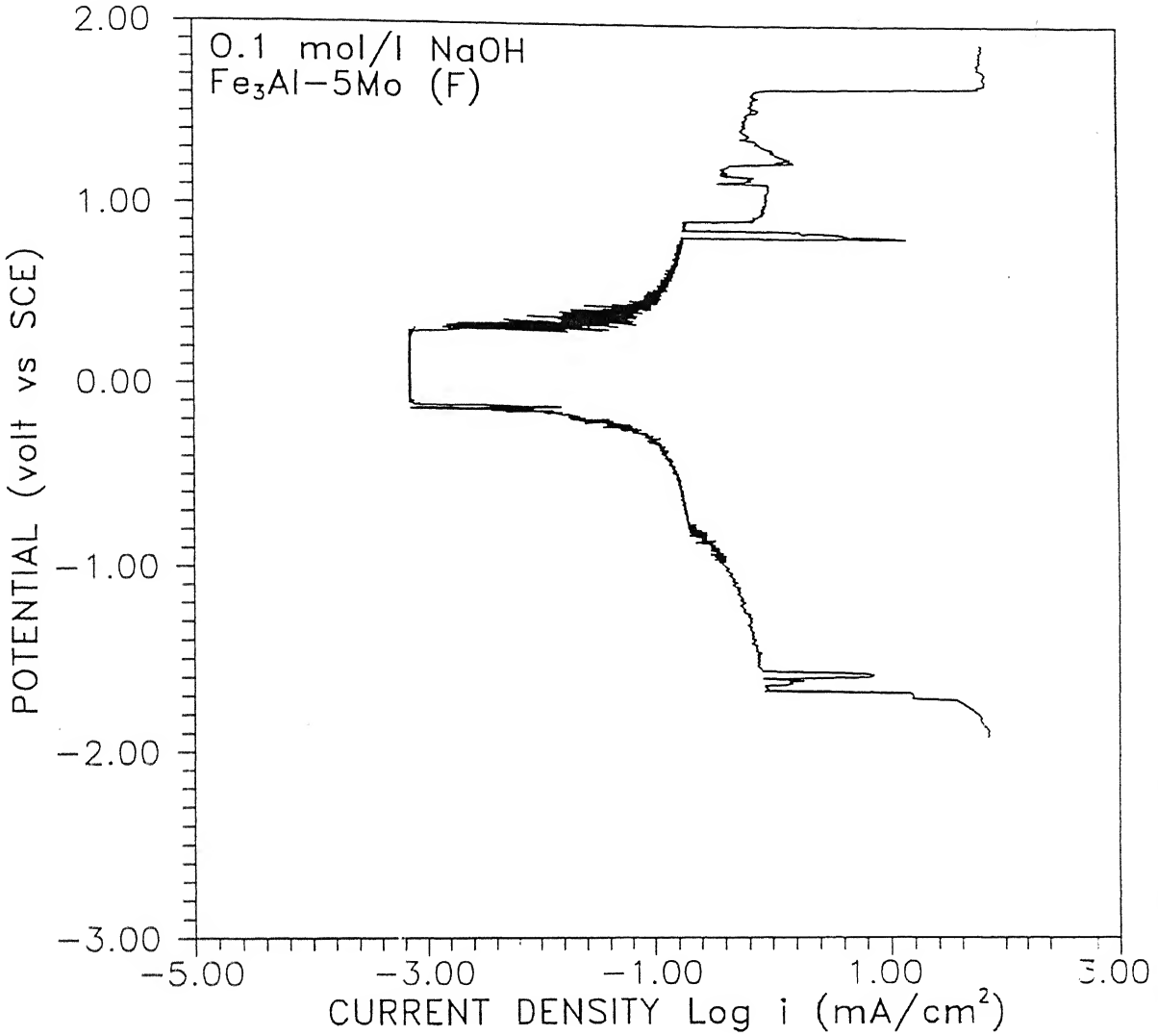

Figure 4.33 Forward polarization curve of Fe_3Al-5Mo intermetallic in 0.1 mol/l NaOH.

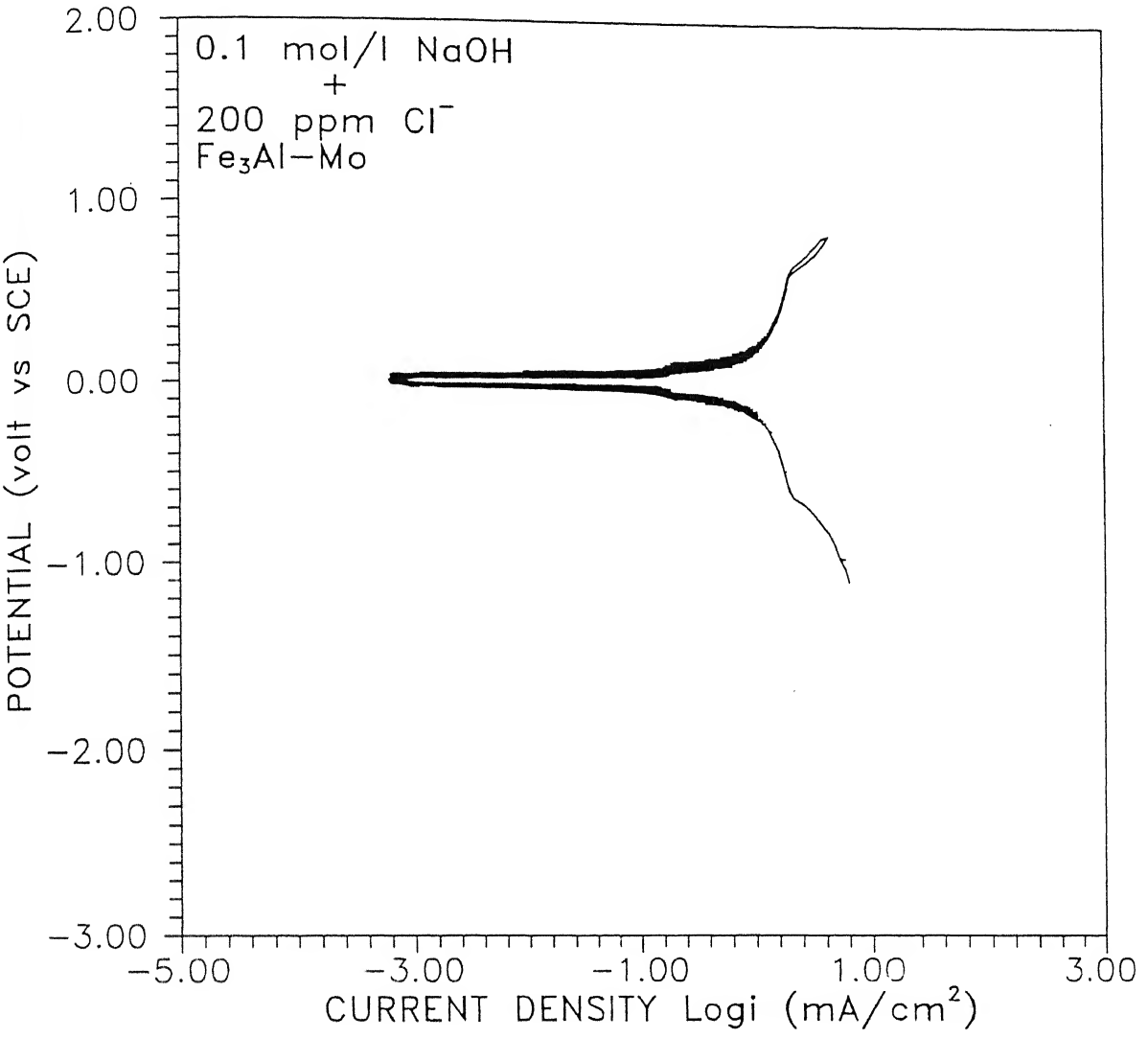

Figure 4.34 Forward polarization curve of Fe_3Al-5Mo intermetallic in 0.1 mol/l NaOH with 200 ppm Cl^-.

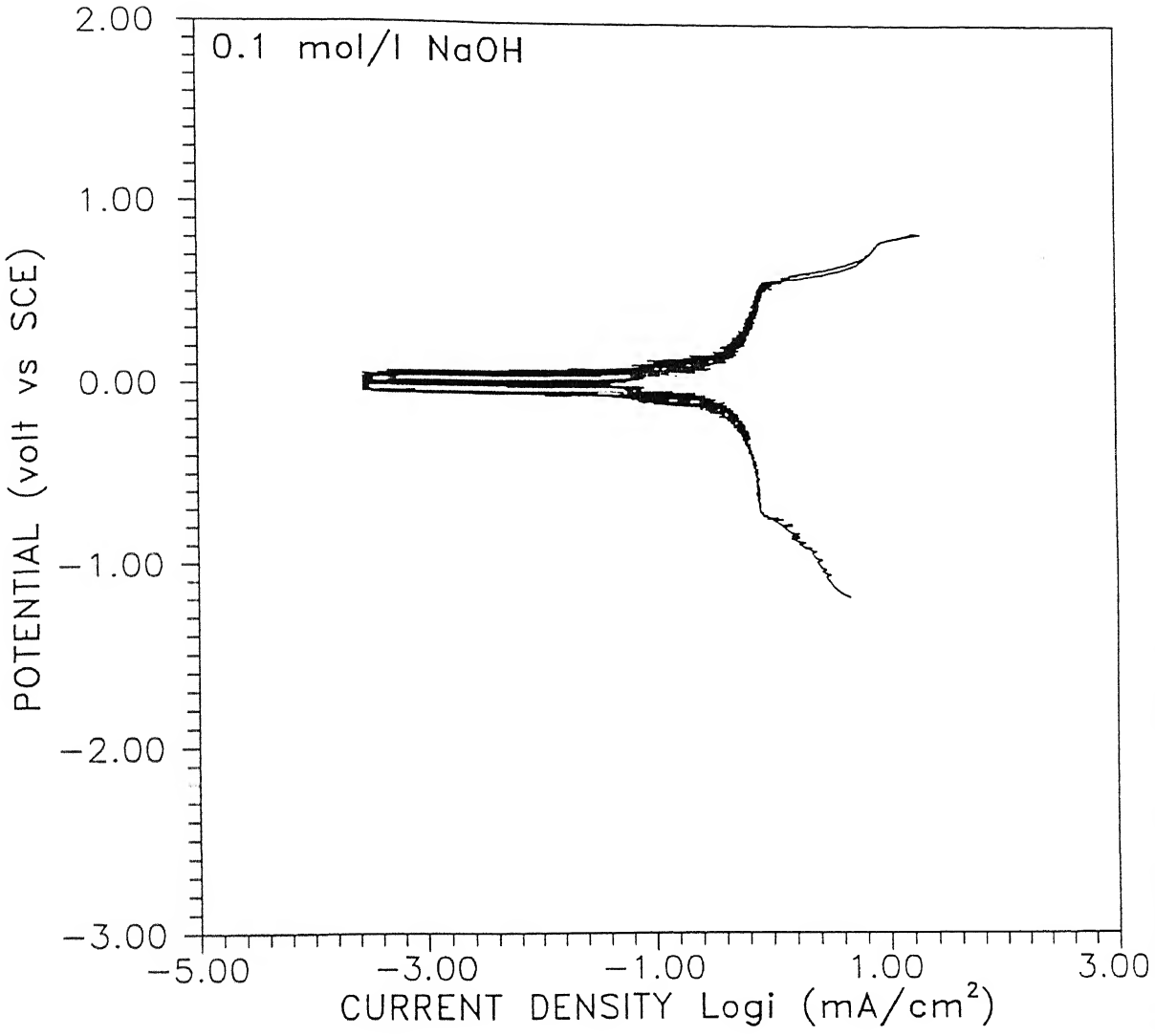

Figure 4.35 Typical polarization curve of Fe_3Al-5M (M = Zr, V, Nb and W) intermetallic in 0.1 mol/l NaOH.

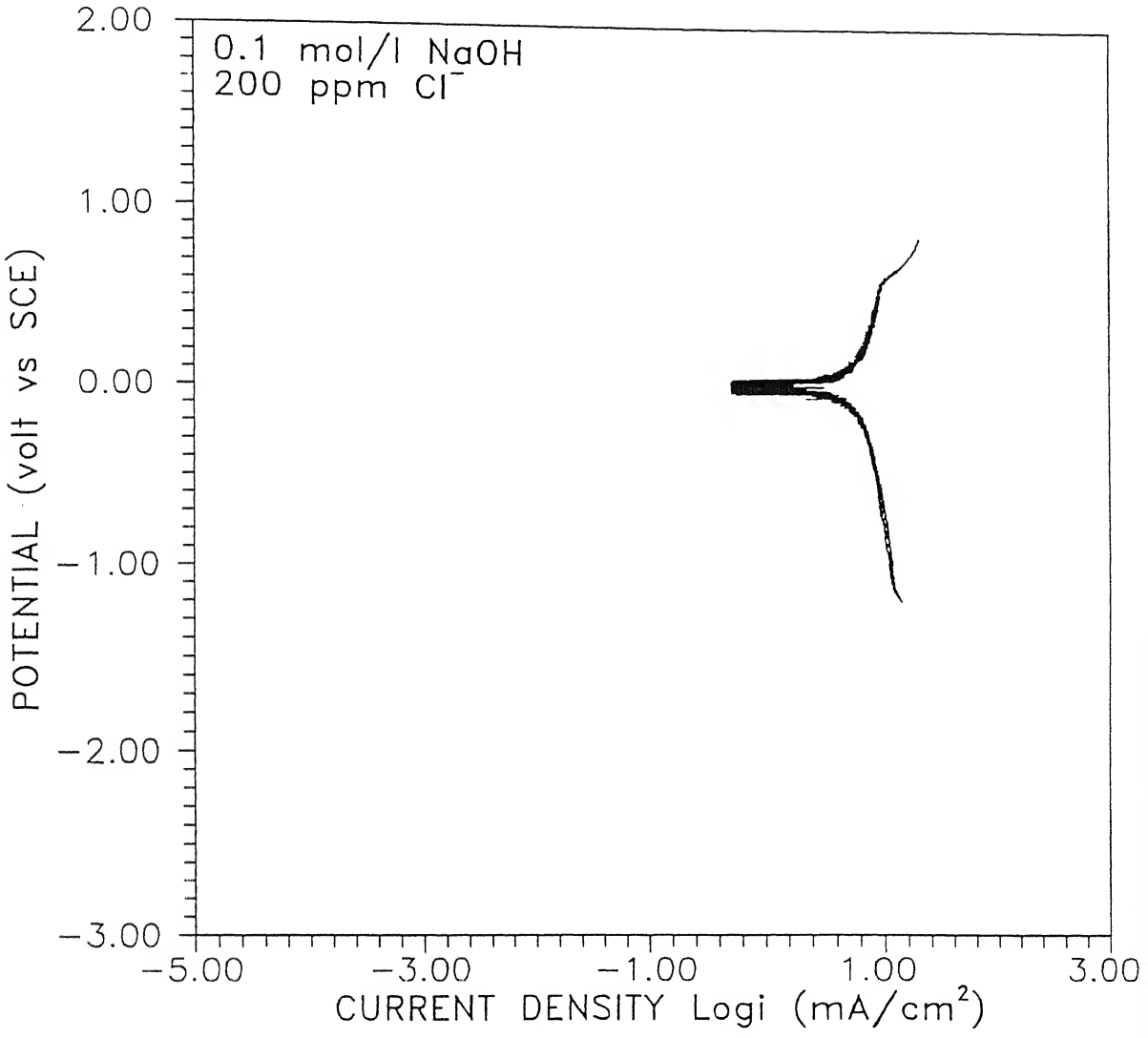

Figure 4.36 Typical polarization curve of Fe_3Al-5M (M = Zr, V, Nb and W) intermetallic in 0.1 mol/l NaOH with 200 ppm Cl^-.

The passive range obtained in the alkaline solution without chlorides for the intermetallics Fe_3Al and Fe_3Al-5M (M = Ti, Ta, Cr and Mo) in the forward polarization scan have been tabulated in Table 4.7. It can be noticed that the passive range obtained is larger in the case of the Ta- and Mo-alloyed intermetallics when compared to the base, Cr- and Ti-alloyed intermetallics. It was earlier also observed that the Ta-alloyed intermetallic exhibited the largest range of passivity in a NaOH solution of pH 8 [10]. It appears that the behavior is also similar in this alkaline solution.

is enhanced. The critical current density for passivation and the passive current density for the alloyed intermetallics are lower than the base intermetallic. The primary passivation potential and the complete passivation potential are lower for the alloyed intermetallic. The breakdown potential and the passive range is higher for the alloyed intermetallics. The variation of these parameters with alloying strongly suggest that passivity is enhanced on alloying.

3. The presence of chloride ions in the acidic solution leads to lowering of the breakdown potential and the passive region thereby indicating that they destabilize the passive layer of the intermetallics in the acidic solution. No systematic trend was noticed as regards the effect of chloride ions on the other parameters characterizing passivity. The primary and complete passivation potentials remain unchanged in the presence of the chloride ions.

4. The repassivation behavior of the intermetallics, as indicated by the loop on reverse scanning from noble potentials, is good in the case of the base Fe_3Al, Nb-, Ta-, Cr-containing intermetallics and moderate in the case of the Ti-, Zr-, Mo- and W-containing intermetallics in the absence of chloride ions in the acidic medium. The presence of chloride ions generally results in poorer repassivation behavior and this is due to the destabilizing effect of chloride ions on the passive layer.

5. The polarization behavior of Fe_3Al and Fe_3Al-5M (M=Ti,Ta, Cr and Mo) in the alkaline solution are similar and they exhibited stable passive behavior in the absence of chloride ions. The passive range was larger for the Ta- and Mo-containing intermetallics compared to that for the others. However, the polarization behavior of the intermetallics in the presence of chloride ions was similar and they exhibited active behavior. The polarization behavior of the other intermetallics Fe_3Al-5M (M=Zr,

V, Nb, and W) are poorly understood.

6. The characterization of the phases that form on alloying the base intermetallic with passivity-inducing elements (Ti, Zr, V, Nb, Ta, Cr, Mo, W, Ni and Si) was performed by x-ray diffraction. The study indicated that Cr and Ti additions dissolve as solid solutions in the base intermetallic whereas additional phases form in the other alloyed intermetallics. They were identified as Fe_2Nb FeNb, $AlNb_2$ and Al_3Nb in Fe_3Al-5Nb, Fe_5Ta_3, Ta_2Al_3 and FeTa in Fe_3Al-5Ta, $Fe_{63}Mo_{37}$ and $Al_{17}Mo_4$ in Fe_3Al-5Mo, FeV in Fe_3Al-5V, Fe_2W and Fe_7W_6 in Fe_3Al-5W, Fe_2Zr in Fe_3Al-5Zr and Al_8Fe_2Si in Fe_3Al-5Si.

5.2. SUGGESTIONS FOR FUTURE WORK

The following suggestions could be incorporated in future work on the polarization behavior of these alloyed intermetallics:

1. The polarization behavior could be studied in other solutions where active-passive behavior could be expected. The effect of normality of the acidic solution could be a variable. In order to study the polarization behavior in near neutral pH, experiments could be conducted using borate buffered solutions as has been employed to study passivity of iron-based alloys.

2. The role of oxygen on the polarization behavior could be investigated by using solutions of different aerations (i.e. completely deaeraed by bubbling with an inert gas and fully aerated by bubbling with oxygen gas prior to experimentation). This would throw some light on the role of oxygen in stabilizing the passive layer and also on the role of the oxygen reduction reaction in affecting the polarization behavior and hence passivity.

3. The polarization behavior of the intermetallics in the alkaline solution was poorly understood in this study. Therefore, this

aspect needs to be studied in greater detail preferably as a function of solution pH.

4. Weight loss measurements could be conducted using small specimens sectioned from the alloyed intermetallics in order to obtain information on actual corrosion rates. This could be obtained in a wide variety of solutions using the same specimens.

5. It was noticed in this study that the intermetallics are susceptible to pitting. The nature of pitting upon free corrosion conditions could be studied by performing scanning electron microscopic studies on the surface of the pit specimens in order to obtain information on the morphology and nature of pitting. The pitting behavior could also be correlated with the precipitates (additional phases that precipitate on alloying) present in the alloyed intermetallics.

6.The effect of processing and state of order in the material on the polarization behavior could also be studied although few studies in this direction indicated that the polarization behavior depended more on the composition of the intermetallic than on the processing method.

7. The effect of temperature on the polarization behavior also needs to be understood. As mentioned in the experimental procedure section, it was noticed that the temperature variation during the time the experiments were conducted was around 13^{o}C. This would have affected the dissolved oxygen concentration in the electrolytes which could also affect the polarization behavior. Therefore, the effect of temperature on polarization behavior merits study. It would also be interesting to study the corrosion of the iron aluminides by weight loss method at high temperatures as this is also an important parameter to be studied if iron aluminides are to replace stainless steels.

REFERENCES

1. N.S.Stoloff and D.J.Duquette, "Moisture and Hydrogen Induced Embrittlement of Iron Aluminides", *Journal of Metals*, **45**, (1993), 30-35.
2. C.T.Liu, V.K.Sikka and C.G.McKamey, "Alloy Development of FeAl Aluminide Alloys for Structural Use in Corrosive Environments", ORNL Report, Martin Marietta Energy Systems, Unpublished Research.
3. C.T.Liu, E.H.Lee and C.G.McKamey, "An Environmental Effect as the Major Cause for Room Temperature Embrittlement in FeAl", *Scripta Metall.*, **23**, (1989), 875-880.
4. C.T.Liu, C.L.Flu, E.P.George and G.S.Painter, "Environmental Embrittlement in FeAl Aluminides (Review), *ISIJ Int.*, **31**, (1991), 1192-1200.
5. D.J.Gaydosh and M.V.Nathal, "Influence of Testing Environment on the Room Temperature Ductility of FeAl Alloys", *Scripta Metall. Mater.*, **24**, (1990), 1281-1284.
6. C.T.Liu and K.S.Kumar, "Ordered Intermetallic Alloys, Part 1: Nickel and Iron Aluminides", *Journal of Metals*, **45**, (1993), 38-44.
7. C.G.McKamey and C.T.Liu, "Chromium Addition and Environmental Embrittlement in Fe_3Al", *Scripta Metall. Mater.*, **24**, (1990), 2119-2122.
8. R.Balasubramaniam, "On the role of Chromium in Minimizing Room Temperature Hydrogen Embrittlement in Iron Aluminides", *Scripta Mater.*, **34**, (1996) 127-133.
9. S.Yangshan, Y.Z.Zhengjun, Z.Zhonghua and H.Haibo, "Mechanical Properties of Fe_3Al-Based Alloys with Cerium Addition", *Acta Metall. Mater.*, **33**, (1995), 811-812.
10. A.Agarwal, M.J.Akhtar and R.Balasubramaniam, "Effect of Alloying on Aqueous Corrosion and Mechanical Behavior of Iron Aluminide Fe_3Al", *Journal of Material Science*, (1996), accepted.

11. K.Vedula, "FeAl and FE_3Al", *in Intermetallic Compounds*, Edited by J.H.Westbrook and R.L.Fleischer, John Wiley New York, USA, **Vol 2**, (1994), 199-209.
12. N.Ridley, *J. Inst. Met.*, **94**, (1966), 255.
13. A.J.Bradley and A.Taylor, *Proc. R. Soc. London. Ser. A*, **136**, (1932), 210.
14. A.J.Bradley and A.Taylor, *Proc. R. Soc. London. Ser. A*, **159**, (1937), 210.
15. J.R.Stephens, *Mater. Res. Soc. Symp. Proc.*, **39**, (1985), 381.
16. K.Ho and R.A.Dodd, "Point Defects in FeAl", *Scripta Metall.*, **12**, (1978), 1055-1058.
17. K.Vedula and J.R.Stephens, *Mater. Res. Soc. Symp Proc.*, **81**, (1987), 381.
18. N.Mantravadi, PhD Thesis, (1986), Case Western Reserve University.
19. M.Mendiratta, S Ehlers, D.Dimiduk, W.Kerr, S.Mazdiyasni and H.A.Lipsitt, *Mater. Res. Soc. Symp. Proc.*, **81**, (1987), 393.
20. M.G.Mandiretta and H.A.Lipsitt, *Mater. Res. Soc. Symp. Proc*, **39**, (1985), 155.
21. B.H.Rabin and R.N.Wright, "Microstructure and Tensile Properties of Fe_3Al Produced by Combustion Synthesis/Hot Isostatic Pressing", *Met. Trans. A*, **23A**, (1992), 35-40.
22. I.Baker and D.J.Gaydosh, "Flow and Fracture of Fe-Al", *Mater. Sci. Eng.*, **96**, (1987), 147-158.
23. C.T.Liu, C.G.McKamey, E.H.Lee, "Environmental Effects on Room-Temperature Ductility and Fracture in Fe_3Al Alloys", *Scripta Metall. Mater.*, **24**, **2**, (1990), 385-390.
24. O.Klein and I.Baker, "Effect of Heat-Treatment on The Tensile Behavior of Iron-Rich FeAl and FeAl + B", *Scripta Metall. Mater.*, **30**, (1994), 627-632.
25. P.G.Sanders, V.K.Sikka, C.R.Howell and R.H.Baldwin, "A Processing Method to Reduce the Environmental Effect In Fe_3Al-Based Alloys", *Scripta Metall. Mater.*, **25**, (1991), 2365-2369. and

C.G.McKamey and D.H.Pierce, "Effect of Recrystallization on Room temperature Tensile Properties of an Fe_3Al-Based Alloy", *Scripta Metall. Mater.*, **28**, (1993), 1173-1176.

26. C.G.McKamey, J.A.Horton, and C.T.Liu, "Effect of Chromium on Room Temperature Ductility and Fracture Mode in Fe_3Al" ,*Scripta Metall.*, **22**, (1988), 1679-1681.
27. C.T.Liu and E.P.George, "Environmental Embrittlement in Boron-Free and Boron Doped FeAl (40 at % Al) Alloys", *Scripta Metall. Mater.*, **24**, (1990), 1285-1290.
28. C.T.Liu and E.P.George, in "*High Temperature Ordered Intermetallic Alloys IV*", Edited by L.A.Johnson, D.P.Pope and J.O.Stiegler, MRS, Pittsburgh, (1991), 527.
29. D.Li, D.Lin, A.Shan and Y.Liu, "Effects of Strain Rate and Mangnese Addition on Room Temperature Ductility of FeAl", *Scripta Metall. Mater.*, **30**, (1994), 655-659.
30. I.Jung, M.Rudy and G.Sauthoff, *Mater. Res. Soc. Symp. Proc*, **81**, (1987), 263.
31. P.R.Swann, W.R.Duff and R.M.Fisher, *Trans. Metall. Soc. AIME*, **245**, (1969), 851.
32. P.R.Swann, W.R.Duff and R.M.Fisher, *Phys. Stat. Sol.*, **37**, (1970), 577.
33. P.R.Swann, W.R.Duff and R.M.Fisher, "The Electron Metallography of Ordering Reactions in Fe-Al Alloys", *Metall. Trans.*, **3**, (1972), 409-419.
34. H.K.Birnbaum, G.M.Bond and I.M.Robertson, "Effect of Hydrogen on Deformation and Fracture Process in High Purity Aluminium", *Acta Metall.*, **36**, (1988) 2193-2198.
35. A.Agarwal, R.Balasubramaniam and S.Bhargava, "Effect of Thermomechanical Treatments on the Room Temperature Mechanical Behavior of Iron Aluminide", *Metallurgical and Materials Transactions* A, (1996), accepted.

C.G.McKamey, J.A.Horton and C.T.Liu, *J Mater Research*, **4**, (1989), 1156.

36. R.A.Buchanan and J.G.Kim, "Chloride-Induced Localized Corrosion of Fe_3Al-Type Iron Aluminides: Beneficial Effects of Cr and Mo Additions", *Mat. Res. Soc. Symp. Proc.*, **213**, (1991), 945-950.

37. A.Agarwal and R.Balasubramanium, "Role of Surface Passive Films in the Hydrogen Embrittlement of Iron Aluminides", *Bulletin of Materials Science*, (1996), in press.

38. A.Shan and D.Lin, "Effects of Strain Rate and Chromium Addition on Room Temperature Ductility and Fracture Mode in Fe_3Al", *Scripta Metall.*, **23**, (1989), 875-880.

39. P.Janavicius and J.H.Payer, "The Dissolution Behavior of Iron Aluminides, *"Environmental Effects On Advanced Materials"*, Edited by R.H.Jones and R.E.Ricker, TMS, Warrendale, USA, (1991), 199-212.

40. R.A.Buchanan, J.G.Kim, R.E.Ricker and L.A.Heldt, "Aqueous Corrosion of Intermetallic Alloys", in, *"Processing and Properties of Intermetallic Compounds"*, Edited by N.S.Stoloff and V.Sikka, Chapman and Hall, London, England, (1996), 536-552.

41. M.J.Akhtar and R.Balasubramaniam, "Corrosion Behavior of Iron Aluminide Fe_3Al", *Corrosion*, (1996) communicated.

42. R.Narayan, *"An Introduction to Metallic Corrosion and its Prevention"*, Oxford and IBH Co. Pvt Ltd, New Delhi, India, (1983), 76-98.

43. D.A.Jones, *"Principles and Prevention of Corrosion"*, Maxwell Macmillan International Publishing Group, New York, USA, (1992), 117-524.

44. Standard Practice for Laboratory Immersion, Corrosion Testing of Metals, G 31-72, *"Annual Book of ASTM Standard"*, ASTM, Philadelphia, USA, 03.02, (1991), 102.

45. K.Oki, M.Hasaka and T.Eguchi, "Process of Order-Disorder Transformation in Iron-Aluminium Alloys", *Japanese Journal of Applied Physics*, **12**, (1973), 1522-1530.

46. N.D.Tomashov and G.P.Chernova, *"Pssivity and Protection of Metals Against Corrosion"*, Plenum Press, USA, (1967), 14-28, 59, 61, 64, 67-79, 128, 167, 168, 169, 295, 675.

47. H.Gerischer, *Angew. Chem.*, **70**, (1958) 285.
48. V.Cihal and M.Prazak, *J. Iron Steel Inst.*, **193**, (1959), 360.
49. E.I.Litvinova, *Zh. Prikl. Khim.*, **28**, (1955) 1285.
50. D.Lin(T.L.Lin), A.Shan and D.Li, "Superplasticity in Fe_3Al-Ti Alloy With Large Grains", *Scripta Metall. Mater.*, **31**, (1994), 1455-1460.
51 M.G.Fontana and N.G.Greene, "*Corrosion Engineering*", 2nd Edition, McGraw Hill, New York, (1983), 56, 57, 63, 71, 81, 237, 242, 337, 367.
52. N.D.Tomashov, G.P.Chernova and O.N.Markova, "*Collection: Corrosion of Metals And Alloys*", Metallurgizdat, Moscow (1963), 73.
53. K.Hashimoto and K. Asami, "Factors Determinig Corrosion Resistance of Chromium Bearing Alloys", in "*Passivity of Metals*",Edited by R.P.Frankenthal and J.Kruger, Electrochemical Society, Princeton, (1978), 749-751.
54. M.Prazak and V.Cihal, *Corrosion Science*, **2**, (1962).
55. G.P.Chernova and N.D.Tomashov, "*Collection: Corrosion of Structural Metals*", Metallurgizdat, Moscow (1959), 7 and *Z. Phys. Chem.*, **226**, (1964), 136.
56. P.F.King and H.H.Uhlig, *J. Phys. Chem.*, **63**, (1959), 2026.

APPENDIX B

ANALYSIS OF X-RAY DIFFRACTION PATTERNS OF THE BASE AND ALLOYED INTERMETALLICS.

TABLE B1 Analysis of XRD pattern of base intermetallic Fe_3Al thermomechanically processed at 1000°C.

TABLE B2 Analysis of XRD pattern of base intermetallic Fe_3Al thermomechanically processed at 1000°C and then ordered at 500°C for 4 days.

TABLE B3 Analysis of XRD pattern of intermetallic Fe_3Al-5Ti thermomechanically processed at 1000°C.

TABLE B4 Analysis of XRD pattern of intermetallic Fe_3Al-5Zr from the homogenized button.

TABLE B5 Analysis of XRD pattern of intermetallic Fe_3Al-5V thermomechanically processed at 1000°C.

TABLE B6 Analysis of XRD pattern of intermetallic Fe_3Al-5Nb thermomechanically processed at 1000°C.

TABLE B7 Analysis of XRD pattern of intermetallic Fe_3Al-5Ta thermomechanically processed at 1000°C.

TABLE B8 Analysis of XRD pattern of intermetallic Fe_3Al-5Cr thermomechanically processed at 1000°C.

TABLE B9 Analysis of XRD pattern of intermetallic Fe_3Al-5Mo thermomechanically processed at 1000°C.

TABLE B10 Analysis of XRD pattern of intermetallic Fe_3Al-5W from the homogenized button.

TABLE B11 Analysis of XRD pattern of intermetallic Fe_3Al-5Si thermomechanically processed at 1000°C.

TABLE B1

Analysis of XRD pattern of base intermetallic Fe_3Al thermomechanically processed at 1000°C.

2θ ($Cr_{k\alpha}$)	d		Int		plane	phase
	Obs	Theor	Obs	Theor		
(deg)	(Å)	(Å)	(%)	(%)	(hkl)	
32.4	4.10					
34.3	3.88					
35.0	3.81					
36.4	3.68					
46.6	2.90	2.89	20	50	(200)	Fe_3Al
54.1	2.52					
58.2	2.36					
68.0	2.05	2.04	100	100	(220)	Fe_3Al
78.3	1.81					
85.3	1.69	1.67	8	10	(222)	Fe_3Al
104.0	1.45	1.45	76	80	(400)	Fe_3Al

TABLE B2

Analysis of XRD pattern of base intermetallic Fe_3Al thermomechanically processed at 1000°C and then ordered at 500°C for 4 days

2θ ($Cr_{k\alpha}$)	d		Int		plane	phase
	Obs	Theor	Obs	Theor		
(deg)	(Å)	(Å)	(%)	(%)	(hkl)	
32.4	4.10					
34.3	3.88					
35.0	3.81					
36.4	3.68					
46.6	2.90	2.89	20	50	(200)	Fe_3Al
54.1	2.52					
58.2	2.36					
68.0	2.05	2.04	100	100	(220)	Fe_3Al
78.3	1.81					
85.3	1.69	1.67	8	10	(222)	Fe_3Al
104.0	1.45	1.45	76	80	(400)	Fe_3Al

TABLE B3

Analysis of XRD pattern of intermetallic Fe_3Al-5Ti thermomechanically processed at $1000^{o}C$.

2θ ($Cr_{k\alpha}$)	d		Int		plane	phase
	Obs	Theor	Obs	Theor		
(deg)	(Å)	(Å)	(%)	(%)	(hkl)	
32.4	4.10					
34.3	3.88					
35.0	3.81					
36.4	3.68					
46.6	2.90	2.89	20	50	(200)	Fe_3Al
54.1	2.52					
58.2	2.36					
68.0	2.05	2.04	100	100	(220)	Fe_3Al
78.3	1.81					
85.3	1.69	1.67	8	10	(222)	Fe_3Al
104.0	1.45	1.45	76	80	(400)	Fe_3Al

TABLE B4

Analysis of XRD pattern of intermetallic Fe_3Al-5Zr from homogenized button.

2θ ($Cr_{k\alpha}$) (deg)	d Obs (Å)	d Theor (Å)	Int Obs (%)	Int Theor (%)	plane (hkl)	phase
26.5	4.99					
28.8	4.61					
32.3	4.12					
54.9	2.48	2.481	40	40	(220)	Fe_2Zr(H)
60.1	2.29	2.278	55	60	(200)	Al_2Zr
64.4	2.15					
65.4	2.12	2.114	85	100	(311)	Fe_2Zr
66.8	2.08					
67.9	2.05					
68.9	2.02	2.03	35	40	(222)	$ZrFe_2$
77.4	1.83					
103.2	1.46	1.46	70	20	(800)	Fe_3Zr
105.3	1.44					
110.1	1.40					
114.8	1.36					
124.1	1.30					

TABLE B5

Analysis of XRD pattern of intermetallic Fe_3Al-5V thermomechanically processed at 1000°C.

2θ ($Cr_{k\alpha}$)	d		Int		plane	phase
	Obs	Theor	Obs	Theor		
(deg)	(Å)	(Å)	(%)	(%)	(hkl)	
32.7						
43.8						
68.3	2.04	2.03	100	100	(110)	FeV
104.4						

TABLE B6

Analysis of XRD pattern of intermetallic Fe_3Al-5Nb thermomechanically processed at 1000°C.

2θ ($Cr_{k\alpha}$)	d		Int		plane	phase
	Obs	Theor	Obs	Theor		
(deg)	(Å)	(Å)	(%)	(%)	(hkl)	
36.0	3.71					
38.0	3.52	3.51	20	60	(101)	Al_3Nb
46.9	2.88					
56.3	2.43	2.42	40	100	(410)	$\sigma AlNb_2$
58.3	2.35					
61.7	2.23					
65.9	2.11	2.12	20	83	(111)	FeNb
67.9	2.05	2.05	100	100	(112)	Fe_2Nb
70.7	1.98	1.98	15	27	(205)	FeNb
76.3	1.85					
79.6	1.81					
100.5	1.49					
102.8	1.47					
103.4	1.46					
104.0	1.45					
104.4	1.45					
114.4	1.36	1.36	22	20	(423)	$AlNb_2$
119.4	1.33					
119.9	1.32					
127.5	1.28					
129.5	1.27					

APPENDIX A

X-RAY DIFFRACTION PATTERNS OF THE BASE AND ALLOYED INTERMETALLICS

FIGURE A1 XRD pattern of base intermetallic Fe_3Al thermomechanically processed at 1000°C.

FIGURE A2 XRD pattern of base intermetallic Fe_3Al thermomechanically processed at 1000°C and then ordered at 500°C for 4 days

FIGURE A3 XRD pattern of intermetallic Fe_3Al-5Ti thermomechanically processed at 1000°C.

FIGURE A4 XRD pattern of intermetallic Fe_3Al-5Zr from homogenized button.

FIGURE A5 XRD pattern of intermetallic Fe_3Al-5V thermomechanically processed at 1000°C.

FIGURE A6 XRD pattern of intermetallic Fe_3Al-5Nb thermomechanically processed at 1000°C.

FIGURE A7 XRD pattern of intermetallic Fe_3Al-5Ta thermomechanically processed at 1000°C.

FIGURE A8 XRD pattern of intermetallic Fe_3Al-5Cr thermomechanically processed at 1000°C.

FIGURE A9 XRD pattern of intermetallic Fe_3Al-5Mo thermomechanically processed at 1000°C.

FIGURE A10 XRD pattern of intermetallic Fe_3Al-5W from the homogenized button.

FIGURE A11 XRD pattern of intermetallic Fe_3Al-5Si thermomechanically processed at 1000°C.

TABLE B10

Analysis of XRD pattern of intermetallic Fe_3Al-5W from the homogenized button.

2θ ($Cr_{k\alpha}$)	d		Int		plane	phase
	Obs	Theor	Obs	Theor		
(deg)	(Å)	(Å)	(%)	(%)	(hkl)	
37.8	3.54					
57.8	2.37	2.37	25	100	(110)	Fe_7W_6
58.3	2.35	2.36	24	100	(110)	Fe_2W
68.2	2.04	2.04	100	80	(0111)	Fe_7W_6
108.8	1.41					
112.5	1.38					

TABLE B11

Analysis of XRD pattern of intermetallic Fe_3Al-5Si thermomechanically processed at 1000°C.

2θ ($Cr_{k\alpha}$)	d		Int		plane	phase
	Obs	Theor	Obs	Theor		
(deg)	(Å)	(Å)	(%)	(%)	(hkl)	
38.5	3.47	3.45	15	34	(124)	Al_8Fe_2Si
58.3	2.35	2.34	20	36	(140)	Al_8Fe_2Si
68.1	2.045					
105.7	1.43					
124.8	1.29					

MME-1996-M-AST-ELE

TABLE B9

Analysis of XRD pattern of intermetallic Fe_3Al-5Mo thermomechanically processed at 1000°C.

2θ ($Cr_{k\alpha}$)	d		Int		plane	phase
	Obs	Theor	Obs	Theor		
(deg)	(Å)	(Å)	(%)	(%)	(hkl)	
32.2	4.13					
37.2	3.59	3.58	10	15	(102)	Al_5Mo
39.7	3.37	3.38				
43.5	3.09	3.10	10	33	(211)	$Al_{12}Mo$
46.3	2.91					
58.6	2.34	2.34	10	20	(018)	$Fe_{63}MO_{37}$
67.4	2.06	2.06	100	70	(410)	$Fe_{63}Mo_{37}$
102.2	1.472					
102.6	1.468					
103.2	1.461	1.46		30	(541)	σFe-Mo

better compared Fe_3Al. Incidentally, the corrosion behavior of the binary Fe_3Al has been investigated in a variety of electrolytes and this has been discussed elsewhere [41]. The potentiodynamic polarization curves of binary Fe_3Al and Fe_3Al-5M (M = Cr, Mo, Ta and Ti) intermetallics in electrolytes of pH 4 and 8 have been presented elsewhere [10]. The corrosion characteristics of these intermetallics in electrolytes of pH 4 and 8 are summarized in Tables 2.6 and 2.7, respectively. The following comparative observations were made for Fe_3Al-5M intermetallics and binary Fe_3Al. The FCP of Fe_3Al-5M intermetallics were noble compared to binary Fe_3Al in both the electrolytes (pH 4 and 8). The complete passivation potentials (E_{cp}) were more negative for Fe_3Al-5M intermetallics compared to binary Fe_3Al, thereby indicating that it should be easier to passivate Fe_3Al-5M compared to Fe_3Al. The pitting potentials (E_{pit}) were noble for Fe_3Al-5M intermetallics compared to binary Fe_3Al in the electrolyte of pH 4 indicating that they retain passivity to much higher potentials without pitting. However, the reverse was the case in the electrolyte of pH 8, where Fe_3Al showed a noble pitting potential compared to the Fe_3Al-5M intermetallics. The passivity range was larger for Fe_3Al-5M intermetallics compared to binary Fe_3Al in both the electrolytes.

2.4 POLARIZATION BEHAVIOR OF PASSIVATING METALS/ALLOYS

For metals exhibiting passivity, the potentiostatic or potentiodynamic methods give full information about passivation behavior. Figure 2.7 shows a typical potentiostatic/dynamic anodic polarization curve of a metal exhibiting passivity. The important points in this curve are described below.

A - corresponds to the equilibrium potential of the metal under a given environment condition.

AB - anodic polarization behavior of a normal corroding metal

B - corresponds to equilibrium potential for initiation of passive film growth E_{ip}.

C - at potential of primary passivation E_{pp} acceleration of metal dissolution occurs.

CHAPTER 3

EXPERIMENTAL PROCEDURE

This chapter describes the materials, test specimens, their preparation, experimental apparatus and electrolytes used for polarization studies. The experimental methods employed to characterize the materials used in the study have also been described.

3.1. MATERIAL

A pancake of iron aluminide (Fe-28 at% Al) of diameter 120 mm and thickness 15 mm was obtained from the Defence Metallurgical Research laboratory (DMRL), Hyderabad. This pancake was processed by the ingot metallurgy route. In order to remove segregation, this pancake was homogenised at 1000^{o}C for 4 hours. A test piece of size 8cm x 4cm x 1.5 cm was later ordered at 550^{0}C for 4 days. After ordering specimen of size 1cm x1cm and thickness of 3mm were machined from this piece. Base Fe_3Al intermetallic specimens for the polarization studies were also obtained from the base Fe_3Al intermetallic that had been thermomechanically processed to 80% deformation at 1000 ^{o}C in multi-pass rolling [35]. They did not exhibit any difference in their polarization behavior indicating that the composition of the material was more important than the processed state of the intermetallic.

In order to prepare the alloyed intermetallics, pieces of about 20 gm each were cut from the homogenized pancake. In the first round of specimen preparation, five atomic percent of passivity-inducing elements Cr, Mo, Ti, Ta, Nb, V, Ni and Si of purity 99.9% was added to binary Fe_3Al to prepare the alloyed intermetallic of type Fe_3Al-5M (M = passivity inducing element). These alloys were melted in an arc furnace in an inert (argon) atmosphere. Each alloy was melted thrice to minimize segregation. Ni could not be alloyed because of a violent with iron aluminide of the composition Fe_3Al.

CHAPTER 4

RESULTS AND DISCUSSIONS

The results obtained in the present study would be presented in this chapter and discussed. The first section of this chapter deals with the characterization of the alloyed iron aluminide intermetallics by x-ray diffraction . The next section discusses the nature of stabilization of the free corrosion potentials of these intermetallics in the various electrolytes studied. The electrochemical behavior of the intermetallics in the acidic medium is individually discussed next in great detail and the section ends with an overall comparison of the intermetallics in this medium. The electrochemical behavior of the intermetallics in the alkaline medium is addressed after this.

4.1 MATERIAL CHARACTERIZATION

The x-ray diffraction patterns obtained from the base iron aluminide and the alloyed intermetallics are presented in Appendix A. The diffraction peaks in these patterns have been indexed according to the standard procedure and the results of the analysis are tabulated in Appendix B. The following features could be concluded from the XRD analysis. The base intermetallic that was thermomechanically processed at 1000^{o}C exhibited the presence of the peaks corresponding the α phase of Fe_3Al (Figure A1). It is to be noted that the peaks corresponding to the DO_3 ordered allotrope of Fe_3Al is generally absent in the XRD patterns of even the ordered intermetallic and the reasons for the same have been elucidated elsewhere [35,45]. This can also be noticed in the XRD pattern of the base intermetallic that was processed at 1000^{o}C and later ordered at 550^{o}C for 4 days (Figure A2). However, the presence of order in the intermetallic that was provided the ordering treatment is indicated by the broadening of the (440)

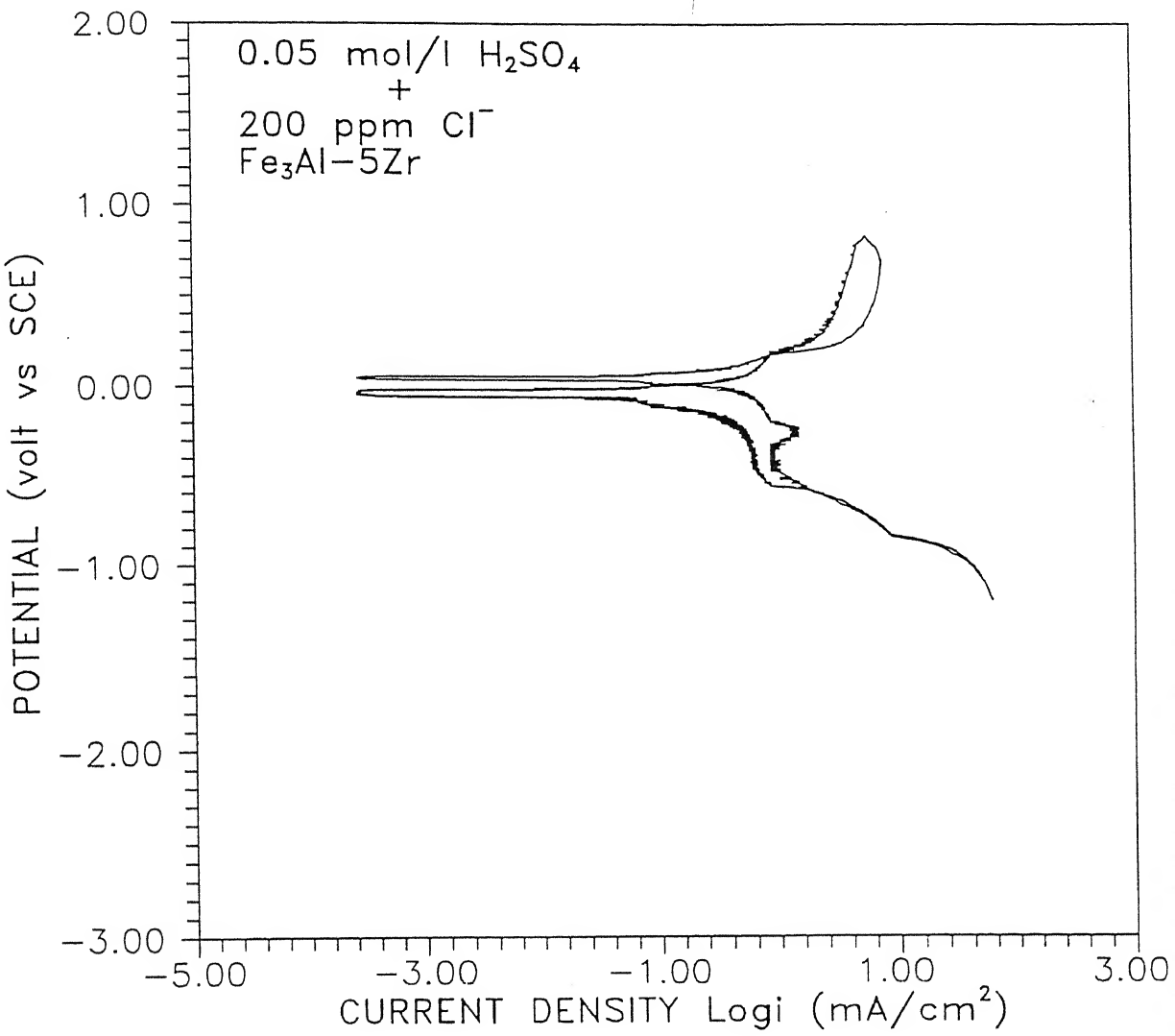

Figure 4.10 Cyclic polarization curve of Fe_3Al-5Zr intermetallic in 0.05 mol/l H_2SO_4 with 200ppm of Cl^-.

higher currents are drawn in the passive region during the reverse scan than in the forward scan and the forward scan is intersected at a potential very close to the ZCP on forward scan indicating that the material is not very resistant to chloride-induced pitting.

It has been reported that Nb addition improves the passivity of stainless steels if the additions are retained in solid solution by annealing at high temperature [48]. Nb additions to stainless steels lower the i_{crit} [49] and a similar effect is seen by alloying Nb to Fe_3Al. In the present case, the i_{crit} is lowered by an order of magnitude. Moreover, E_{pp} and E_{cp} are lowered while E_b is increased on alloying with Nb. Therefore, it appears that the addition of Nb results in the enhancement of passivity of the base intermetallic.

4.3.6 Fe_3Al-5Ta

The potentiodynamic polarization curves (forward and reverse scans) for Fe_3Al-5Ta in the acidic H_2SO_4 solution without chloride ions are presented in Figures 4.16. The intermetallic exhibited active-passive behavior in this electrolyte as can be seen from the forward scan and this is different from the active behavior observed earlier for the base Fe_3Al intermetallic. The stabilized FCP for this intermetallic was -0.6 V vs SCE and the zero current potential (ZCP) on scanning from the cathodic to the anodic (active to noble) direction is -0.45 V vs SCE. The value of i_{crit} is 3.98 mA/cm^2 and this is lower than the i_{crit} of unalloyed Fe_3Al during the reverse scan in the same electrolyte. The passive range extends to about 1.0V and this is very much higher than the passive range obtained in unalloyed Fe_3Al in the reverse scan. Two breakdown potentials can be identified from the forward polarization curve (namely at 1.0 V and 1.6 V). The nature of the curve on reverse scanning indicates the relatively good re-passivation characteristics of the Ta-alloyed intermetallic as the reverse scan closely traces the original forward scan all the way to the ZCP. The noble value of the first breakdown potential

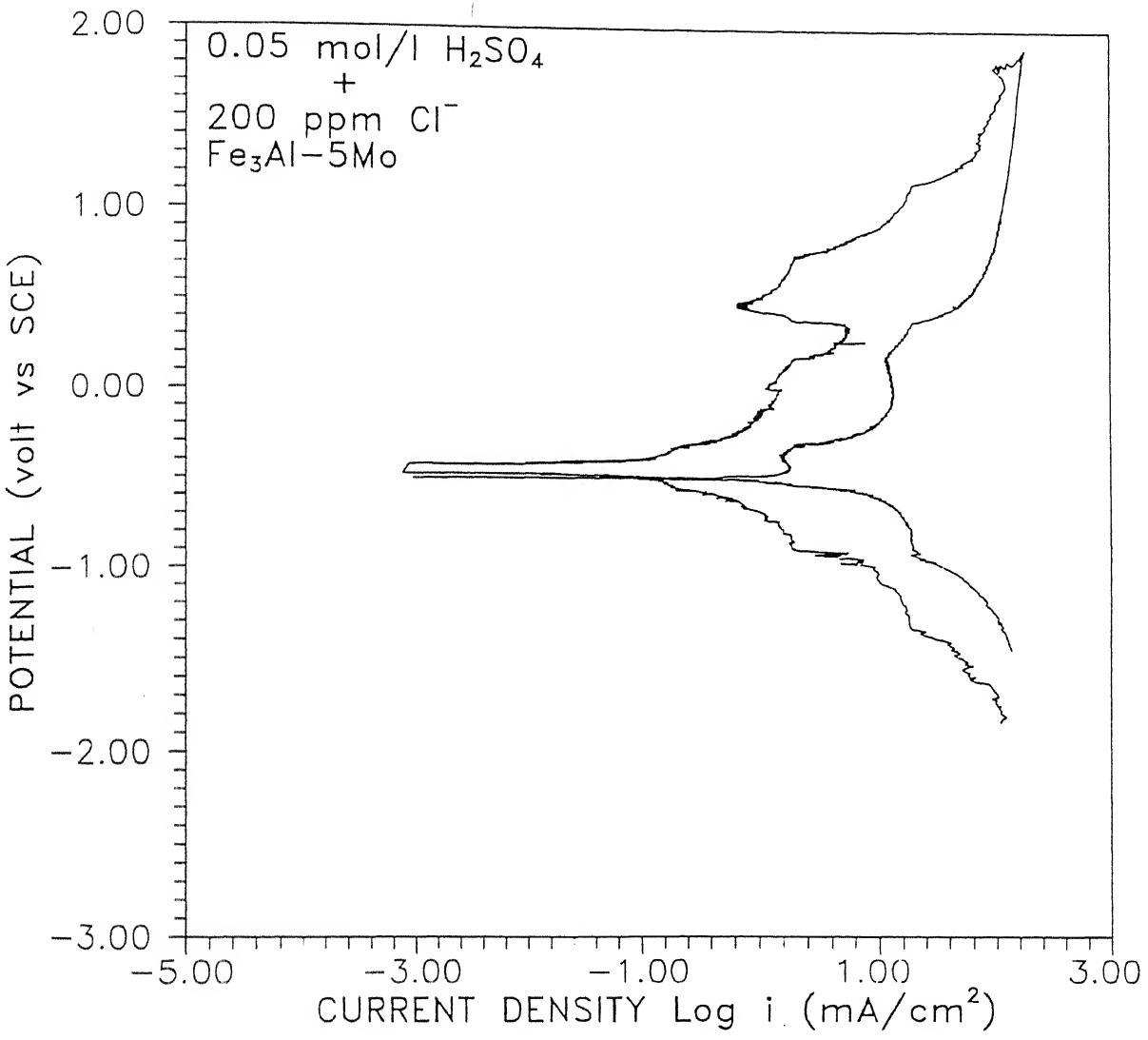

Figure 4.22 Cyclic polarization curve of Fe_3Al-5Mo intermetallic in 0.05 mol/l H_2SO_4 with 200ppm of Cl^-.

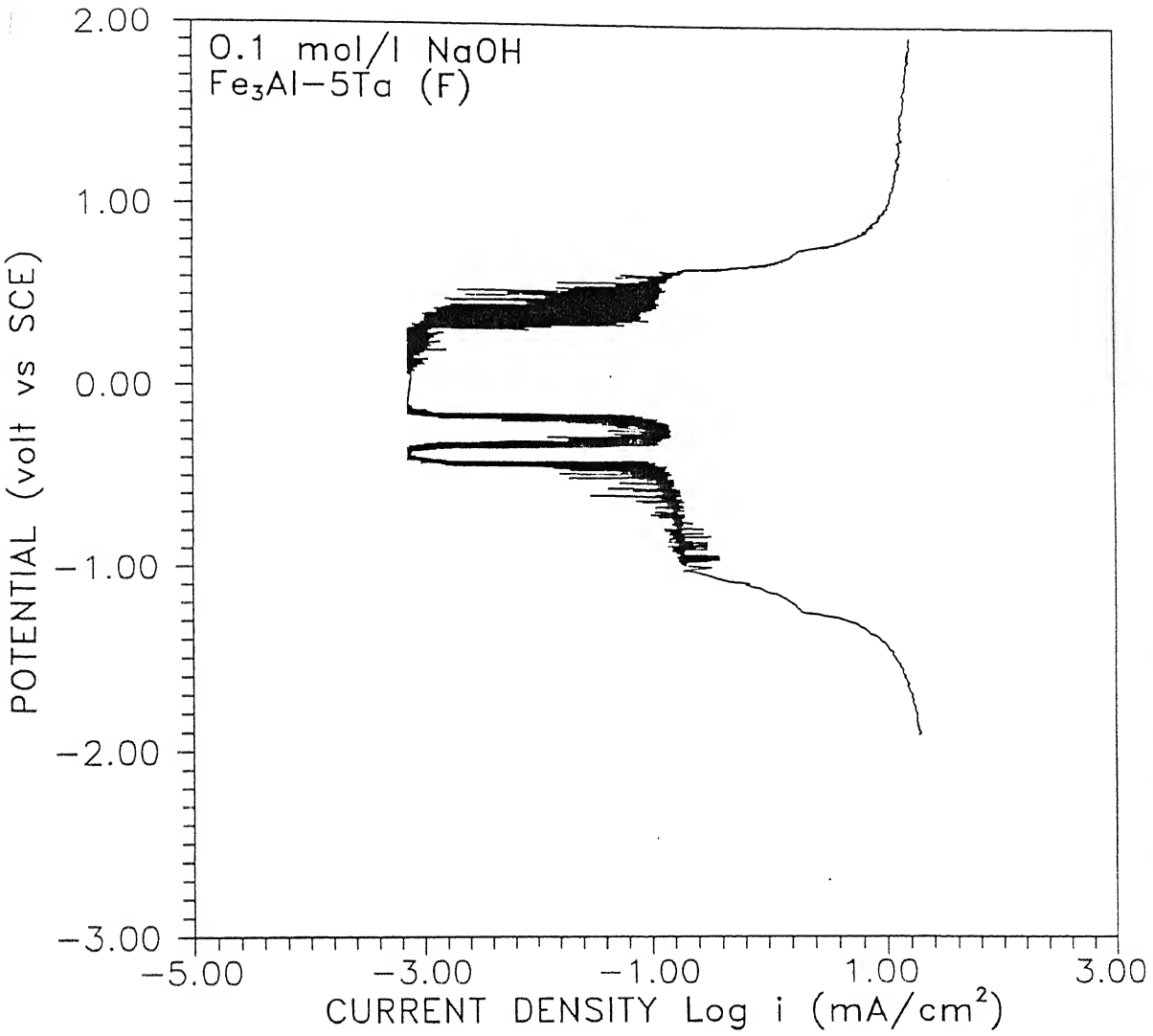

Figure 4.29 Forward polarization curve of Fe_3Al-5Ta intermetallic in 0.1 mol/l NaOH.

CHAPTER 5

CONCLUSIONS

5.1 CONCLUDING REMARKS

The stoichiometric iron aluminide of composition Fe_3Al has been alloyed with passivity-inducing elements (Ti, Zr, V, Nb, Ta, Cr, Mo, W, Ni and Si) in order to minimize the room temperature hydrogen embrittlement problem in these intermetallics according to a recently proposed iron aluminide alloy development philosophy [8]. In order to understand the passivity-inducing abilities of these alloying additions, the polarization behavior of alloyed iron aluminide intermetallics has been studied by the potentiodynamic polarization method. The intermetallics studied were Fe_3Al and Fe_3Al-5M (M=Ti, Zr, V, Nb, Ta, Cr, Mo and W). The electrochemical polarization behavior was studied in 0.05 mol/l H_2SO_4 and 0.1 mol/l NaOH solutions, with and without 200 ppm of chloride ions. The following are the important conclusions of the present study.

1. The base intermetallic exhibited active behavior in the acidic solution. In contrast, all the alloyed intermetallics, except the V-containing one, exhibited active-passive behavior in the same medium. Therefore, the addition of these elements induced passivity to the base iron aluminide in the acidic medium. The V-containing intermetallic exhibited active behavior both in the forward and reverse polarization scans. However, the base intermetallic exhibited passive behavior in the reverse polarization scan.

2. On comparing the reverse polarization curve for the base intermetallic and the forward polarization curves of the alloyed intermetallic in the acidic medium, it was observed that passivity